Master of Science Thesis

Incorporating Geovectors into the Process of Conflict Resolution for UAV Airspace

M.A. Giliam

06 July 2022

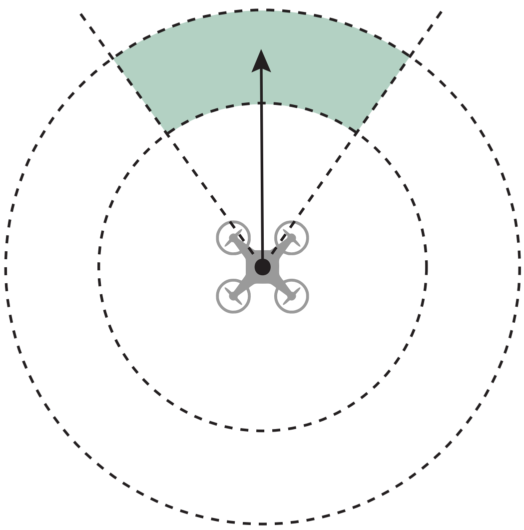

Faculty of Aerospace Engineering · Delft University of Technology

TU Delft Delft University of Technology

Challenge the future

Incorporating Geovectors into the Process of Conflict Resolution for UAV Airspace

Master of Science Thesis

For obtaining the degree of Master of Science in Aerospace Engineering at Delft University of Technology

M.A. Giliam

06 July 2022

Faculty of Aerospace Engineering · Delft University of Technology

Delft University Of Technology
Department Of
Control and Simulation

The undersigned hereby certify that they have read and recommend to the Faculty of Aerospace Engineering for acceptance a thesis entitled **"Incorporating Geovectors into the Process of Conflict Resolution for UAV Airspace"** by **M.A. Giliam** in partial fulfillment of the requirements for the degree of **Master of Science**.

Dated: 06 July 2022

Head of department: ______________________
prof.dr.ir. J.M. Hoekstra

Supervisor: ______________________
dr.ir. J. Ellerbroek

Reader: ______________________
dr. A. Bombelli

Acknowledgements

I wish to thank my supervisors, dr.ir. J. Ellerbroek and prof.dr.ir. J.M. Hoekstra, for providing me with the opportunity to work on this challenging topic. They helped me to improve my thesis work throughout the entire process, always taking the time to provide me with useful insights, lifting my research to a higher level. In addition, I would like to thank ir. A. Badea and ir. A. Morfin for their numerous advices regarding my thesis work.

Delft, The Netherlands M.A. Giliam
06 July 2022

Contents

List of Figures

List of Tables

Nomenclature

Latin Letters

$\mathbf{d}$	Distance vector
$\mathbf{n}$	Unit vector
$\mathbf{V}$	Velocity vector
$\mathbf{x}$	Position vector
alt	Altitude
CR	Conflict rate
d	Distance (magnitude)
GS	Ground speed
hdg	Heading
n	Integer (count)
p	Probability
R	Rotation matrix
S	Separation minimum between aircraft
t	Time
V	Speed (velocity vector magnitude)
VS	Vertical speed

Greek Letters

χ	Course
Δ	Difference between two parameters
η	Efficiency

ε	Correction factor

Subscripts

conf	Conflict
cpa	At the Closest Point of Approach
cur	Current
E	In the easterly direction
g	Describing a geovector course limit
h	In the horizontal plane
int	Intruder
intru	Intrusion
LA	Lookahead (conflict detection)
LoS	Loss of Separation / intrusion
max	Maximum limit
min	Minimum limit
N	In the northerly direction
own	Ownship
r	Conflict resolution (vector)
rel	Relative
sol	Conflict solution
t	Tangent to the Protected Zone
v	In the vertical plane

Superscripts

OFF	without conflict resolution
ON	with conflict resolution

Abbreviations

ADS-B	Automatic Dependent Surveillance-Broadcast
AGL	Above Ground Level
ARV	Allowed Reachable Velocities
ATCO	Air Traffic Controller
BVLOS	Beyond Visual Line Of Sight
CC	Collision Cone
CD	Conflict Detection

CD&R	Conflict Detection & Resolution
CPA	Closest Point of Approach
CR	Conflict Resolution
DEP	Domino Effect Parameter
FMS	Flight Management System
FRV	Forbidden Reachable Velocities
FV	Set of Forbidden Velocities
GNSS	Global Navigation Satellite System
IPR	Intrusion Prevention Rate
LoS	Loss of Separation
MVP	Modified Voltage Potential
PZ	Protected Zone
RV	Set of Reachable Velocities
SERA	Standardised European Rules of the Air
SESAR JU	SESAR Joint Undertaking
SSD	Solution Space Diagram
SSR	Secondary Surveillance Radar
UAM	Urban Air Mobility
UAV	Unmanned Aerial Vehicle
UPP	UTM Pilot Program
UTM	Unmanned Traffic Management
VLL	Very Low Level
VO	Velocity Obstacle

Part I

Scientific Article

A Tactical Conflict Resolution Method for UAVs in Geovector Airspace

M.A. Giliam*, J. Ellerbroek†, A. Badea, A. Morfin, J.M. Hoekstra†
Control and Simulation, Faculty of Aerospace Engineering
Delft Univertsity of Technology, Delft, The Netherlands
*MSc student †Thesis supervisor

Abstract – **In order to enable the safe and efficient integration of Unmanned Aerial Vehicles into very low level airspace, modern day research focuses on the development of new traffic services and procedures. One of these is the geovectoring protocol, which aims to reduce traffic complexity by setting limits on the allowed ground speed, course, and vertical speed. A geovector can be used to increase the capacity of an airspace by lowering the conflict rate. However, problems with priorities emerge when performing avoidance maneuvers in geovector airspace, as the limits are ignored in this process. A powerful conflict resolution algorithm is the Modified Voltage Potential (MVP). This paper proposes an extension to the MVP ruleset, based on Velocity Obstacle theory. Making use of an alternative conflict resolution maneuver which respects the geovector, five resolution strategies are defined with different priority settings for the separate limits. The performance of these strategies is compared to pure MVP on geovector, safety, and stability measures, making use of fast-time simulations in a corridor airspace. All resolution strategies show improvements on the ability to perform conflict resolution maneuvers within the geovector limits, albeit at the expense of safety and stability. It is recommended to further investigate the performance of the geovector resolution strategies for other types of airspace, to verify whether the observed reduction in conflict rate from the geovectors can be reinforced by the resolution strategies.**

Keywords – **UAVs - drones - U-Space - geovectoring - conflict detection & resolution - detect & avoid**

I. INTRODUCTION

Rapid advancements in the technology of Unmanned Aerial Vehicles (UAVs) enable the use this relatively new type of air traffic for various applications, such as public safety, maintenance, and parcel delivery. It is expected that 7 million leisure drones and 400,000 commercial/government drones will be present across Europe by 2050, where the majority will operate at altitudes below 150 meters [1]. Current estimates sit at over 78 thousand parcel-delivery drone and over 24 thousand food-delivery drone movements per hour for the metropolitan area of Paris by the year 2035 [2]. The safe and efficient integration of this new type of air traffic in urban areas, with high air traffic densities, is a key component of novel research on UAV airspace.

In Europe, new air traffic services and procedures are being developed for UAVs, called U-Space [3]. In order to accommodate the expected large number of UAVs, it is necessary to maximize the capacity of the airspace. Hoekstra et al. [4] identify that the conflict rate is a limiting factor for airspace capacity. Therefore, they propose to add a novel concept to the set of U-Space services: the geovectoring protocol. Specifically, a geovector consists of a set of limits on the allowed ground speed, course, and vertical speed of UAVs. These limits are implemented in a finite section of the airspace. A reduction in conflict rate is obtained by reducing the relative velocity between aircraft.

In a previous study, Jacobse et al. [5] succesfully implemented geovectors as a conflict prevention tool in converging traffic flows. In the experiments, conflict resolution maneuvers were always prioritized over abiding by the geovector rules. As a result, a negative correlation was observed between traffic density and the conflict rate reduction attributed to the geovectors. The increase in number of conflicts at higher traffic densities leads to an increase geovector rule violations.

This study aims to improve the effectiveness of the geovector rules by incorporating them into the process of conflict resolution in the horizontal plane. A horizontal conflict resolution maneuver is derived based on velocity obstacle theory. Various resolution strategies are defined, with varying priority settings for the conflict and the geovector constraints. The benefits of the resolution strategies are experimentally verified, comparing them on geovector, safety, and stability metrics for varying geovector settings. Experiments are performed using BlueSky, an open source air traffic management simulator developed at TU Delft [6].

The present paper is structured as follows: Section II. provides necessary background on UAV traffic management concepts. This is followed by literature on conflict detection & resolution methods in Section III. These topics from literature are combined in Section IV., introducing the proposed resolution method in geovector airspace. The methodology is presented in Section V., followed by the experiment results in Section VI. The paper concludes with the discussion and conclusions in Section VII. and Section VIII., respectively.

II. UAV TRAFFIC MANAGEMENT

This section provides a brief introduction of European UAV airspace services in Subsection A., followed by a description of the geovectoring protocol in Subsection B. The concept of layered airspace is shortly presented in Subsection C.

A. U-Space

New procedures and air traffic services are being developed in Europe, in order to safely and efficiently integrate UAVs into the existing airspace. These services are called U-Space. The roll-out of U-Space services is envisioned in four major steps listed below, where U3 and U4 are focused on enabling high traffic density UAV operations [3]:

- **U1**: *Foundation services:* registration of UAVs, provision of restricted flight areas (geofencing)
- **U2**: *Initial services:* routine UAV operations, flight beyond visual line of sight
- **U3**: *Advanced services:* conflict resolution, dynamic airspace capacity management
- **U4**: *Full services:* complete roll-out of U-Space

B. Geovectoring

Hoekstra et al. [4] mention that the capacity of an airspace can be increased by decreasing the conflict rate. Furthermore, Sunil et al. [7] mention that a driving factor for the conflict rate is the relative velocity between aircraft. Hoekstra et al. experimentally verified that reducing the relative velocity does indeed lead to a reduction in conflict rate.

In order to achieve relative velocity reduction to increase the capacity of the airspace, Hoekstra et al. [4] introduce the geovectoring protocol. As indicated in Equation 1, a geovector specifies minimum and maximum limits on the allowed ground speed, course, and vertical speed of aircraft. These rules are applied in a finite section of the airspace, being a function of latitude, longitude, and altitude. Hoekstra et al. propose to add geovectoring as a tool to the U3 services of U-Space to enable high traffic densities in future UAV airspace.

$$\mathbf{V}_{geo} = \left\{ \begin{matrix} [GS_{min}, GS_{max}] \\ [\ \chi_{min}\ ,\ \chi_{max}\ ] \\ [VS_{min}, VS_{max}] \end{matrix} \right\} = f(lat, lon, alt) \tag{1}$$

A geovector can be visualized in velocity vector space, showing the set of allowed velocity vectors. Figure 1 indicates how limits are represented in the horizontal plane. For an arbitrary aircraft in a geovector area with velocity vector $\mathbf{V}$, ground speed limits (GS) can be visualized as circles centered at the point-mass representation of the aircraft, while course limits (χ) are represented by radials originating at the aircraft. The set of allowed velocities is represented by the area enclosed by the limits, colored green in Figure 1.

C. Layered Airspace Structure

In the Metropolis project performed by Sunil et al. [8], four concepts for urban airspace structure were proposed and compared on airspace capacity, safety, and route efficiency metrics. The concepts varied in level of structure in increasing order: unstructured, layers, zones, and tubes. The layered airspace concept, previously investigated in several studies [9, 10, 11], was found to perform best in terms of maintaining a balance between safety and route efficiency.

The layered airspace concept consists of vertically stacked altitude bands (layers) with fixed height equal to the vertical separation minimum between UAVs. Each layer only allows flight in a certain heading range. This range differs per layer, such that aircraft on the same altitude all fly in approximately the same direction. By separating traffic this way, the overall conflict rate can be reduced [12].

The present study assumes a layered airspace concept. Analysis throughout this paper is performed in the horizontal plane inside one layer, ignoring the vertical dimension.

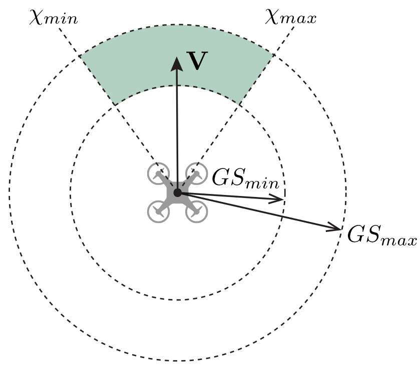

Fig. 1. Illustrating the set of allowed velocity vectors constrained by the minimum and maximum geovector ground speed (GS) and course (χ) limits in the horizontal plane.

III. CONFLICT DETECTION AND RESOLUTION

In order to prevent collisions, a safe zone is defined around each UAV which should not be entered by other UAVs. This so called Protected Zone (PZ) is shaped like a disc with radius equal to the horizontal separation minimum (S_h). An intrusion occurs when a UAV passes through the PZ of another UAV. A conflict is a predicted intrusion which will happen within a certain lookahead time.

The process of Conflict Detection and Resolution (CD&R) is aimed at detecting conflicts and performing a maneuver to maintain a safe separation distance. A wide variety of methods has been developed for this purpose, summarized by Ribeiro et al. [13]. The present study is aimed at decentralized separation methods, each UAV will perform CD&R without involvement of centralized air traffic control. The process consists of three major steps: detection, resolution, and recovery.

A. Detection: State-Based Trajectory Propagation

Conflicts are found by predicting the future trajectory of UAVs and checking whether the separation minima will be violated. Trajectory propagation can either be intent-based or state-based [13]. The former relies on comparing the actual flight plans of UAVs. While this method can prevent false conflict warnings due to planned turns or altitude changes, it requires constantly sharing the intented trajectory with other traffic. The latter, state-based trajectory propagation, only relies on the current state of UAVs (position and velocity). Linear extrapolation of state-information up to the lookahead time provides linear predicted flight paths for all UAVs. If the flight path of the UAV will cross the boundary of the PZ of another UAV within the lookahead time, a conflict warning is issued. The present study assumes state-based trajectory propagation, as this method only requires sharing current position and velocity using a broadcast system such as ADS-B.

B. Resolution: Modified Voltage Potential

In order to resolve a conflict before an intrusion occurs, an avoidance maneuver is performed. A commonly applied method for decentralized separation is the Modified Voltage Potential (MVP) designed by Hoekstra et al. [14]. Using MVP, a velocity vector change for conflict resolution can be computed based solely on the geometry of the conflict.

Figure 2 illustrates the conflict geometry used by MVP. The UAV performing CD&R is referred to as the *ownship*, the other UAV is called the *intruder*. The PZ of the intruder is represented by a circle with radius equal to the horizontal separation minimum S_h. As indicated in Equation 2, subtracting the intruder velocity vector ($\mathbf{V}_{int}$) from the ownship velocity vector ($\mathbf{V}_{own}$) provides the velocity of the ownship relative to the intruder ($\mathbf{V}_{rel}$).

$$\mathbf{V}_{rel} = \mathbf{V}_{own} - \mathbf{V}_{int} \tag{2}$$

A conflict exists because the distance between the UAVs at the closest point of approach (CPA) is smaller than the horizontal separation minimum. In order to resolve the conflict, the relative velocity should be changed such that it does not cross the PZ of the intruder. This change in velocity ($\Delta\mathbf{V}_{\texttt{MVP}}$) is computed by dividing the predicted amount of intrusion at the CPA (I_h) by the time left until the CPA is reached (t_{CPA}), refer to Equation 3. I_h slightly exceeds the edge of the PZ in order to make sure the new relative velocity vector does not cross the PZ of the intruder. This is illustrated by the enlarged portion in Figure 2. $\Delta\mathbf{V}_{\texttt{MVP}}$ is always orthogonal to $\mathbf{V}_{rel}$. Schaberg et al. [15] showed that applying the velocity change in this direction results in the smallest possible path deviation for a conflict.

$$\Delta\mathbf{V}_{\texttt{MVP}} = \frac{I_h}{t_{CPA}} \tag{3}$$

The conflict free relative velocity which is a solution for the conflict ($\mathbf{V}_{rel,sol}$) is obtained by adding the required change in velocity ($\Delta\mathbf{V}_{\texttt{MVP}}$) to the current relative velocity ($\mathbf{V}_{rel}$):

$$\mathbf{V}_{rel,sol} = \mathbf{V}_{rel} + \Delta\mathbf{V}_{\texttt{MVP}} \tag{4}$$

MVP ensures the solution is implicitly coordinated by always using the "shortest way out" of the intruder PZ. Since the conflict geometry is rotationally symmetric, the velocity change computed from the intruder perspective points in exactly the opposite direction ($-\Delta\mathbf{V}_{\texttt{MVP}}$).

In case multiple conflicts exist at the same time, a separate velocity change is computed for each intruder. As indicated by Equation 5, the solution velocity for the ownship is found by adding the sum of the separate solutions for all n conflicts to the current ownship velocity.

$$\mathbf{V}_{own,sol} = \mathbf{V}_{own} + \sum_{i=1}^{n} \Delta\mathbf{V}_{\texttt{MVP},i} \tag{5}$$

C. Recovery: Two-Criteria Method

The solution velocity for a conflict ($\mathbf{V}_{own,sol}$) needs to be maintained until the UAVs have actually passed each other. With MVP, recovery to the intended velocity is normally started when the CPA has been reached. CPA recovery, however, can lead to problems depending on the convergence angle between two aircraft. As shown by Schaberg et al. [15], repetitive conflicts between aircraft can occur as the CPA does not ensure conflict-free recovery for a solution velocity grazing the intruder PZ. Furthermore, repetitive conflicts are more likely to occur when relative velocities between aircraft are small, such as in shallow-angle conflicts. Since geovector rules aim to reduce the relative velocity between aircraft, CPA recovery can lead to significant problems in geovector airspace. Therefore, the present study employs the two-criteria method designed by Schaberg et al. to overcome this problem. A Free To Revert (FTR) point is determined where it is safe to start recovery. It was shown that two-criteria recovery significantly reduces conflict count compared to CPA recovery, especially for shallow-angle conflicts.

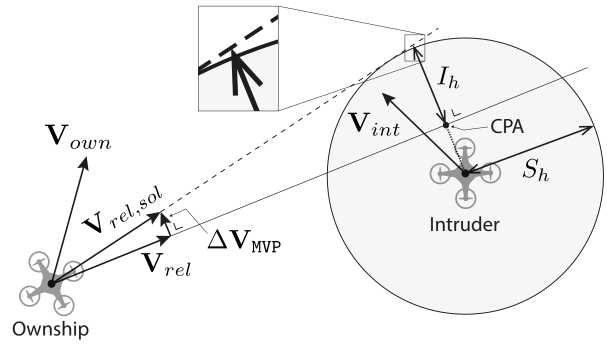

Fig. 2. Illustration of conflict geometry using the Modified Voltage Potential (not to scale)

As the name suggests, two criteria should be met before the ownship can start recovery. Reverting to the intended velocity of the ownship should not result in a new conflict with the intruder, given that:

1. the intruder maintains its current velocity
2. the intruder also reverts back to its intended velocity

Note that, since the intended velocity of the intruder is unknown, the initial velocity of the intruder at the start of the conflict is used as a best guess. This data needs to be stored internally by the ownship at the start of the conflict.

IV. CONFLICT RESOLUTION WITH GEOVECTOR CONSTRAINTS

Both the geovectoring protocol and self separation methods are proposed procedures for the U3 services of U-Space. Previous research on geovectors used the MVP method to resolve conflicts in geovector areas. However, the direction and magnitude of the velocity change vector dictated by MVP is solely determined by the geometry of the conflict. It is not ensured that geovector limits are respected in the process of conflict resolution. This chapter describes an alternative resolution method, which aims to solve a conflict within the constraints imposed by the geovector limits.

A. Visualizing Conflicting Velocities Using the Velocity Obstacle

A useful tool to visualize the set of solution velocities for a conflict is the Velocity Obstacle (VO) [16] [17]. A VO represents the set of ownship velocities yielding a conflict with the intruder. Any velocity vector outside the VO would resolve the conflict, assuming the velocity change would be instantaneous and the intruder does nothing.

Ellerbroek [18] describes how the VO can be derived, as explained hereafter. Consider the example conflict in Figure 3. As shown in Equation 6, the unit vector pointing from the ownship to the intruder ($\mathbf{n}_d$) is computed by dividing the relative distance vector from ownship to intruder ($\mathbf{d}$) by the magnitude of the distance (d). The relative distance vector is obtained by subtracting the absolute ownship position vector

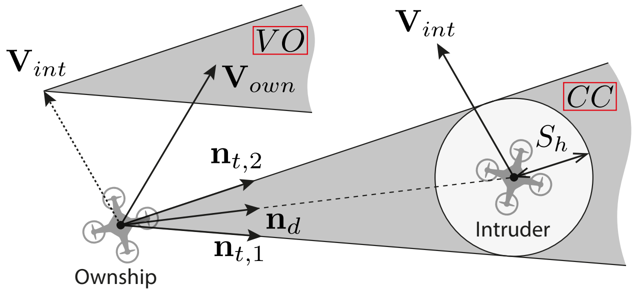

Fig. 3. Example of the construction of a Collision Cone (CC) and Velocity Obstacle (VO) from the ownship perspective in an arbitrary conflict (not to scale)

($\mathbf{x}_{own}$) from the absolute intruder position vector ($\mathbf{x}_{int}$).

$$\mathbf{n}_d = \frac{\mathbf{d}}{d} = \frac{\mathbf{x}_{int} - \mathbf{x}_{own}}{||\mathbf{x}_{int} - \mathbf{x}_{own}||} \tag{6}$$

The Collision Cone (CC), shown in grey in figure Figure 3, indicates the set of *relative* velocities which are not conflict free. The edges or "legs" of the CC can be described using two tangent unit vectors: $\mathbf{n}_{t,1}$ and $\mathbf{n}_{t,2}$. These are found by rotating $\mathbf{n}_d$ using rotation matrix R, where R^T represents the transpose of the matrix (refer to Equation 7). The amount of rotation is dictated by the horizontal separation minimum S_h and the distance d to the intruder (Equation 8). Translating the CC along the intruder velocity vector results in the VO, also shown in grey in Figure 3. The VO indicates all *absolute* ownship velocities yielding a conflict.

$$\begin{aligned} \mathbf{n}_{t,1} &= R\mathbf{n}_d \\ \mathbf{n}_{t,2} &= R^T\mathbf{n}_d \end{aligned} \tag{7}$$

$$R = \begin{bmatrix} \sqrt{1-\left(\frac{S_h}{d}\right)^2} & \frac{S_h}{d} \\ -\frac{S_h}{d} & \sqrt{1-\left(\frac{S_h}{d}\right)^2} \end{bmatrix} \tag{8}$$

B. Conflict Resolution Constrained by Geovector Limits

The VO can be combined with the representation of geovector constraints in velocity vector vector space, which was previously illustrated in Figure 1. In Figure 4, an arbitrary conflict is depicted from the perspective of the ownship. The set of velocity vectors allowed by the geovector is shown in green, a VO is constructed in grey. In order to solve the conflict, the ownship should apply a velocity change such that its velocity vector $\mathbf{V}_{own}$ is pushed outside the VO. As illustrated in the figure, the velocity change computed using MVP ($\Delta\mathbf{V}_{\texttt{MVP}}$), which is orthogonal to the relative velocity, pushes $\mathbf{V}_{own}$ beyond the maximum GS limit of the geovector.

Nevertheless, a subset of the allowed geovector velocities is conflict-free for the example conflict. This subset is denoted by *SOL*, shown in dark green. In order to ensure implicit coordination, no resolution maneuvers should cross the span of the unit vector $\mathbf{n}_d$, as they would not end up at the closest leg of the VO. Denoting this set of uncoordinated velocity vectors as U and the set of allowed geovector velocities as G, the conflict solution space within the geovector limits is defined as the difference between the set of geovector velocities and the union of conflicting velocities and uncoordinated velocities:

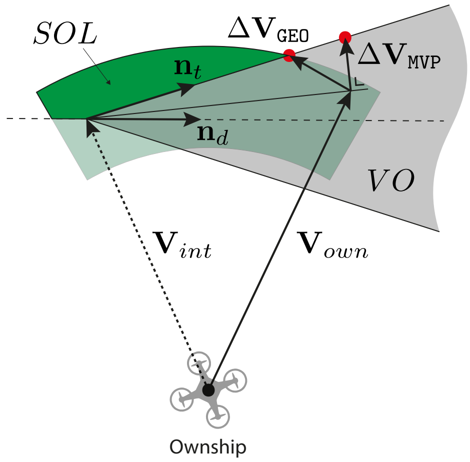

Fig. 4. Illustration of the set of coordinated conflict solutions for the ownship within the geovector limits, denoted by *SOL* in dark green. In this example, the MVP maneuver will lead to a violation of the geovector limits. An alternative conflict resolution maneuver can be defined within the geovector limits, denoted as "GEO".

$$SOL = G \setminus (VO \cup U) \tag{9}$$

In case the solution set defined in Equation 9 is not empty, as seen in Figure 4, an alternative conflict resolution maneuver can be defined within the geovector limits. Let this geovector maneuver be denoted by "GEO". In order to prevent over-solving the conflict, the alternative maneuver GEO is chosen such that the ownship velocity vector ends up at the coordinated leg of the VO. Let $\mathbf{n}_t$ be the unit vector describing the coordinated leg of the VO. Any coordinated solution for the ownship ($\mathbf{V}_{own,sol}$) can be expressed as the sum of the intruder velocity and $\mathbf{n}_t$ times a positive scalar c, where c represents the magnitude of the relative velocity after resolution ($||\mathbf{V}_{rel,sol}||$):

$$\mathbf{V}_{own,sol} = \mathbf{V}_{int} + c\mathbf{n}_t \tag{10}$$

In order to find the most optimal value for the scalar factor c inside the solution space *SOL*, a comparison is made with the MVP maneuver. Let the value of the scalar factor c corresponding to the MVP maneuver be denoted by $c_{\texttt{MVP}}$. As previously mentioned, the MVP maneuver results in the smallest possible path deviation for a conflict. Therefore, the alternative resolution maneuver GEO is chosen such that the difference along the leg of the VO with the resolution vector for MVP is minimized ($||c_{\texttt{MVP}} - c_{\texttt{GEO}}||$). Applying this logic for the example conflict displayed in Figure 4, the solution for the ownship velocity vector using the GEO maneuver is found at the intersection between the leg of the VO and the maximum ground speed limit, as shown in the figure. Note that, in case the MVP maneuver does not lead to a violation of any geovector limit in the first place, the GEO maneuver simply coincides with the MVP maneuver.

It is possible that the ownship is already violating a limit at the start of the conflict, for example if it just entered the geovector sector. In this case, it is possible that the closest velocity vector inside the geovector limits with respect to $\mathbf{V}_{own}$ corresponds to a coordinated solution for the conflict, while

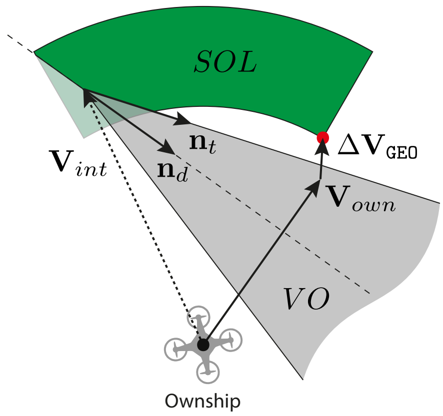

Fig. 5. Example conflict where the closest point inside the geovector limits corresponds to a coordinated conflict solution.

this solution does not lie on the leg of the VO. This situation is illustrated in Figure 5. Let the closest point inside the goevector limits be denoted by $\mathbf{V}'_{own}$. This velocity vector, by definition, always corresponds to a smaller state-change than the intersection on the leg of the VO (except if they are exactly the same). Furthermore, $\mathbf{V}'_{own}$ corresponds to what the UAV would do in case no conflicts were present at all, assuming $\mathbf{V}_{own}$ corresponds to the current autopilot setting (clipping the ownship velocity to the geovector limits). The present study therefore assumes that, in this case, the solution dictated by the GEO maneuver corresponds to $\mathbf{V}'_{own}$.

C. Threshold for Relative Velocity after Resolution

If the GEO maneuver does not correspond to $\mathbf{V}'_{own}$, the solution lies on the coordinated leg of the VO. The location of the GEO solution on the coordinated leg of the VO depends both on the geometry of the conflict and on the geovector limits. Consider the example conflict depicted in Figure 6. The intersection between the coordinated leg of the VO and the solution space *SOL* lies significantly closer to the tip of the VO than the MVP solution. Solutions close to the tip of the VO can yield a significant reduction in relative velocity. Although this behaviour is in line with the objective of the geovector, it can yield undesired behaviour. In case the intruder would also perform a maneuver to a solution close to the tip of the VO, the UAVs could start diverging instantly and would not be able to pass each other. On the other hand, choosing a solution far away from the tip of the VO leads to a significant increase in relative velocity, which is not in line with the objective of the geovector as well.

In order to prevent these negative effects, thresholds are installed indicating the minimum and maximum allowed magnitude of relative velocity after performing the conflict resolution maneuver ($\mathbf{V}_{rel,sol}$). A comparison is made with the MVP maneuver, which is the baseline solution for each pairwise conflict. Thresholds are set at 50% and 150% of the magnitude of the relative velocity after the MVP maneuver would be performed ($c_{\texttt{MVP}}$). If the GEO solution exceeds one of the thresholds, the maneuver is rejected:

$$\text{Strategy} = \begin{cases} \text{Accept}, & \text{if } \frac{1}{2}c_{\texttt{MVP}} \leq c_{\texttt{GEO}} \leq \frac{3}{2}c_{\texttt{MVP}} \\ \texttt{Reject}, & \text{otherwise} \end{cases}$$

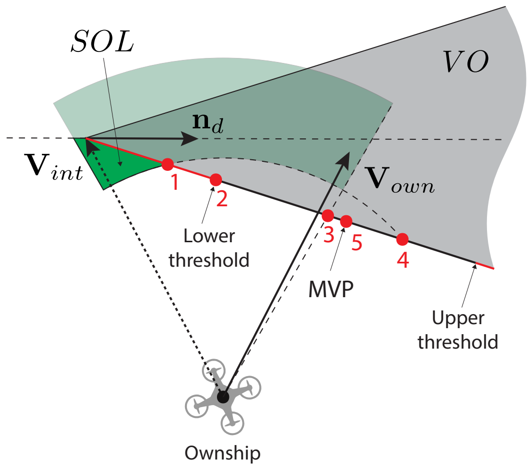

Fig. 6. Categorization of intermediate resolution maneuvers to mitigate the negative effects of very large state changes to satisfy all geovector limits

TABLE I

Geovector resolution strategies used when the solution satisfying all limits exceeds the lower or upper threshold

Label	Strategy	Description
1	ALL	Satisfy all limits (ignore thresholds)
2	LIM	Clip to the thresholds
3	CRS	Ignore ground speed limits (MVP if no alternative)
4	GS	Ignore course limits (MVP if no alternative)
5	NONE	Ignore all limits (= MVP)

It should be noted that the present study assumes uncooperative conflict resolution: the ownship always assumes that the intruder will do nothing. Furthermore, no thresholds are used in case the GEO maneuver corresponds to the closest point in the geovector limits ($\mathbf{V}'_{own}$), reasoning that the UAV would also perform this maneuver if no conflict were present. The GEO maneuver is always accepted in this case.

The effects of setting a threshold on the solution space are visualized in Figure 6. The available solution space on the coordinated leg of the VO is constrained to a subset of velocities on the leg of the VO, bound by the points designated as "lower threshold" and "upper threshold". The parts of the leg where solutions exceed the threshold are colored red. As can be seen in the figure, the solution which satisfies all limits (1) exceeds the lower threshold.

D. Alternative Resolution Strategies

Once the GEO maneuver satisfying all limits gets rejected, multiple alternative maneuvers can be executed. Five resolution strategies are identified in the present study, summarized in Table I. The corresponding maneuvers are indicated for the example conflict in Figure 6.

Using the *ALL* strategy, the ownship will still pick the solution satisfying all limits (1), even though it exceeds the threshold. For *LIM*, *CRS*, and *GS*, one or multiple limits are ignored. The former clips the solution to the threshold (2) such that it is not exceeded. Using *CRS*, the geovector constraints on the solution space are relaxed by ignoring the ground speed

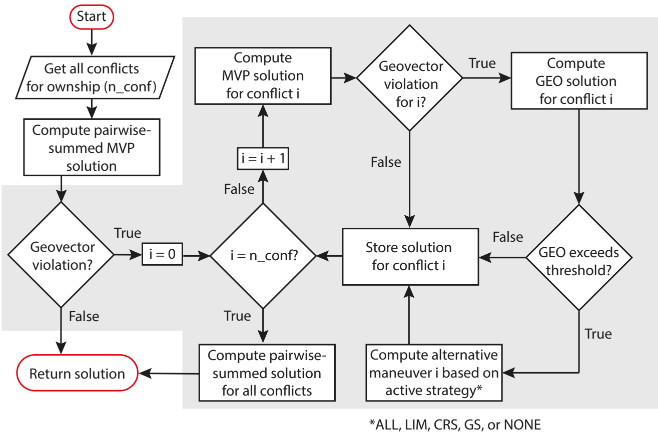

Fig. 7. Conflict resolution ruleset integrating alternative maneuvers in the process of MVP. The additional ruleset taking into account the geovector limits is covered in grey.

limits (3). The opposite is done for *GS*, where course limits are ignored (4). Note that for both *CRS* and *GS*, it is not ensured that an alternative maneuver exists within the threshold. If not, the resolution strategy will default to the MVP maneuver. Finally, using *NONE*, all limits are ignored and the ownship will simply pick the MVP maneuver (5).

Finally, in case the available solution space within the geovector limits is empty, all geovector resolution strategies listed in Table I will default to the MVP maneuver for the pairwise conflict under consideration.

E. Total Resolution Ruleset

Using the GEO maneuver is only necessary when the MVP maneuver leads to a violation of the geovector rules. This also holds when the ownship is in conflict with multiple intruders at once. MVP finds one overall solution by summing the resolution vector for each separate intruder (conflict pair). Therefore, it is possible that the final solution does not violate any limit while the solutions for the individual conflict pairs do. In this case, the MVP solution can be accepted for every conflict.

Figure 7 indicates the conflict resolution process performed by each UAV. The grey area represents the extra ruleset proposed in the present study. First of all, all conflicts for the ownship (conflict count = `n_conf`) are returned by the conflict detection algorithm. Using only MVP, one solution is found for all conflicts by summing the resolution vectors for each conflict pair. Subsequently, it is checked whether this pairwise-summed solution will lead to a violation of the geovector limits. If not, the solution can be returned. Otherwise, the algorithm will consider each conflict separately.

For each conflict, it is checked whether the MVP solution corresponding to that conflict pair will lead to a violation of the geovector limits. If it does not, the MVP solution will be stored for this conflict. Otherwise, the GEO maneuver is computed, satisfying all limits. It is checked whether this maneuver exceeds the threshold. If so, an alternative maneuver is determined based on the strategy that is applied (refer to Table I). The alternative maneuver is stored for the current conflict. After all conflicts have been considered, one solution is found by summing the separate resolution vectors for all conflict pairs (identical to the baseline MVP method, refer to Equation 5).

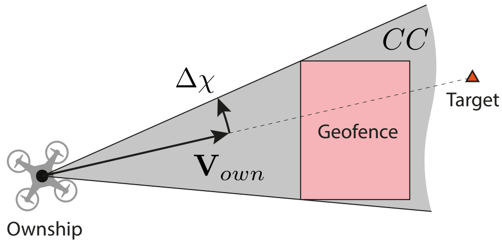

Fig. 8. Applying a course change to avoid a geofence.

F. Geofence Avoidance and Hierarchy

UAV airspace can contain static obstacles in the form of geofences. An avoidance method can be used based on the collision cone approach proposed by Chakravarthy et al. (1998) [19]. Assuming a geofence in the shape of a polygon, a CC can be constructed around the outermost vertices of the shape. Subsequently, a course change is applied to the edge of the CC, which corresponds to the closest difference between target course and avoidance course. This process is illustrated in Figure 8. Once the ownship has reached the corresponding vertex, it reverts back to its target course.

The geofence avoidance algorithm, conflict resolution algorithm, and autopilot (route following within the geovector limits) all provide different steering directions for the UAV. In the present study, it is assumed that geofence avoidance takes precedence over avoiding other UAVs. Therefore, the following hierarchy is used in decreasing order:

1. **Geofence avoidance:** avoid forbidden flight areas
2. **Conflict resolution:** avoid other UAVs
3. **Autopilot:** satisfy geovector limits
4. **Autopilot:** fly to next waypoint

While performing a geofence avoidance maneuver, the UAV ignores all conflicts with other UAVs and the autopilot directions. Furthermore, the autopilot directions are also ignored while performing a conflict resolution maneuver to avoid another UAV. If no conflicts exist with geofences or other UAVs, the geovector rules are prioritized over the directions to the next waypoint.

V. EXPERIMENT DESIGN

This chapter provides a description of the design of the experiments, used to verify the effectiveness of the proposed conflict resolution ruleset in geovector airspace.

A. Simulation Platform

Simulations are performed in the open-source Air Traffic Management Simulator "BlueSky". The "OpenAP" library is used for aircraft performance models [20]. The autopilot model for the UAVs has been updated to include geovector constraints and an area avoidance functionality. Furthermore, the proposed resolution ruleset has been implemented as separate plugin. More information on BlueSky can be found in [6].

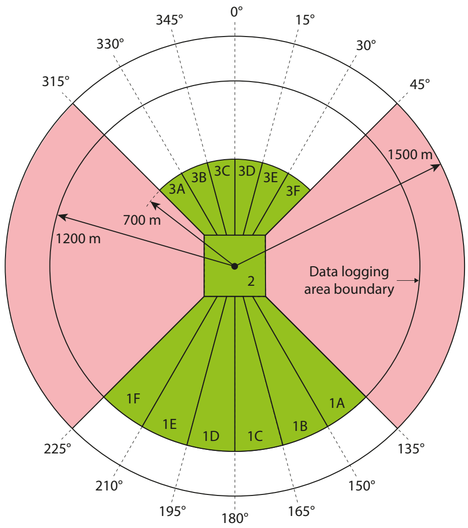

Fig. 9. Layout of the airspace, showing geofences in red and geovector sectors in green.

B. Airspace Design

In order to create a significant number of conflicts, a corridor airspace is used, similar to the design used by Jacobse et al. (2020) [5]. The layout of this corridor is shown in Figure 9. The experiment area is shaped like a circle with a radius of 1500 m, centered on coordinate with latitude 0°N and longitude 0°E. Two geofences, shown in red in the figure, are implemented in order to create an airspace corridor through the center of the experiment area. The width and length of the corridor are set at 400 m.

The area where the experiment data is collected is also shaped like a circle, but has a radius of 1200 m. The margin between the experiment area boundary and the data logging area boundary is implemented in order to account for instantaneous conflicts when the UAVs are spawned.

The airspace is subdivided into several geovector sectors. This sector division is shown in Figure 9. Sector 1 and 3 correspond to the converging and diverging parts of the airspace, respectively. Sector 1 extends from the corridor entry up to the boundary of the data logging area, sector 3 from the corridor exit up to the circle with radius 700 m. They are subdivided into parts A-F. Sector boundaries are defined by the bearing from the center of the experiment area relative to the true north, as indicated in the figure. Sector 2 represents the corridor section at the center of the airspace.

C. Flight Route Assignment

Figure 10 shows the airspace layout relevant for route assignment. The flight direction for all UAVs is from south to north, throuh the corridor section. UAVs are spawned randomly (with a uniform probability distribution) on the spawn arc at the south of the experiment area. They get assigned a random destination (with a uniform probability distribution) on the destination arc, north of the experiment area. The radius of the desination arc is set at 3000 m, in order to prevent excessive headings close to the destination arc to reach the destination waypoint [5]. UAVs are automatically deleted when exiting the experiment area. A small margin of 3° is used to prevent flight routes from lying too close to the geofence boundaries.

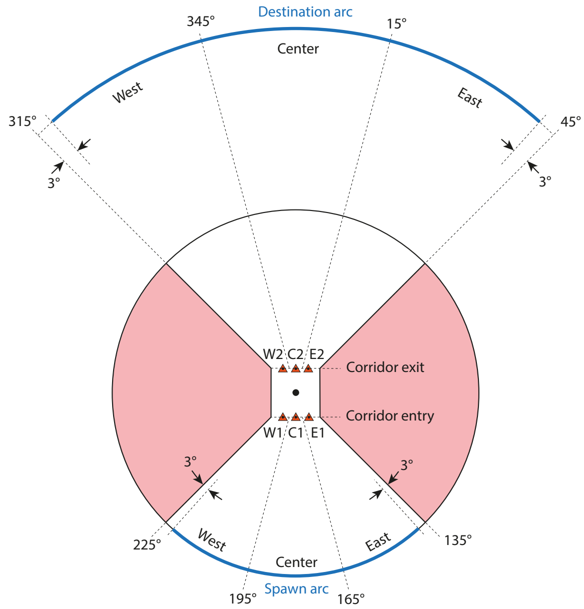

Fig. 10. Layout of spawn and destination sectors and the waypoints implemented at the corridor entry and exit.

In order to prevent flight routes from crossing the geofences, three sets of intermediate waypoints are defined at the corridor entry and exit: west (W1, W2), center (C1, C2), and east (E1, E2). The waypoints are spaced 100 m in the easterly direction, such that the 400 m wide corridor entry and exit are divided into four equal parts. Waypoints in the same set lie on the same meridian.

A different corridor waypoint set is allocated depending on the bearing from the center of the experiment area to the spawn and destination waypoints, relative to the true north. Three sectors with a central angle of 30° are defined on both the spawn arc and the destination arc: West, Center, and East. The bearings corresponding to the sector edges are indicated in Figure 10. Each UAV selects either the set corresponding to the spawn sector or the set corresponding to the destination sector (both with a probability of 50%). For example, a UAV spawning in sector West with a destination in sector East can either cross the corridor via waypoints W1 and W2 or via waypoints E1 and E2. A UAV having the same spawn and destination sector will always cross the corridor using the waypoints corresponding to that sector.

Finally, it is possible that conflict resolution maneuvers or geovectors prevent a UAV from reaching its assigned waypoint. In order to prevent UAVs from flying back south in the airspace, a waypoint is considered to be reached when the latitude of the UAV position is equal to or north of the latitude of the waypoint, irrespective of its longitude.

D. Control Variables

Control variables are listed in Table II. Conflict detection and resolution is performed with a lookahead time of 10 s and a horizontal separation minimum of 25 m [21]. The lookahead time for conflicts with geofences is also set at 10 s. Furthermore all UAVs are spawned at an altitude of 100 ft and are not allowed to change this altitude. The speed setting of the autopilot is chosen randomly on an interval between 7 and 13 m/s (with a uniform probability distribution). The traffic

TABLE II
Control variables

Variable	Setting	Unit
Conflict detection lookahead time	10	s
Horizontal separation margin	25	m
Geofence avoidance lookahead time	10	s
Flight altitude	100	ft
Autopilot speed	[7,13]	m/s
Traffic spawn rate	720	UAVs/h
Corridor width	400	m
Corridor length	400	m

spawn rate is set at 720 UAVs/h, in order to simulate high traffic density airspace. This results in an average of 1 UAV entering the corridor section on one of the three waypoints every 5 seconds.

Finally, one type of UAV is used in the experiments, which is the DJI Matrice 600. Characteristics of this UAV taken from the OpenAP library are listed in Table III.

TABLE III
Characteristics of the DJI Matrice 600 UAV

Parameter	Value
Reachable airspeeds	[-18, 18] m/s
Number of rotors	6
Maximum take-off weight	15.1 kg
Maximum altitude	2500 m

E. Independent Variables

Two independent variables are used for the experiments: the conflict resolution strategy and geovector settings. All variations of both are shown in Table IV and seperately explained hereafter. The five geovector settings allow comparison of all resolution strategies for varying limits. The seven resolution methods and six geovector settings are combined into 7x5 = 35 combinations. For each combination of independent variables, 50 experiments are performed. Per experiment, data is logged over a period of 1 hour, using 10 minutes build-up time before data logging is started.

TABLE IV
Variations of independent variables

Independent variable	Variations
Resolution method	OFF, pure MVP (baseline), NONE, LIM, CRS, GS, ALL
Geovectors	SEV, EXT-GS, MED, EXT-CRS, WIDE

1) Resolution method: For the resolution method, all geovector resolution strategies listed in Table I are chosen. Furthermore, the pure MVP algorithm is added as baseline scenario. Finally, experiment repetitions are also performed without conflict resolution (OFF). The latter is only used for computation of the dependent measures.

2) Geovector settings: All geovectors used in the experiments are composed of both [min, max] ground speed limits and [min, max] course limits. In order to quantify the available maneuvering space within the geovector limits, the geovector settings are defined as intervals. The interval size equals the difference between the maximum and the minimum limit. The intervals for the ground speed limits are always centered on the average autopilot speed of 10 m/s, as shown in Table V. Three intervals are chosen: narrow (1 m/s), medium (3 m/s), and wide (5 m/s). All geovector sectors use the same minimum and maximum limit per ground speed interval setting.

TABLE V
[min, max] ground speed limits (m/s) in all geovector sectors for varying ground speed interval sizes

Interval	Ground speed limits
1 m/s	[9.5, 10.5]
3 m/s	[8.5, 11.5]
5 m/s	[7.5, 12.5]

Course limits vary between the sectors. In order to make sure a UAV is always allowed to stay within one geovector sector, the course limits implemented in that sector should at least allow flight parallel to its boundaries. Therefore, the minimum course interval using the sector division shown in Figure 9 equals the 15° central angle of sectors A-F. The subdivision of sectors is simplified with increasing course interval. Using an interval of 30° only requires three sectors to make sure UAVs can reach the corridor entry. In case of 45°, only two sectors remain. Table VI shows the minimum and maximum course limits per sector for varying interval sizes. Three intervals are chosen: narrow (15°), medium (30°), and wide (45°).

TABLE VI
[min, max] course limits (°) per sector for varying course intervals sizes

		Course interval		
		15°	**30°**	**45°**
Sector	**1A, 3A**	[315, 330]	[315, 345]	[315, 0]
	1B, 3B	[330, 345]	[315, 345]	[315, 0]
	1C, 3C	[345, 0]	[345, 15]	[315, 0]
	1D, 3D	[0, 15]	345, 15]	[0, 45]
	1E, 3E	[15, 30]	[15, 45]	[0, 45]
	1F, 3F	[30, 45]	[15, 45]	[0, 45]
	2	[352.5, 7.5]	[345, 15]	[337.5, 22.5]

Five different combinations of the ground speed and course intervals are used for the experiments. Four combinations consist of either a narrow or a wide ground speed interval, as well as either a narrow or a wide course interval. A fifth combination is added with both medium ground speed interval and medium course interval, such that data can be compared across geovectors in a variety of ways. The five combinations are as follows:

- **SEV**: GS interval 1 m/s, course interval 15°
- **EXT-GS**: GS interval 1 m/s, course interval 45°
- **MED**: GS interval 3 m/s, course interval 30°
- **EXT-CRS**: GS interval 5 m/s, course interval 15°
- **WIDE**: GS interval 5 m/s, course interval 45°

F. Dependent Measures

Dependent variables used to analyze the behaviour of the resolution methods for varying geovector constraints are split up in three groups: geovector, safety, and airspace stability. These are separately introduced hereafter and summarized in Table VII.

1) Geovector measures: In order to verify whether the proposed geovector resolution strategies are succesful in taking the geovector limits into account during conflict resolution maneuvers, it is measured whether the resolution maneuvers determined by the resolution module stay within the limits. Since all resolution strategies behave the same without geovector limits, only the maneuvers performed inside the geovector sectors are considered. A subdivision is made between ground speed limits and course limits: %manv$_{GS}$ and %manv$_{\chi}$ respectively indicate the percentage of all resolution maneuvers in the airspace which were chosen outside the ground speed limits and course limits. The lower these values, the better the performance of a resolution strategy.

Another measure is added with respect to the resolution maneuvers performed inside the geovector sectors. In order to verify whether the geovectors still allow conflict resolution maneuvers inside the limits in the first place, the percentage of maneuvers for which the available solution space inside the limits was empty is considered as well (%manv$_{\emptyset}$).

The actual ability of a UAV to respect the geovector limits can differ from the ability to take the limits into account when computing a resolution maneuver. Therefore, measures are included to quantify the actual geovector violations which are observed during the experiment. Violations can occur due to conflict resolution maneuvers, but also upon entering a new geovector sector, since it takes time to adapt to the new limits. In order to test the actual contribution of the conflict resolution module, only the time intervals are considered where the conflict resolution module of a UAV was active. Here, it is important to mention that the UAV's resolution module turns on when a conflict is detected and stays active until the free-to-revert (FTR) point is reached. A geovector breach starts when the limit under consideration is violated and the resolution module is active. A breach ends when the violation stops, or when the resolution module switches off.

The cumulative duration of all geovector breaches observed during the data logging period is used to assess the system of UAVs as a whole. One value is determined per experiment repetition. A subdivision is made, such that ground speed and course limits can be separately assessed. $\sum t_{GS}$ and $\sum t_{\chi}$ indicate the cumulative duration of ground speed limit and course limit violations, respectively. Again, performance of a resolution strategy is deemed to be better when values are lower.

Furthermore, the actual deviation from a limit is measured in terms of the average excess from a limit observed over the time interval the breach occurred. Since both minimum and maximum limits can be violated, the absolute value of the deviation is used. Again, a subdivision is made between ground speed and course limits: DEV_{GS} and DEV_{χ} respectively indicate the (absolute) average deviation from ground speed and course limits per geovector breach. It is said that the lower the average deviation, the better a resolution strategy performs.

TABLE VII

Overview of dependent measures

Metric	Type	Description
%manv$_{GS}$	Geovector	Percentage of resolution maneuvers in geovector sectors chosen outside the ground speed limits
%manv$_{\chi}$	Geovector	Percentage of resolution maneuvers in geovector sectors chosen outside the course limits
%manv$_{\emptyset}$	Geovector	Percentage of resolution maneuvers in geovector sectors where no maneuver was possible inside the geovector limits
$\sum t_{GS}$	Geovector	Cumulative duration of all ground speed limit violations
$\sum t_{\chi}$	Geovector	Cumulative duration of all course limit violations
DEV_{GS}	Geovector	(Absolute) average deviation from ground speed limits per geovector breach
DEV_{χ}	Geovector	(Absolute) average deviation from course limits per geovector breach
n_{conf}	Safety	Filtered number of conflicts
n_{intru}	Safety	Number of intrusions
LOS_{sev}	Safety	Intrusion severity
$\%MACC$	Safety	Percentage of (unfiltered) conflict pairs involving multiple UAVs simultaneously
$f_{V_{rel}}$	Safety	Change in magnitude of relative velocity per conflict resolution maneuver
$\|\|\Delta\chi_{CR}\|\|$	Safety	Absolute course change per conflict resolution maneuver
DEP	Stability	Domino Effect Parameter
ρ_{inst}	Stability	Instantaneous airspace density

2) Safety measures: Safety metrics indicate the ability of the resolution module to prevent collisions between UAVs. First of all, the number of conflicts (n_{conf}) indicates how often protected zone intrusions were predicted to occur within the conflict detection lookahead time. The lower the observed number of conflicts, the better a resolution strategy performs on this measure.

A filter is applied on the number of conflicts to account for noise in the data coming from repetitive conflicts (refer to Section III.). If a conflict between a unique UAV pair re-occurs within 15 seconds, the conflict is not counted again. Two exceptions are added: both UAVs should not have encountered a conflict with another UAV in the meantime (secondary conflicts should be counted), and both UAVs should not have entered a different geovector sector since the first conflict was resolved. More information on the conflict count filter can be found in Appendix A.

Two other metrics that give an indication about safety are the number of intrusions (n_{intru}) and the severity per intrusion (LOS_{sev}). The latter is defined as difference between the required separation margin (S_h) and the actual closest distance of approach (d_{CPA}), expressed as percentage of the separation margin [13] (refer to Equation 11). For both these measures, a resolution strategy is said to show an increase in performance when the measured values decrease.

$$LOS_{sev} = \frac{S_h - d_{CPA}}{S_h} \cdot 100 \qquad (11)$$

The performance of the geovector resolution strategies can be affected by multi-aircraft conflicts (MACC), since pairwise-summation of the individual resolution vectors can still lead to a geovector violation. Therefore, the percentage of (unfiltered) conflicts which involved multiple intruders at once (*%MACC*) is included in the list of dependent measures. It should be noted that, in case only one UAV in the conflict pair was in conflict with multiple intruders simultaneously, the conflict is still counted as multi-aircraft conflict.

In an effort to capture the behaviour of the resolution strategies, the change in magnitude of the relative velocity is measured for each conflict. Let the solution relative velocity be denoted as $\mathbf{V}_{rel,sol}$ and the initial relative velocity at the start of the conflict as $\mathbf{V}_{rel}$ (refer to Figure 2). Since the relative velocity after conflict resolution is determined by the combination of maneuvers performed by both UAVs, one value can be computed per unique conflict pair. The change in magnitude is expressed as factor f_{Vrel}:

$$f_{Vrel} = \frac{||\mathbf{V}_{rel,sol}||}{||\mathbf{V}_{rel}||} \tag{12}$$

Finally, it is known that large resolution vectors have a destabilizing effect on the airspace, since a UAV will scan a larger portion of the airspace for new conflicts while performing the maneuver [22]. For the airspace used in the experiments, this especially holds for large course changes, since all UAVs fly at approximately parallel tracks through the corridor. In order to capture the behaviour of the resolution strategies, the absolute course change applied by each UAV per conflict resolution maneuver is logged ($||\Delta\chi_{CR}||$).

3) Stability measures: The stability of the airspace is measured using the Domino Effect Parameter (*DEP*) [23]. This metric gives an indication of the number of secondary conflicts that emerged in the airspace. Let the number of conflicts with conflict resolution on be denoted by n_{conf}^{ON} and without conflict resolution by n_{conf}^{OFF}. For the latter, the unfiltered conflict count is used, since repetitive conflicts do not occur without conflict resolution. The Domino Effect Parameter is computed as shown in Equation 13. Positive values indicate a destabilizing effect of a resolution method, as performing resolution maneuvers triggers secondary conflicts. It is possible that negative values are observed as well, showing a stabilizing effect. In general, a resolution strategy performs better on this measure when values are lower.

$$DEP = \frac{n_{conf}^{ON}}{n_{conf}^{OFF}} - 1 \tag{13}$$

Finally, the number of UAVs flying in the data logging area is measured every 10 seconds. Dividing this figure by the size of the data logging area excluding geofences (0.683 NM^2) yields the instantaneous airspace density (ρ_{inst}). An increase in density indicates a lower traffic flow in the experiment area, which would be deemed a decrease in performance.

G. Hypotheses

Two hypotheses are posed for the experiments. First of all, different from the baseline method (pure MVP), the proposed geovector resolution strategies actively consider the geovector limits in the conflict resolution process. Therefore, it is hypothesized that all these strategies will show improved performance on the geovector measures for all geovectors, compared to pure MVP.

Furthermore, it is known that geovectors can reduce the conflict rate in the airspace [4] [5]. In line with the expected reduction in geovector violations, it is hypothesized that the observed number of conflicts will be lower for the geovector resolution strategies in comparison to pure MVP. After all, the conflict reduction observed from the geovector is expected become more apparent when UAVs are confined to the geovector limits during conflict resolution maneuvers.

VI. RESULTS

This section presents the results of the metrics listed in Table VII. Data is shown in the form of box plots. Statistical tests have been performed to verify differences between resolution strategies. Each data sample for pure MVP was compared to the five other data samples for the geovector resolution strategies corresponding to the same geovector setting. Not all data samples follow a normal distribution, therefore Wilcoxon signed rank-tests [24] and Mann-Whitney U tests [25] were used for the paired and unpaired data samples, respectively. The threshold for rejecting the null-hypothesis of the statistical tests was set to $p \leq 0.05$. Furthermore, a Bonferroni correction [26] was applied to account for the fact that pure MVP is compared to five other resolution strategies. Therefore, differences between data samples are deemed statistically significant when $p \leq 0.01$. All p-values and medians are reported in Appendix C, p-values supporting an observation are also mentioned in the article.

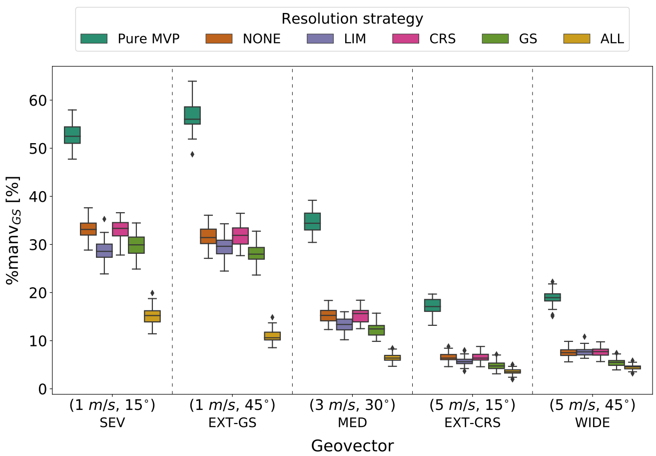

Fig. 11. Percentage of resolution maneuvers chosen outside the ground speed limits (%manv$_{GS}$)

A. Results of geovector measures

The percentage of resolution maneuvers chosen outside the ground speed limits is shown in Figure 11. As can be observed, all geovector resolution strategies show significant improvements compared to pure MVP ($p = 7.557E-10$). Resolution strategy ALL performs best on this measure for all geovectors under consideration. Furthermore, resolution strategies LIM and GS outperform methods NONE and CRS for almost all geovectors. An exception is found for geovector WIDE, where only GS appears to result in a lower percentage of ground speed violations.

Two more observations can be made with respect to the differences across geovectors in Figure 11. Firsly, the percentage of maneuvers chosen outside the ground speed limit decreases for all resolution methods when the size of the ground speed interval is increased (compare geovector SEV to EXT-CRS and EXT-GS to WIDE). Secondly, an observation is made considering pure MVP. When the ground speed interval is kept constant, increasing the interval size of the course limits increases the percentage of maneuvers chosen outside the ground speed limits. This effect is observed for both narrow and wide ground speed limits (compare SEV to EXT-GS and EXT-CRS and WIDE).

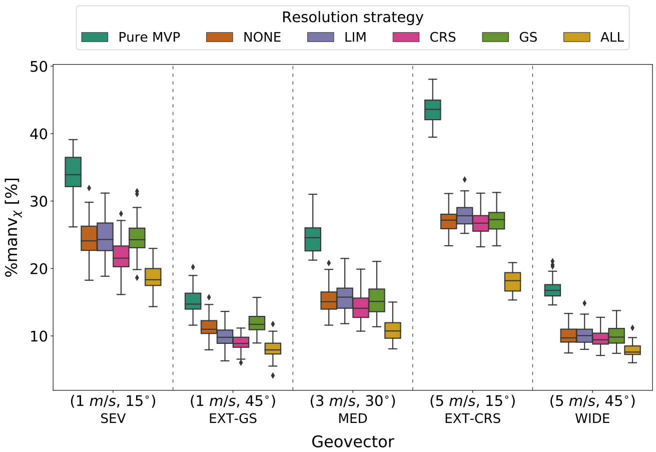

Fig. 12. Percentage of resolution maneuvers chosen outside the course limits ($\%manv_\chi$)

Figure 12 shows the percentage of maneuvers which exceeded the course limits. Again, all geovector resolution strategies show significant improvements compared to pure MVP ($p \leq 8.031E-10$) and resolution strategy ALL shows the best performance overall. Furthermore, it can be observed that resolution strategy CRS resulted in fewer maneuvers exceeding the course limits than NONE, LIM, and GS for geovectors with narrow ground speed interval (SEV and EXT-GS). These differences are less notable when the ground speed interval is increased. Furthermore, LIM appears to perform better than NONE and GS for geovector EXT-GS, while the opposite is observed for geovector EXT-CRS.

Comparing samples across different geovectors, similar trends are observed as in Figure 11 (which considered ground speed limit violations). Firstly, increasing the size of the course limit interval reduces the percentage of maneuvers chosen outside the course limits for all resolution strategies (compare geovector SEV to EXT-GS and EXT-CRS to WIDE). Secondly, the percentage of maneuvers chosen outside the course limits using pure MVP increases when the course limit interval is kept constant while the ground speed interval is increased. This effect is especially notable for narrow course limits (compare SEV to EXT-CRS).

Figure 13 shows the percentage of resolution maneuvers inside the geovector sectors where the available solution space

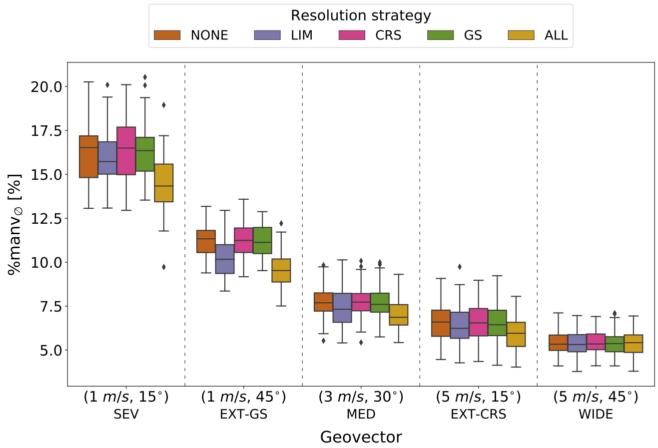

Fig. 13. Percentage of resolution maneuvers for which the available solution space inside the geovector limits was empty ($\%manv_\emptyset$)

inside the geovector limits was empty. Pure MVP is not shown, since this resolution strategy does not take into account the geovector at all. A clear trend can be observed in the figure: the more constraining the combination of limit intervals, the higher the percentage of maneuvers for which the solution space was empty.

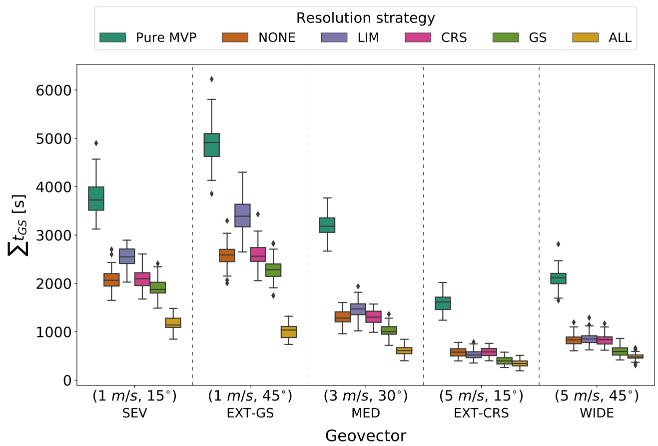

Fig. 14. Cumulative duration of all ground speed limits violations over the hour long data period ($\sum t_{GS}$)

The cumulative duration of all ground speed limit violations observed over the data logging period is shown in Figure 14. Statistical analysis confirms that all geovector resolution strategies show significantly lower values than pure MVP for all geovectors ($p = 7.557E-10$). Furthermore, ALL shows the lowest values for all geovectors, followed by resolution strategy GS. Finally, considering LIM, the observed cumulative conflict duration appears significantly higher than for the other geovector resolution strategies at geovectors with narrow and medium ground speed interval (SEV, EXT-GS, and MED).

Finally, looking at the differences between geovectors, the same two trends are found as in Figure 11. Firstly, the cumulative duration of ground speed violations for all conflict resolution strategies reduces when the size of the ground speed intervals is increased (compare SEV to EXT-CRS and EXT-GS to WIDE). Secondly, keeping the ground speed limit interval size constant but increasing the course limit interval size, an increase in the median can be observed for pure MVP (compare SEV to EXT-GS and EXT-CRS to WIDE).

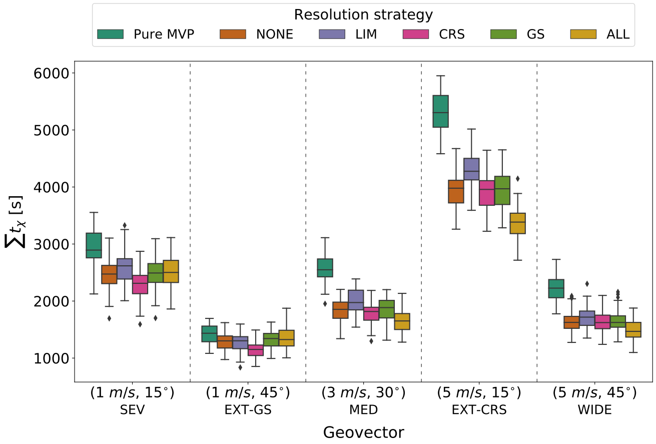

Fig. 15. Cumulative duration of all course limits violations over the hour long data period ($\sum t_\chi$)

Figure 15 shows the cumulative duration of all course limit violations observed over the data logging period. It immediately becomes clear that differences between pure MVP and the geovector resolution strategies are not as pronounced as in Figure 14, especially for the geovectors with narrow ground speed interval size (SEV and EXT-GS). Still, statistical analysis shows that almost all the geovector resolution strategies significantly lower the cumulative duration of course limit violations for all geovectors, compared to pure MVP ($p \leq 4.924E-05$). One exception is found: differences between pure MVP and ALL on geovector EXT-GS could not be proven to be statistically significant.

Comparing all the resolution strategies across the different geovectors, the cumulative duration of course violations is reduced for all resolution methods when the size of the course intervals is increased (compare SEV to EXT-GS and EXT-CRS to WIDE). Furthermore, keeping the course limit interval constant and increasing the ground speed limit interval, an increase can be observed for pure MVP (compare SEV to EXT-CRS and EXT-GS to WIDE).

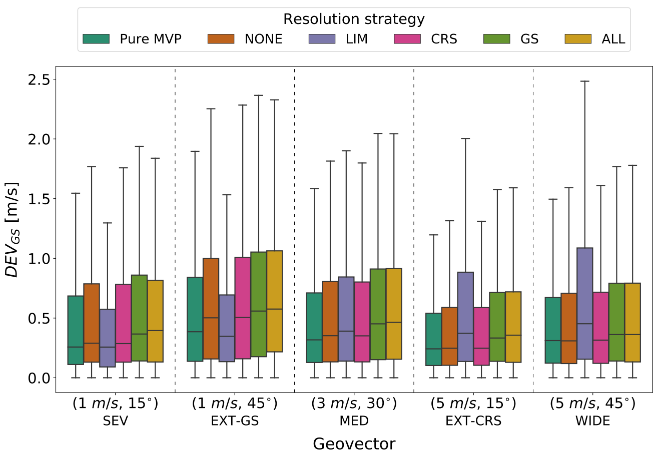

Fig. 16. (Absolute) average deviation from ground speed limits per geovector breach (DEV_{GS}). Outliers are not shown.

Figure 16 shows the average deviation from the ground speed limits sustained by the conflict resolution per geovector breach. Improvements compared to the baseline (pure MVP) are only found for resolution strategy LIM. For geovectors with a narrow ground speed interval (SEV and EXT-GS), using this resolution strategy resulted in a statistically significant smaller average deviation from the ground speed limits ($p \leq 2.723E-05$).

Furthermore, as can be observed in the figure, LIM performed worst of all resolution strategies for the geovectors with wide ground speed interval (EXT-CRS and WIDE). Finally, statistical analysis reveals that all other data samples show a significant increase in deviation from the ground speed limits compared to pure MVP ($p \leq 0.00763$). Two exceptions to the last observation are NONE and CRS for the WIDE geovector, where no differences could be proven.

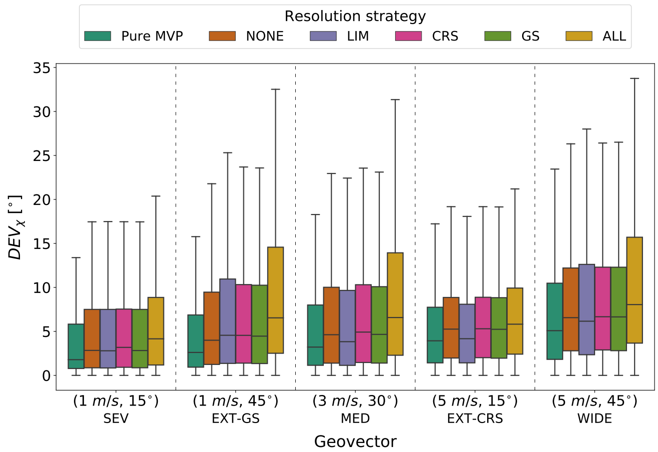

Fig. 17. (Absolute) average deviation from course limits per geovector breach (DEV_χ). Outliers are not shown.

Last of the geovector measures, the average heading deviation from the course limits is shown in Figure 17. First of all, statistical analysis shows that all geovector resolution strategies perform significantly worse than pure MVP ($p \leq 1.806E-08$). Secondly, it can be observed that ALL performs worst of all resolution methods for all geovectors. Finally, the average deviation from the course limits per violation appears to decrease overall when the individual limit interval sizes are reduced.

B. Results of safety measures

Figure 18 shows the (filtered) total number of conflicts observed over the hour long data logging period. First of all, a positive correlation can be observed between the overall conflict count for any resolution method and the size of both ground speed and course intervals. For the combination of airspace layout and geovectors used in the experiments, ground speed limits appear to induce a greater reduction in conflict count than course limits (consider the differences between geovectors EXT-GS, MED, and EXT-CRS).

Considering the resolution methods for each geovector separately, statistical analysis shows a significant increase in number of conflicts for resolution strategy LIM compared to pure MVP on both geovectors with wide ground speed interval (EXT-CRS and WIDE) ($p \leq 0.0017$). Furthermore, resolution

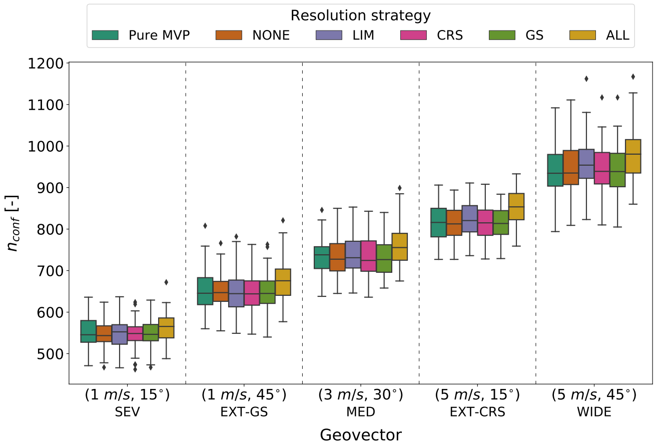

Fig. 18. Number of conflicts (n_{conf}) over the logging period of 1 hour (repetitive conflicts are filtered out)

strategy ALL shows a statistically significant increase in number of conflict for all geovector settings ($p \leq 0.00638$). Other differences could not be proven to be significant.

Figure 19 shows the total number of intrusions observed over the data logging time interval. Statistical analysis shows that resolution strategy LIM induces a significant reduction in number of intrusions compared to pure MVP for geovectors EXT-GS and MED ($p \leq 0.00225$). Furthermore, resolution strategy ALL also shows an increase in performance: a small reduction is observed for geovectors SEV, EXT-GS, and MED with narrow and medium ground speed intervals ($p \leq 9.692E-04$). The other data samples showed no statistically significant differences when compared to pure MVP.

Finally, it should be noted that, since the overall intrusion count is very small, observed differences between methods can be sensitive to small changes in data. One should be careful when drawing conclusions.

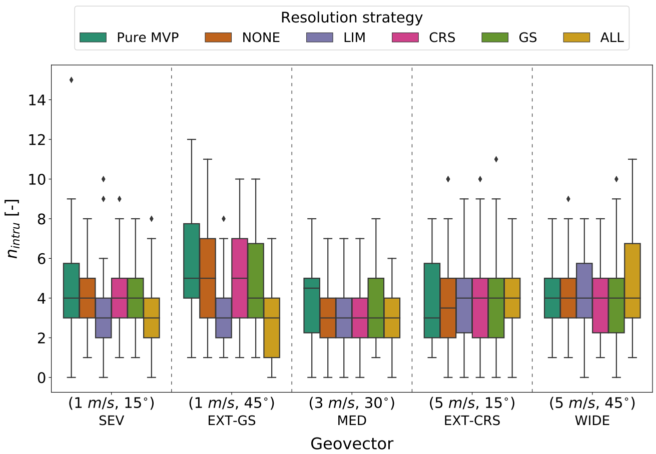

Fig. 19. Number of intrusions ($\mathbf{n}_{intru}$) over the 1 hour data logging period

The intrusion severity is shown in Figure 20. Similar to the trends observed for the number of intrusions, statistical analysis reveals significant differences are only found for resolution strategies LIM and ALL, compared to pure MVP. Intrusion severity is higher for LIM for geovectors EXT-GS and MED ($p \leq 0.00484$). For ALL, intrusion severity is significantly higher for geovectors SEV, EXT-GS, MED, and

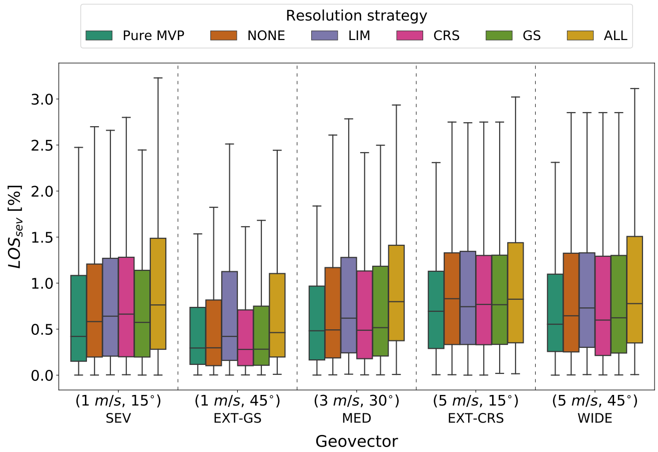

Fig. 20. Intrusion severity (LOS_{sev}) computed for each intrusion. Outliers are not shown.

WIDE ($p \leq 0.00125$).

Furthermore, it can be observed that for all resolution strategies, most values are concentrated around only a few percent. The severity of intrusions of the outliers never exceeded about 20% of the required separation minimum (see Appendix B).

Figure 21 shows the percentage of conflicts where multiple intruders were involved at once. Comparing the geovector resolution strategies to pure MVP, ALL shows a statistically significant increase for geovectors MED, EXT-CRS, and WIDE ($p \leq 6.214E-04$). Furthermore, LIM shows a significant reduction for geovector EXT-GS ($p = 0.00783$). Other differences were not proven to be statistically significant.

Finally, still considering Figure 21, it can be observed that the overall percentage of multi-aircraft conflicts for all methods appears to be positively correlated with the size of the course limit interval size of a geovector.

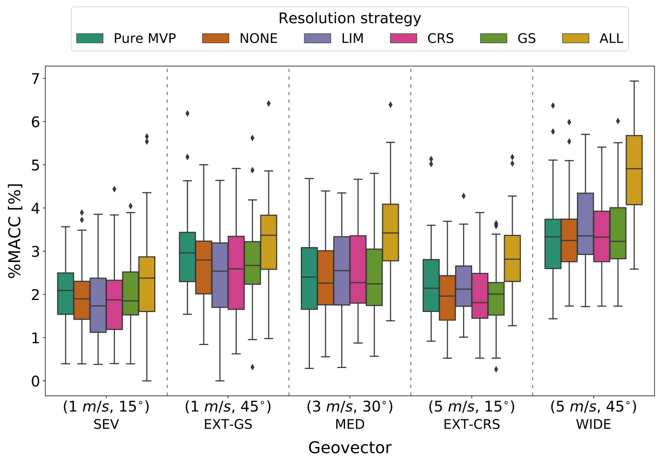

Fig. 21. Percentage of resolution maneuvers involving multiple intruders at once ($\%MACC$)

The change in relative velocity per conflict resolution maneuver is shown in Figure 22. Although the medians of the datasets lie close together, the spread appears to be larger for the geovector resolution strategies than for pure MVP. As can be observed in the figure, resolution strategy ALL shows the highest spread for all geovectors, closely followed by LIM. Differences in spread between NONE, CRS, and GS are hardly visible. Pure MVP shows the smallest spread overall.

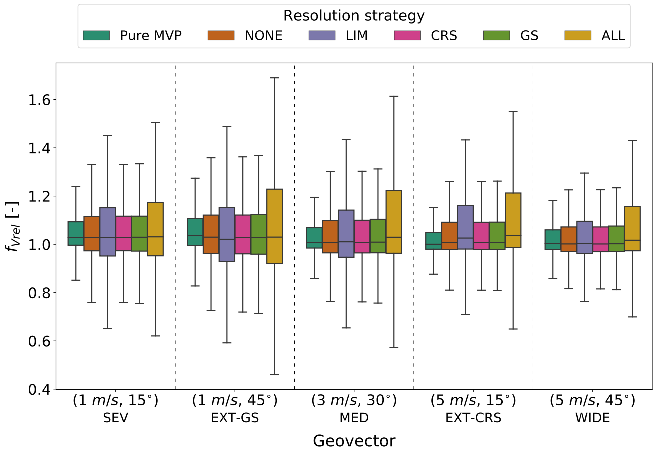

Fig. 22. Change in magnitude of relative velocity per combined conflict resolution maneuver of two UAVs in a unique conflict pair (f_{Vrel}). Outliers are not shown.

Finally, Figure 23 shows the absolute course change applied per conflict resolution maneuver. All geovector resolution strategies show statistically significant differences compared to pure MVP for all geovectors ($p \leq 7.176E-09$). For all geovectors except EXT-CRS, the geovector resolution strategies show an increase in absolute applied course change compared to pure MVP. When considering geovector EXT-CRS, all resolution strategies show a minor but statistically significant decrease in median of applied course change compared to pure MVP ($p \leq 1.917E-25$). Finally, it can be observed that ALL and LIM show a significant increase in median for geovectors with a narrow ground speed interval size (SEV and EXT-GS).

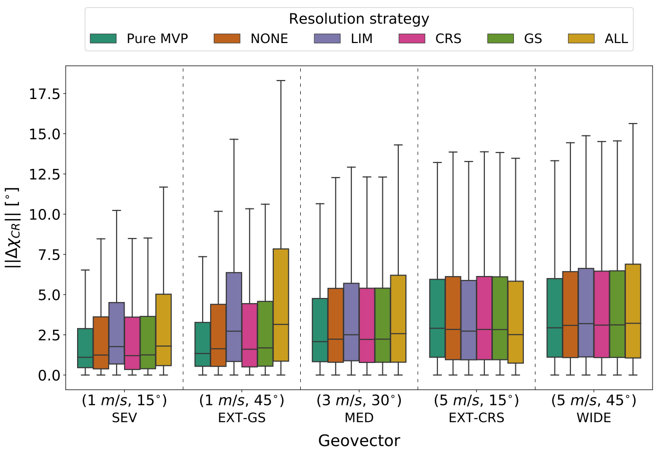

Fig. 23. Absolute course change per resolution maneuver performed by each individual UAV ($||\Delta\chi_{CR}||$). Outliers are not shown.

C. Results of stability measures

The Domino Effect Parameter, shown in Figure 24, is closely tied to the number of conflicts (Figure 18). Considering statistically significant differences, this measure follows a trend similar to the one observed for the number of conflicts (Figure 18): LIM performs worse than pure MVP for geovectors EXT-CRS and WIDE ($p \leq 0.00157$), ALL performs worse on all geovector settings, when compared to pure MVP ($p \leq 0.00603$). The largest differences are observed between pure MVP and ALL, indicating that resolution strategy ALL tends to lead to the largest increase of the Domino Effect Parameter.

Furthermore, it can be observed that the DEP increases slightly both from geovector SEV to EXT-GS and from SEV to EXT-CRS (all strategies), indicating a positive correlation between the DEP and the interval size of both geovector limits.

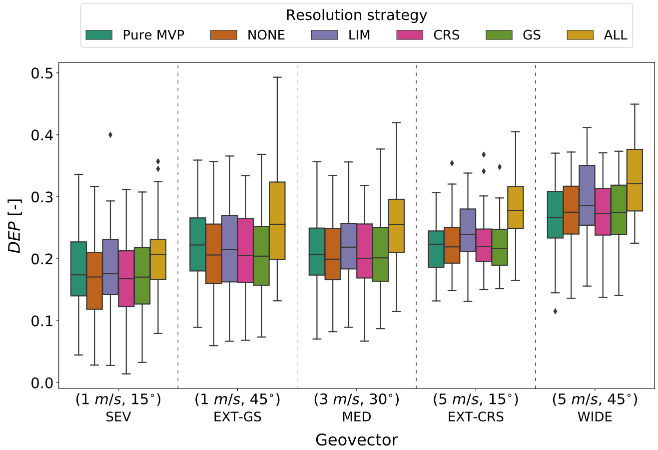

Fig. 24. Domino Effect Parameter (DEP)

Finally, Figure 25 shows the measured instantaneous airspace density every 10 seconds during the data logging period. No statistically significant differences are found when comparing the geovector resolution strategies to pure MVP.

It is further observed that the median of the airspace density stays constant for geovectors SEV, MED, and WIDE (49 UAVs/NM^2). A small shift in the median of the datasets can be observed for geovectors EXT-GS and EXT-CRS, where the former shows a slight reduction (48 UAVs/NM^2) and the latter a slight increase (50 UAVs/NM^2). Furthermore, it can be observed that the spread of all data sets is significant compared to the median, indicating fluctuations in the traffic density. These fluctuations appear to be larger for geovector MED than for the other geovectors.

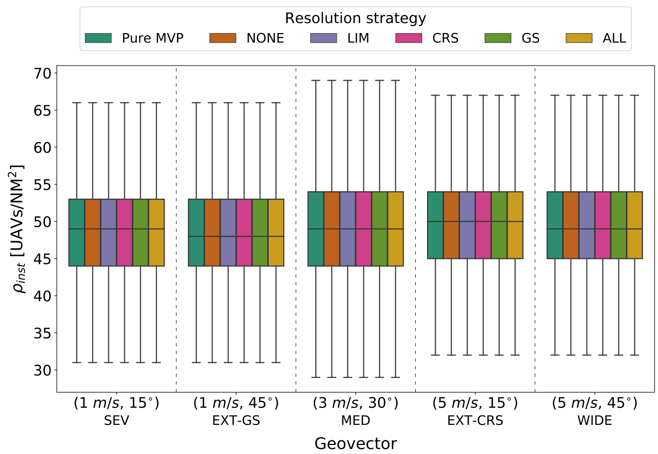

Fig. 25. Instantaneous airspace density (ρ_{inst})

VII. DISCUSSION

The results of the experiments show interesting behaviour, which was not always as expected. In this section, the observations made in the previous Section are further analyzed and used to evaluate the hypotheses.

A. Evaluation of hypotheses

Two hypotheses were posed for the present research. These are separately assessed hereafter.

First of all, it was hypothesized that all geovector resolution strategies show improved performance compared to pure MVP on the geovector measures. Regarding the ability of the UAVs to take into account the geovector limitations while computing a resolution maneuver, the geovector resolution strategies indeed show clear improvements over pure MVP (Figure 11 and Figure 12). This observation also holds when regarding the cumulative duration of all ground speed limit violations (Figure 14). Nonetheless, differences are less pronounced with respect to the cumulative duration of course limit violations (Figure 15). An exception was found for geovector EXT-GS, where differences between pure MVP and ALL were not even found to be statistically significant. Finally, considering the observed average deviation from the limits (Figure 16 and Figure 17), the geovector resolution rulesets appear to violate the limits with larger average deviations. The hypothesis can therefore only be partially accepted: although the system of UAVs generally sustains violations over shorter periods of time, the actual observed deviation appears to be larger.

A remark should be made with respect to the last statement. Although it appears that the geovector resolution strategies lead to an increase in average deviation from a limit, the observed correlation does not necessarily imply causation. Instead of looking at the data which is present in the graph, one could consider the data that is actually missing. It may be that the geovector resolution strategies are successful in preventing geovector violations which would result in only small average deviations, while conflicts resulting in more severe breaches can not be resolved within the limits. In that case, it would indeed appear as if a resolution strategy causes an increase in average deviation, while in fact the observed increase could be merely a result of the way the measure is defined.

The second hypothesis states that the geovector resolution strategies reduce the number of conflicts compared to pure MVP. Considering Figure 18, the effects of the resolution strategy on the number of conflicts appear to be very marginal. The geovector resolution strategies did not result in a lower number of conflicts for any geovector. Considering geovectors with wide ground speed limit interval size, ALL and LIM even showed a statistically significant increase compared to the baseline MVP method. This hypothesis should therefore be rejected.

To prompt discussion on why no reduction in number of conflicts is observed, while the geovector is successfully incorporated in the conflict resolution process, a variety of speculations can be made.

It was observed that, compared to pure MVP, all the geovector resolution strategies tend to increase the absolute course change applied during conflict resolution maneuvers (Figure 23). This effect is especially notable for geovectors with a narrow ground speed interval (SEV and EXT-GS). After all, when the available maneuvering space within the ground speed limits is small, the conflict resolution maneuver should consist of a larger course change to still resolve the conflict within the limits. Larger course changes can yield undesired effects, since a larger portion of the airspace is searched for new conflicts [7]. This could especially be problematic for the type of airspace used in the current research, where all UAVs fly at approximately parallel trajectories towards the center of the experiment area. In turn, it could be expected that the number of secondary conflicts increases when the resolution maneuvers consist of larger course changes.

Furthermore, considering the change in magnitude of the relative velocity due to the conflict resolution maneuvers (Figure 22), a clear trend is observed. All geovector resolution strategies show an increase in spread of data compared to pure MVP. Considering that the MVP maneuver represents the most optimal solution for a given conflict in terms of path deviation [15], it can be said that the UAVs perform less efficient conflict resolution maneuvers in an effort to abide by the geovector rules. Once again, this behaviour could potentially yield more secondary conflicts.

Indeed, a conflict of interests is observed with regards to the objective of the geovector. On the one hand, a greater reduction in closure speed brings about a greater reduction in conflict rate [4]. Nevertheless, once a conflict does emerge, choosing the most optimal solution could potentially be more beneficial in terms of airspace safety and stability measures.

Considering the bigger picture, the reduction in conflict rate caused by the geovector is not reinforced by the geovector resolution strategies for the specific airspace design used in the present study. Nevertheless, the geovector resolution strategies do show improvements regarding the ability to satisfy the geovector limitations in the process of conflict resolution. Furthermore, the observed number of intrusions and corresponding intrusion severity show that the resolution strategies are successful in resolving conflicts. It can therefore be stated that the geovector resolution strategies do achieve their intended goal: resolving conflicts while taking into account the geovector limits.

B. Other observations

A variety of observations were made from the results, these are separately discussed hereafter.

First of all, a few general trends can be observed when comparing the five geovector resolution strategies to each other. ALL outperforms all the other resolution strategies on almost all geovectors measures. Nonetheless, this strategy also tends to show the worst performance on the safety and stability measures. Secondly, data samples for NONE, GS, and CRS often closely resemble each other. This could indicate that, perhaps, for a significant number of conflicts, resolution strategies GS and CRS can not find a maneuver within the thresholds set on the coordinated leg of the Velocity Obstacle (Figure 6). In this case, they will default to the pure MVP maneuver, which equals the solution found by NONE.

Secondly, considering the pure MVP method, the percentage of multi-aircraft conflicts seems to be positively correlated with the size of the course intervals. This could potentially result from the geovector design. Considering the geovector sectors in the converging part of the airspace, UAVs are not allowed to cross through different sectors. As soon as a boundary of a sector is crossed, the geovector in the new sector dictates a flight path parallel to that boundary (consider Figure 9 and Table VI). This way, the geovector sectors actually achieve both a relative velocity reduction and a segmentation effect. While the former reduces the probability that a conflict occurs, the latter reduces the number of conflict pairs by separating traffic [4]. Nevertheless, these are only speculations. Further research is required to verify this kind of behaviour.

Also regarding the subdivision of the airspace into different geovector sectors for the course limits, a failure mode of the resolution strategies comes to light. Although the geovector limits are actively considered during the conflict resolution phase, any limit violation occurring after that time is ignored. If a new geovector sector is entered while the Free to Revert point has not yet been reached, the avoidance maneuver is not reconsidered. As a result of these violations, a discrepancy can be observed between the percentage of conflict resolution maneuvers chosen outside the course limits (Figure 12) and the actually observed cumulative duration of course limit violations (Figure 15).

Furthermore, considering intrusion severity (Figure 20), the majority of measurements is concentrated around only a few percent of the required separation minimum. For no intrusion did the intrusion severity exceed more than 20% of the required separation minimum (Appendix B). UAVs are highly agile, hence responses to an observed intrusion can be quick. One could argue whether the required separation minimum of 25 m is actually unnecessarily high for the airspace under consideration. Indeed, reducing this value could greatly affect the capacity of the airspace.

Finally, regarding the instantaneous airspace density measurements (Figure 25), it was observed that the spread in data is large. This is a direct result of the way in which traffic was spawned: instead of spawning UAVs using a fixed time interval, each UAV was assigned a random spawn time over the entire duration of the simulation, using a uniform probability distribution. This resulted in fluctuations of the actual number of UAVs present in the airspace over the data logging period. Although one could say that these fluctuations might more closely resemble reality, the results of the experiments could become more difficult to interpret.

C. Recommendations

One of the limitations of the current research is the fact that traffic spawn rate was used as a control variable. It is important to gain a better understanding of the effects of traffic spawn rate on the performance of the geovector resolution strategies. Further experiments should be performed for varying traffic densities.

In order to gain better understanding into the effects of the separate geovector limits on the geovector resolution strategies, it is proposed to also perform analysis of airspace involving only ground speed limits or course limits.

Furthermore, although the resolution strategies showed no reduction in conflict rate compared to pure MVP for the airspace design used in the current research, other types of airspace could render different behaviour. After all, the available maneuvering space for a UAV highly depends on the limits that are imposed. It is therefore recommended to further analyze the performance of the proposed geovector resolution rulesets for other types of traffic scenario's.

Although the present study investigated the differences between the geovector resolution strategies on a macroscopic level, not all observed behaviour can be fully understood. It is therefore recommended to further assess each method separately, also focusing on microscopic effects. This could provide useful insights which might help in drawing more definitive conclusions on the topics of discussion from the present paper.

It is also recommended to investigate whether the conflict resolution strategies can be further extended to account for geovector violations occurring during the recovery phase of a conflict. This is especially important for geovector designs with high granularity.

Furthermore, the influence of the geofences on the performance of the resolution strategies has not been extensively tested. Previous research indicates that the geofence avoidance method employed in the current study is not always successful in preventing geofence intrusions [5]. It is therefore recommended to perform further investigation into the effects that the geofences have on the performance of the geovector resolution strategies for an airspace design similar to the one used in the present study.

The current study did not focus on efficiency of the proposed geovector resolution strategies. Nonetheless, it could be insightful to also investigate the effects of the resolution strategies on these measures.

Finally, the simulation of UAVs was assumed to be turbulence and wind free. Furthermore, it was assumed that the required state-information (position and velocity) for conflict detection and resoluton was noise free and instantly available to all other UAVs in the airspace. These assumptions might not closely represent reality. It is therefore recommended to further investigate the effects of these assumptions on the geovector resolution strategies and geovectors used in the experiments.

VIII. CONCLUSIONS

The present paper introduced the existing literature gap on the combination of the geovector protocol and conflict resolution methods. In an effort to incorporate geovector limits into the process of conflict resolution, an alternative resolution maneuver was derived based on Velocity Obstacle theory. Using this maneuver, five geovector resolution strategies were developed, which assign different priorities to the individual geovector limits. Fast-time air traffic simulations were performed to test the performance of the proposed resolution strategies in high-density UAV airspace. Comparisons were made to the pure MVP method on geovector, safety, and stability metrics. The following conclusions can be drawn from the research:

- Regarding the geovector design used in the experiments, a clear reduction in conflict rate was observed.

- The geovector resolution strategies show clear improvements over pure MVP on the majority of geovector metrics.
- Although a reduction in geovector violations is obtained, the conflict rate reduction from the geovector could not be reinforced by the geovector resolution strategies.
- All geovector resolution strategies were successful in preventing intrusions, where in no case the observed intrusion severity exceeded 20% of the horizontal separation minimum.

REFERENCES

[1] SESAR JU. *European Drones Outlook Study*. November 2016. doi: 10.2829/085259.

[2] M. Doole, J. Ellerbroek, and J.M. Hoekstra. Estimation of traffic density from drone-based delivery in very low level urban airspace. *Journal of Air Transport Management*, 88, sep 2020. doi: 10.1016/j.jairtraman.2020.101862.

[3] SESAR JU. *U-space Blueprint*. 2017. doi: 10.2829/335092.

[4] J. Hoekstra, J. Ellerbroek, E. Sunil, and J. Maas. Geovectoring: Reducing Traffic Complexity to Increase the Capacity of UAV airspace. *2018 International Conference on Research in Air Transportation*, 2018. URL `http://resolver.tudelft.nl/uuid:790ea9d2-bdb2-439b-b7eb-ee811bbfaaa5`.

[5] R. Jacobse. *Extending the Modified Voltage Potential algorithm for use in converging traffic flows*. Master thesis, Delft University of Technology, 2020. URL `http://resolver.tudelft.nl/uuid:efe1071e-5704-4a46-956f-a6a94d74818f`.

[6] J. Hoekstra and J. Ellerbroek. BlueSky ATC Simulator Project: An Open Data and Open Source Approach. *7th International Conference on Research in Air Transportation: Philadelphia, USA*, 2016. URL `http://resolver.tudelft.nl/uuid:d1131a90-f0ea-4489-a217-ad29987689a1`.

[7] E. Sunil, J. Ellerbroek, J.M. Hoekstra, and J. Maas. Three-dimensional conflict count models for unstructured and layered airspace designs. *Transportation Research Part C: Emerging Technologies*, 95:295–319, oct 2018. doi: 10.1016/j.trc.2018.05.031.

[8] E. Sunil, J. Hoekstra, J. Ellerbroek, F. Bussink, D. Nieuwenhuisen, A. Vidosavljevic, and S. Kern. Metropolis: Relating airspace structure and capacity for extreme traffic densities. *Proceedings of the 11th USA/Europe Air Traffic Management Research and Development Seminar, ATM 2015*, 2015. URL `http://resolver.tudelft.nl/uuid:1019a338-5f69-409a-a06c-6c8346cd343e`.

[9] R.A. Paielli. A Linear Altitude Rule for Safer and More Efficient Enroute Air Traffic. *Air Traffic Control Quarterly*, 8 (3):195–221, jul 2000. doi: 10.2514/atcq.8.3.195.

[10] R. Irvine and H. Hering. Towards Systematic Air Traffic Management in a Regular Lattice. *7th AIAA Aviation Technology, Integration and Operations Conference (ATIO)*, 2007. doi: 10.2514/6.2007-7780.

[11] K. Leiden, S. Peters, and S. Quesada. Flight Level-based Dynamic Airspace Configuration. *9th AIAA Aviation Technology, Integration and Operations Conference (ATIO)*, 2009. doi: 10.2514/6.2009-7104.

[12] J.M. Hoekstra, J. Maas, M. Tra, and E. Sunil. How Do Layered Airspace Design Parameters Affect Airspace Capacity and Safety ? *7th International Conference on Research in Air Transportation: Philadelphia, USA*, 2016. URL `http://resolver.tudelft.nl/uuid:37969f88-44be-4435-aaa4-20185d548827`.

[13] M. Ribeiro, J. Ellerbroek, and J. Hoekstra. Review of conflict resolution methods for manned and unmanned aviation. *MDPI Aerospace*, 7(6), jun 2020. doi: 10.3390/AEROSPACE7060079.

[14] J.M. Hoekstra. *Designing for safety: The free flight air traffic management concept*. Doctoral thesis, Delft University of Technology, 2001. ISBN: 90-806343-2-8.

[15] W. Schaberg, J. Ellerbroek, and J. Hoekstra. *A Decentralized Recovery Method for Air Traffic Conflicts*. Master thesis, Delft University of Technology, 2020. URL `http://resolver.tudelft.nl/uuid:529b6868-f0b4-49e3-94c3-82e52ebe0c7d`.

[16] P. Fiorini and Z. Shiller. Motion planning in dynamic environments using the relative velocity paradigm. *Proceedings - IEEE International Conference on Robotics and Automation*, 1:560–566, 1993. doi: 10.1109/robot.1993.292038.

[17] P. Fiorini and Z. Shiller. Motion planning in dynamic environments using velocity obstacles. *International Journal of Robotics Research*, 17(7):760–772, 1998. doi: 10.1177/027836499801700706.

[18] J. Ellerbroek. *Airborne Conflict Resolution In Three Dimensions*. Doctoral thesis, Delft University of Technology, 2013. ISBN: 9789461918277.

[19] A. Chakravarthy and D. Ghose. Obstacle avoidance in a dynamic environment: A collision cone approach. *IEEE Transactions on Systems, Man, and Cybernetics Part A:Systems and Humans.*, 28(5):562–574, 1998. doi: 10.1109/3468.709600.

[20] J. Sun, J.M. Hoekstra, and J. Ellerbroek. OpenAP: An open-source aircraft performance model for air transportation studies and simulations. *Aerospace*, 7(8), aug 2020. doi: 10.3390/AEROSPACE7080104.

[21] M. Doole, J. Ellerbroek, and J.M. Hoekstra. Investigation of Merge Assist Policies to Improve Safety of Drone Traffic in a Constrained Urban Airspace. *Aerospace 2022, Vol. 9, Page 120*, 9(3):120, feb 2022. doi: 10.3390/AEROSPACE9030120.

[22] E. Sunil, J. Ellerbroek, J. Hoekstra, and J. Maas. Modeling Airspace Stability and Capacity for Decentralized Separation. *12th Seminar Papers: 12th USA/Europe Air Traffic Management Research and Development Seminar*, page 12, 2017. URL `http://resolver.tudelft.nl/uuid:3e7e2f4a-57ac-4045-8a01-e0e9a4db0a00`.

[23] K.D. Bilimoria, K.S. Sheth, H.Q. Lee, and S.R. Grabbe. Performance evaluation of airborne separation assurance for free flight. *18th Applied Aerodynamics Conference*, 2000. doi: 10.2514/atcq.11.2.85.

[24] F. Wilcoxon. Individual Comparisons of Grouped Data by Ranking Methods. *Journal of Economic Entomology*, 39(2): 269–270, 1946. doi: 10.1093/JEE/39.2.269.

[25] H. B. Mann and D. R. Whitney. On a Test of Whether one of Two Random Variables is Stochastically Larger than the Other. 18(1):50–60, 1947. doi: 10.1214/AOMS/1177730491.

[26] Olive Jean Dunn. Multiple Comparisons among Means. *Journal of the American Statistical Association*, 56(293):52–64, 1961. doi: 10.1080/01621459.1961.10482090.

Part II

Appendices

Appendix A

Repetitive Conflict Filter

The airspace design used in the experiments can yield a large number of repetitive conflicts, considering the fact that the geovectors can significantly reduce the closure speed of the UAVs. In order to prevent this type of conflict from significantly affecting measaurements of the conflict rate in the airspace, the number of conflicts was filtered based on three criteria. For any unique conflict pair, a follow-up conflict is not counted if the difference in time with the previous conflict is smaller than the *filter time*. Two exceptions are made based on the following assumptions:

1. It is assumed that secondary conflicts should not be filtered from the data. Both UAVs for this unique conflict pair should therefore not have encountered a conflict with any other UAV since the previous conflict was observed for this unique conflict pair.
2. It is assumed that both UAVs for this unique conflict pair should not have entered a different geovector sector, compared to the sector in which the first conflict was observed. The reason for this choice is the fact that autopilot directions can change when a new sector is entered (governed both by the geovector limits and by the next waypoint in the FMS).

In case it is determined a conflict should not be counted, it is still used as the last observed conflict to evaluate if future conflicts should be counted. This way, repetitive conflicts occurring over large time intervals can also be accounted for.

For each geovector, the effect of the filter time on the number of conflicts n_{conf} was investigated. The observed difference between the filtered number of conflicts and unfiltered (total) number of conflicts is expressed as filter factor:

$$\text{filter factor} = \frac{n_{conf,filtered}}{n_{conf,unfiltered}} \tag{A.1}$$

Figure A.1 - Figure A.5 show the observed filter factor for all geovectors used in the experiments. The lines show the medians of the datasets, the shading the 95% confidence intervals. As can be seen for all geovectors, no conflicts are filtered out using a filter time of 0 seconds (as can be expected). Furthermore, a steep decrease is observed for all resolution strategies (except OFF) between 0 and 15 seconds. Afterwards, the filter factor stays approximately constant. Based on the observed behaviour, the *filter time* was set at **15 s**.

OFF was included in the figures to verify the performance of the conflict filter, since hypothetically speaking, no conflicts should be filtered out at all for this resolution strategy. Since UAVs do not entirely fly in straight lines, but follow a flight plan over various waypoints which is also constrained by the geovector limits, a unique pair of UAVs can be in conflict more than once during a scenario without conflict resolution. Therefore, the filter shows an increasing error over time. Nonetheless, for a filter time of 15 seconds, the error is very small. Furthermore, it should be noted that for the computation of the dependent measures, the unfiltered conflict count was always used for resolution strategy OFF. Finally, Figure A.6 shows the unfiltered conflict count from the experiments.

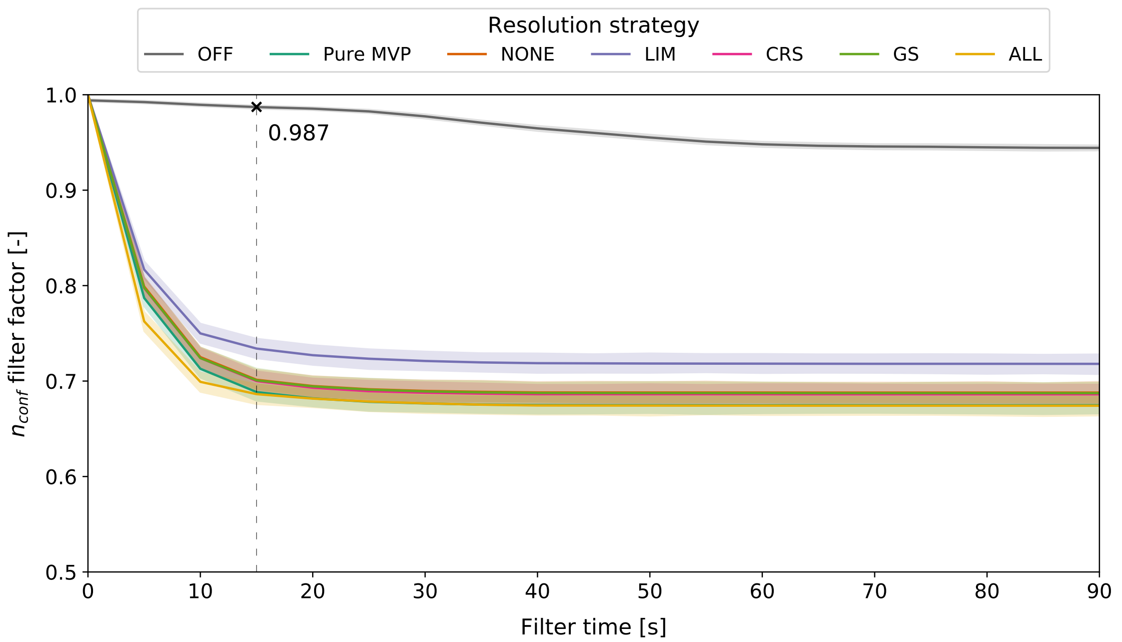

Figure A.1: Effect of the filter time on the filter factor for all resolution strategies and geovector SEV (1 m/s, 15°)

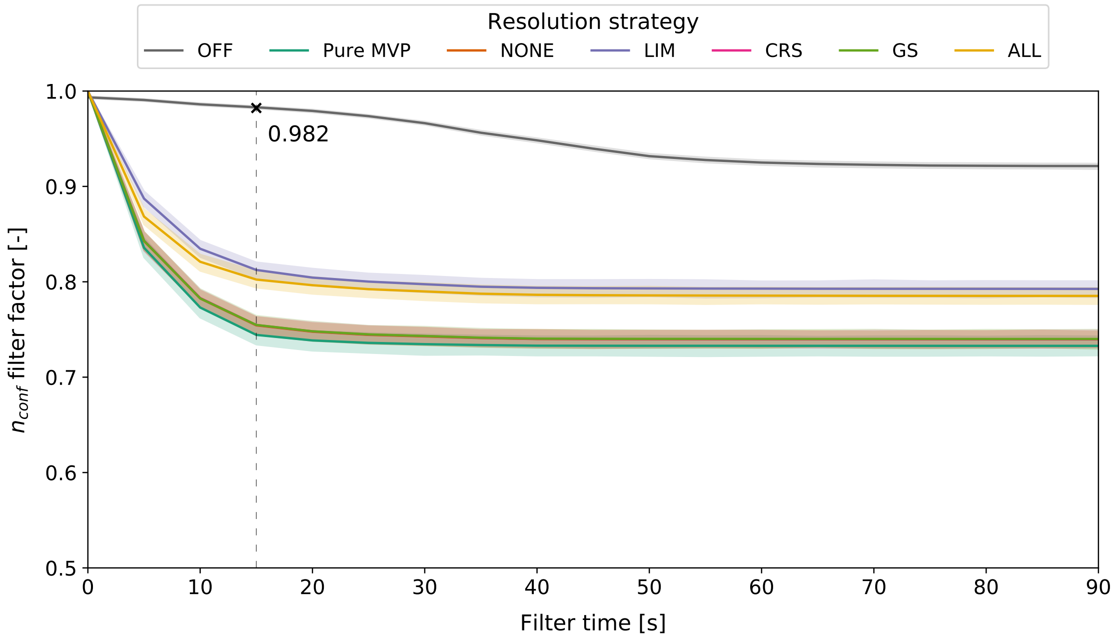

Figure A.2: Effect of the filter time on the filter factor for all resolution strategies for geovector EXT-GS (1 m/s, 45°)

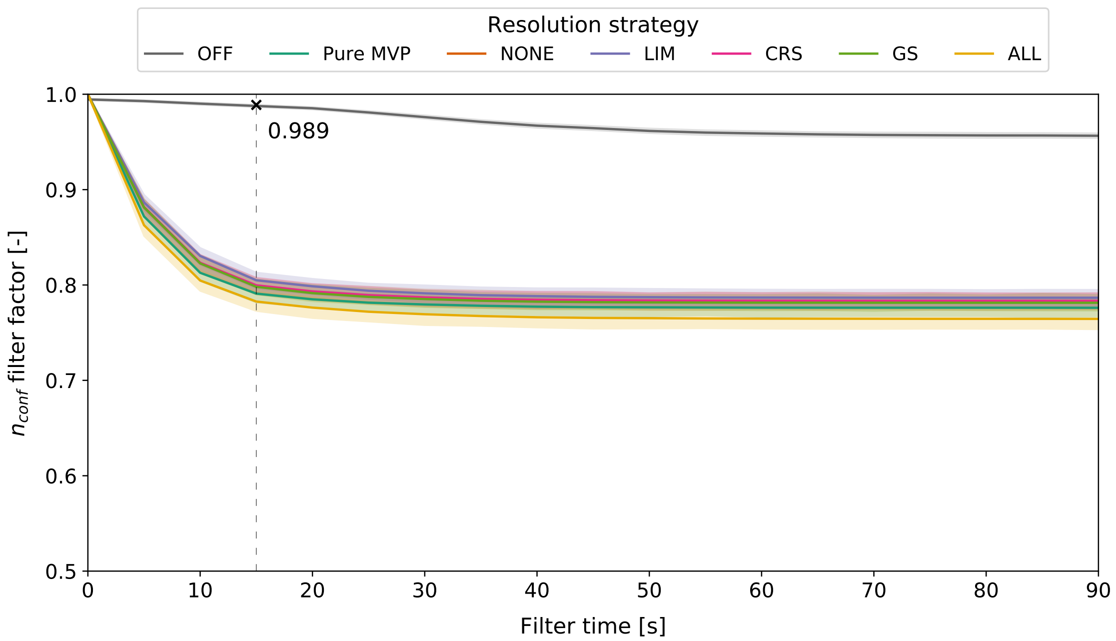

Figure A.3: Effect of the filter time on the filter factor for all resolution strategies for geovector MED (3 m/s, 30°)

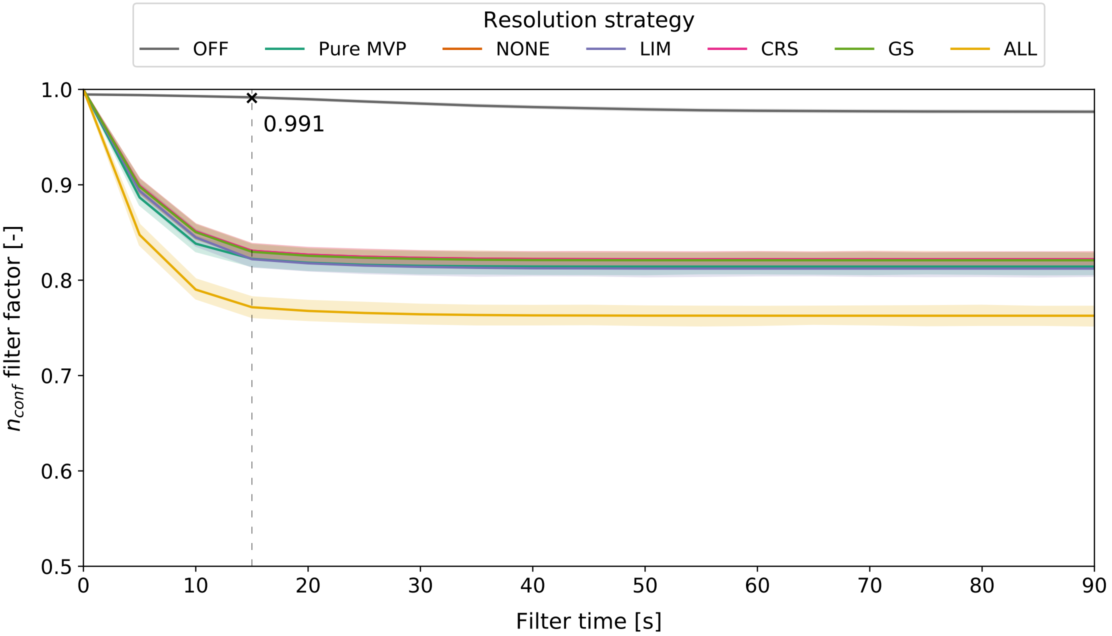

Figure A.4: Effect of the filter time on the filter factor for all resolution strategies for geovector EXT-CRS (5 m/s, 15°)

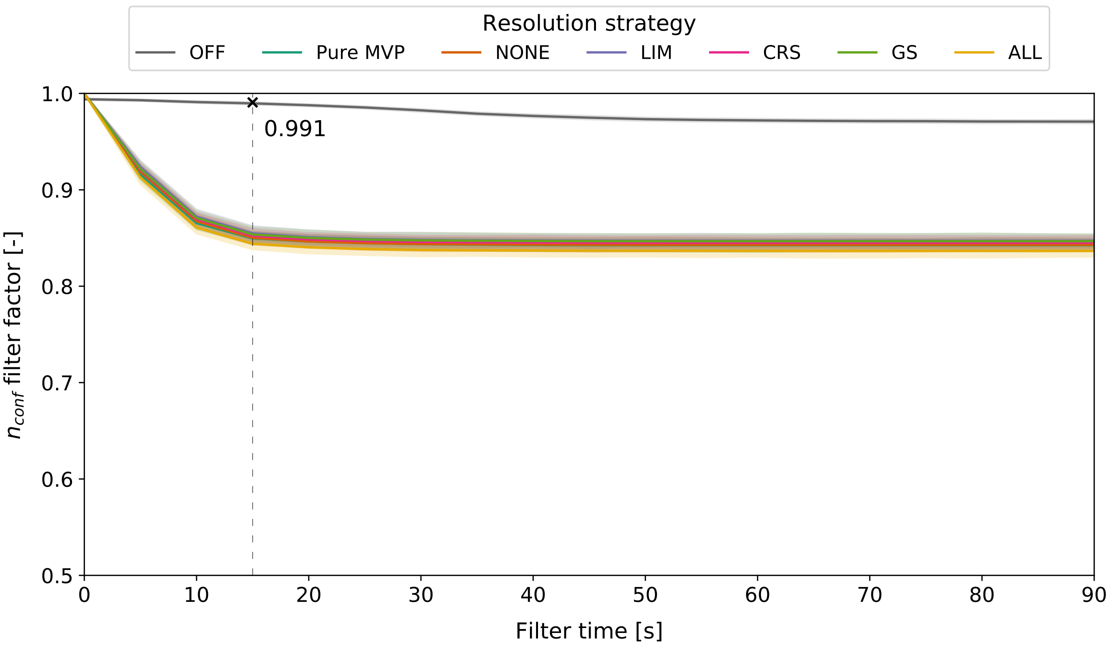

Figure A.5: Effect of the filter time on the filter factor for all resolution strategies for geovector WIDE (5 m/s, 45°)

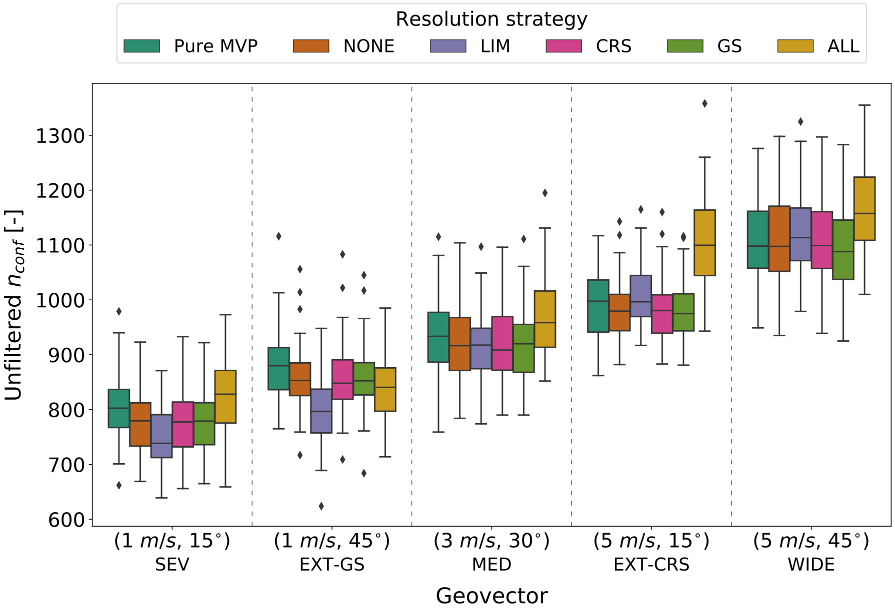

Figure A.6: Unfiltered number of conflicts

Appendix B

Additional Results

Similar to the average deviation from the geovector limits per geovector violation, the duration can also be computed per geovector violation. Figure B.1 and Figure B.2 show the measured duration over which ground speed limit violations and course limit violations were sustained by the conflict resolution module, respectively. One value was stored per observed geovector violation. Outliers are not shown.

Secondly, the intrusion severity was shown without outliers in the article. Figure B.3 shows the intrusion severity (LOS_{sev}) including outliers.

Thirdly, efficiency of a resolution method can be expressed in terms of the distance flown through the data logging area, compared with the direct route to the destination (measured using conflict resolution OFF). The efficiency of a resolution method decreases with increasing extra flight distance. However, for the airspace used in the experiments, an increase in flight distance can not be attributed to the path deviation caused by the resolution maneuver alone. Rather, it is an effect of the combination of resolution maneuvers and geovector limitations. A UAV can end up in a more favorable geovector sector with respect to its destination after performing a resolution maneuver which exceeds the geovector limitations. The opposite can also happen. As shown in Figure B.4, the extra distance flown decreases for approximately half of the portion of all flights. It should be noted that the exit point of a UAV at the boundary of the data logging area might differ between the scenario with and without conflict resolution, which could affect the measurements.

Furthermore, Figure B.5 shows the influence of the geovectors, compared to the scenario without geovectors, on the unfiltered conflict count when using pure MVP. The unfiltered conflict count is shown, since the exception based on assumption 2 from the conflict filter (Appendix A) does not work for the case without geovectors. This can result in an unjust number of conflicts being removed from the data by the conflict filter.

Finally, Figure B.6 shows the filtered number of conflicts for resolution strategy pure MVP and OFF, where the latter means no conflict resolution was performed.

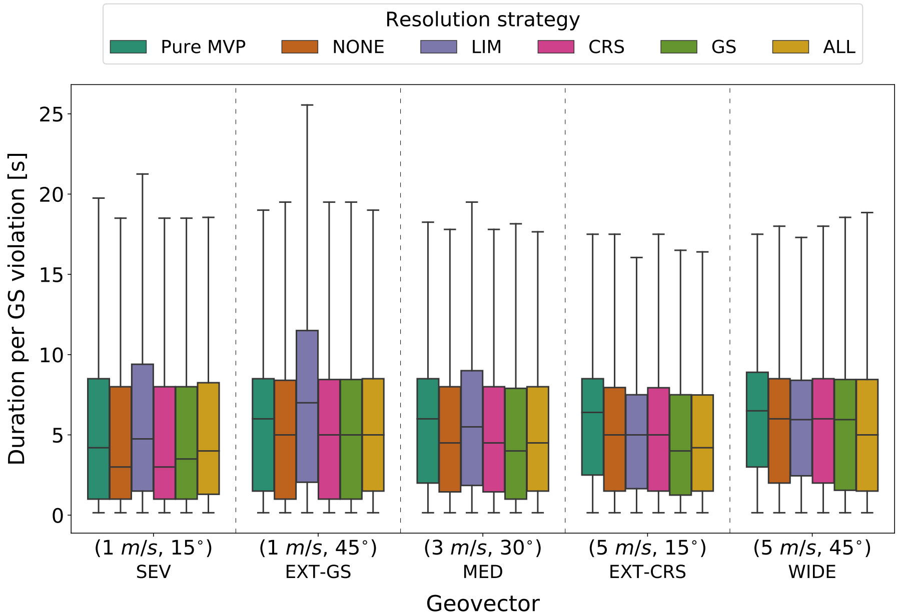

Figure B.1: Effect of geovector settings and conflict resolution strategies on the average duration of ground speed limit violations

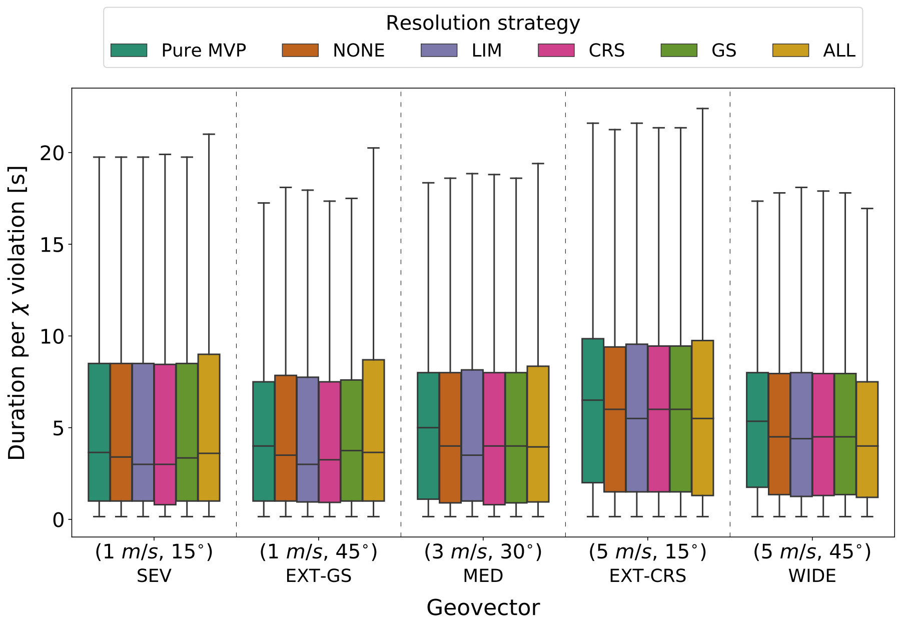

Figure B.2: Effect of geovector settings and conflict resolution strategies on the average duration of course limit violations

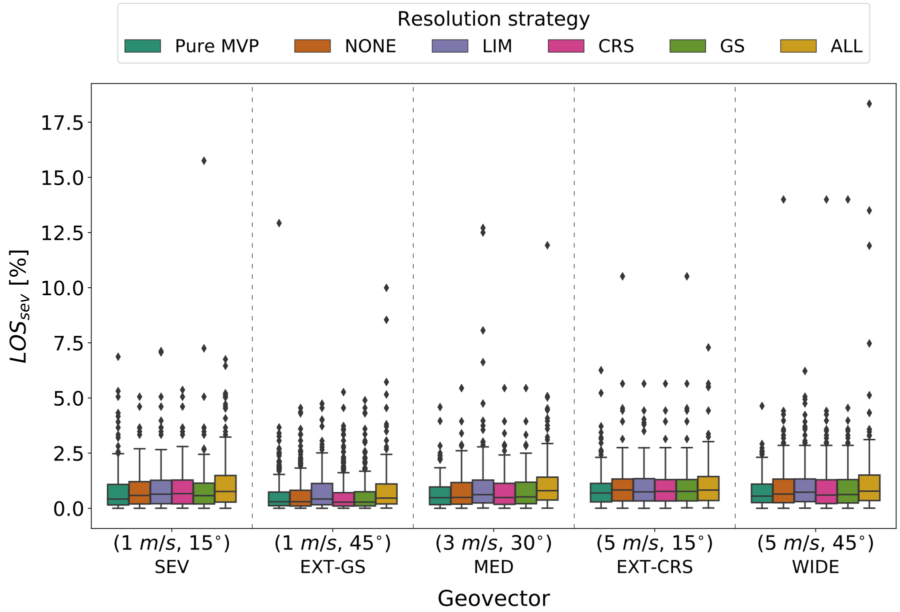

Figure B.3: Intrusion severity (LOS_{sev}) computed for each intrusion, including outliers

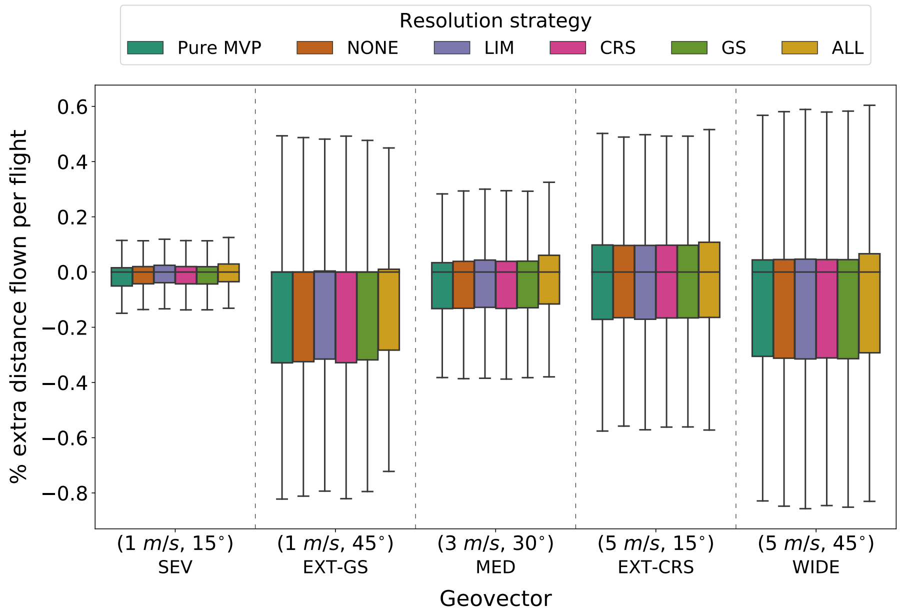

Figure B.4: Percentage increase in distance flown $(\%d_{extra})$ with conflict resolution

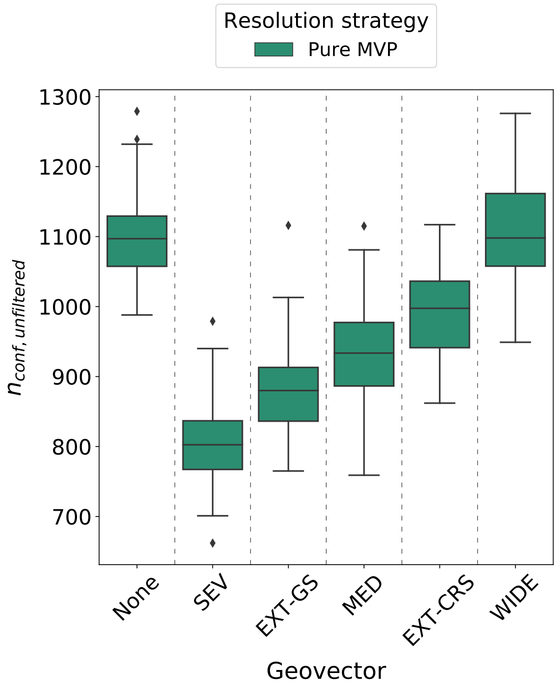

Figure B.5: Effect of geovector settings on the unfiltered number of conflicts for pure MVP. For geovector None, no geovectors are implemented in the airspace.

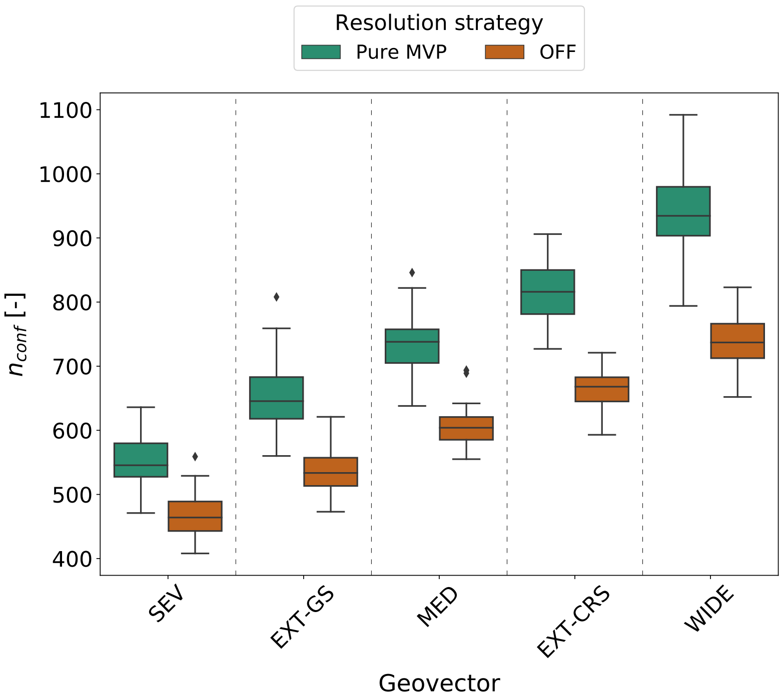

Figure B.6: Effect of geovector settings on the filtered number of conflicts for pure MVP and no conflict resolution (OFF).

Appendix C

Statistical Analysis

This appendix reports the p-values determined using the Wilcoxon signed rank-tests and Mann-Whitney U tests. The test used per measure is indicated in Table C.1. For each table containing p-values, the conflict resolution methods vary between table rows and geovector settings vary between table columns. Each sample of data is compared with the sample from the (baseline) pure MVP method corresponding to the same geovector settings. Each p-value corresponds to the probability that the null-hypothesis of the corresponding statistical test is true. Differences are considered statistically significant when $p \leq 0.01$. Both tests are used to determine if the samples for the geovector resolution strategies differ significantly from the baseline MVP method. Next to p-values, the median of each data sample is also reported.

Table C.1: Overview of statistical tests performed per dependent measure

Metric	Statistical test
$\%\text{manv}_{GS}$	Wilcoxon signed rank-test
$\%\text{manv}_{\chi}$	Wilcoxon signed rank-test
$\sum t_{GS}$	Wilcoxon signed rank-test
$\sum t_{\chi}$	Wilcoxon signed rank-test
DEV_{GS}	Mann-Whitney U test
DEV_{χ}	Mann-Whitney U test
n_{conf}	Wilcoxon signed rank-test
n_{intru}	Wilcoxon signed rank-test
LOS_{sev}	Mann-Whitney U test
$\%MACC$	Wilcoxon signed rank-test
f_{Vrel}	Mann-Whitney U test
$\|\|\Delta\chi_{CR}\|\|$	Mann-Whitney U test
DEP	Wilcoxon signed rank-test
ρ_{inst}	Mann-Whitney U test

Table C.2: P-values of the Wilcoxon signed rank-tests performed on samples for the percentage of resolution maneuvers chosen outside the ground speed limits (%manv$_{GS}$)

Median	**(1** m/s**, 15°)**	**(1** m/s**, 45°)**	**(3** m/s**, 30°)**	**(5** m/s**, 15°)**	**(5** m/s**, 45°)**
NONE	7.557E-10**	7.557E-10**	7.557E-10**	7.557E-10**	7.557E-10**
LIM	7.557E-10**	7.557E-10**	7.557E-10**	7.557E-10**	7.557E-10**
CRS	7.557E-10**	7.557E-10**	7.557E-10**	7.557E-10**	7.557E-10**
GS	7.557E-10**	7.557E-10**	7.557E-10**	7.557E-10**	7.557E-10**
ALL	7.557E-10**	7.557E-10**	7.557E-10**	7.557E-10**	7.557E-10**

$^*p \leq 0.05$, $^{**}p \leq 0.01$

Table C.3: Medians of all data samples for for the percentage of resolution maneuvers chosen outside the ground speed limits (%manv$_{GS}$)

Median	**(1** m/s**, 15°)**	**(1** m/s**, 45°)**	**(3** m/s**, 30°)**	**(5** m/s**, 15°)**	**(5** m/s**, 45°)**
MVP	52.489	56.037	34.409	17.09	18.948
NONE	33.126	31.437	15.259	6.3814	7.5074
LIM	28.565	29.621	13.372	5.6417	7.6801
CRS	33.343	31.898	15.637	6.3775	7.724
GS	29.922	27.987	12.444	4.7531	5.5056
ALL	15.224	10.603	6.388	3.5597	4.5572

Table C.4: P-values of the Wilcoxon signed rank-tests performed on samples for the percentage of resolution maneuvers chosen outside the course limits (%manv$_{\chi}$)

P-value	**(1** m/s**, 15°)**	**(1** m/s**, 45°)**	**(3** m/s**, 30°)**	**(5** m/s**, 15°)**	**(5** m/s**, 45°)**
NONE	7.557E-10**	8.031E-10**	7.557E-10**	7.557E-10**	7.557E-10**
LIM	7.557E-10**	7.557E-10**	7.557E-10**	7.557E-10**	7.557E-10**
CRS	7.557E-10**	7.557E-10**	7.557E-10**	7.557E-10**	7.557E-10**
GS	7.557E-10**	7.557E-10**	7.557E-10**	7.557E-10**	7.557E-10**
ALL	7.557E-10**	7.557E-10**	7.557E-10**	7.557E-10**	7.557E-10**

$^*p \leq 0.05$, $^{**}p \leq 0.01$

Table C.5: Medians of all data samples for for the percentage of resolution maneuvers chosen outside the course limits (%manv$_{\chi}$)

Median	**(1** m/s**, 15°)**	**(1** m/s**, 45°)**	**(3** m/s**, 30°)**	**(5** m/s**, 15°)**	**(5** m/s**, 45°)**
MVP	33.909	14.721	24.566	43.595	16.75
NONE	24.092	10.987	15.066	27.164	9.7104
LIM	24.302	9.7944	15.751	27.818	10.048
CRS	21.534	8.8801	14.098	26.722	9.4254
GS	24.263	11.714	15.12	27.249	9.8291
ALL	18.333	7.9286	10.738	18.186	7.6074

Table C.6: P-values of the Wilcoxon signed rank-tests performed on samples for the cumulative duration of all ground speed limit violations ($\sum t_{GS}$)

P-value	(1 m/s, 15°)	(1 m/s, 45°)	(3 m/s, 30°)	(5 m/s, 15°)	(5 m/s, 45°)
NONE	7.557E-10**	7.557E-10**	7.557E-10**	7.557E-10**	7.557E-10**
LIM	7.557E-10**	7.557E-10**	7.557E-10**	7.557E-10**	7.557E-10**
CRS	7.557E-10**	7.557E-10**	7.557E-10**	7.557E-10**	7.557E-10**
GS	7.557E-10**	7.557E-10**	7.557E-10**	7.557E-10**	7.557E-10**
ALL	7.557E-10**	7.557E-10**	7.557E-10**	7.557E-10**	7.557E-10**

$*p \leq 0.05$, $**p \leq 0.01$

Table C.7: Medians of all data samples for the cumulative duration of all ground speed limit violations ($\sum t_{GS}$)

Median	(1 m/s, 15°)	(1 m/s, 45°)	(3 m/s, 30°)	(5 m/s, 15°)	(5 m/s, 45°)
MVP	3726.3	4914.1	3183.7	1614.7	2117.4
NONE	2064.8	2588.1	1284.2	578.8	833.55
LIM	2550.2	3389.9	1472.4	521.72	852.9
CRS	2096.6	2562.1	1303.2	584.67	837.6
GS	1874.2	2284.4	1001.4	398.5	590.78
ALL	1140.0	1036.6	609.95	343.45	480.32

Table C.8: P-values of the Wilcoxon signed rank-tests performed on samples for the cumulative duration of all course limit violations ($\sum t_{\chi}$)

P-value	(1 m/s, 15°)	(1 m/s, 45°)	(3 m/s, 30°)	(5 m/s, 15°)	(5 m/s, 45°)
NONE	8.031E-10**	1.130E-07**	7.557E-10**	7.557E-10**	7.557E-10**
LIM	3.785E-09**	1.016E-07**	7.557E-10**	7.557E-10**	7.557E-10**
CRS	7.557E-10**	9.634E-10**	7.557E-10**	7.557E-10**	7.557E-10**
GS	8.031E-10**	4.924E-05**	7.557E-10**	7.557E-10**	7.557E-10**
ALL	1.655E-09**	0.0197*	7.557E-10**	7.557E-10**	7.557E-10**

$*p \leq 0.05$, $**p \leq 0.01$

Table C.9: Medians of all data samples for the cumulative duration of all course limit violations ($\sum t_{\chi}$)

Median	(1 m/s, 15°)	(1 m/s, 45°)	(3 m/s, 30°)	(5 m/s, 15°)	(5 m/s, 45°)
MVP	2893.5	1435.2	2548.4	5304.2	2226.5
NONE	2473.8	1301.6	1854.3	3978.7	1625.6
LIM	2617.5	1303.1	1973.7	4275.7	1718.2
CRS	2311.1	1151.4	1816.5	3957.8	1622.5
GS	2491.9	1342.7	1884.8	3969.2	1624.4
ALL	2501.6	1325.0	1651.3	3384.6	1468.0

Table C.10: P-values of the Mann-Whitney U tests performed on samples for the (absolute) average deviation from ground speed limits per geovector breach (DEV_{GS})

P-value	**(1** m/s**, 15°)**	**(1** m/s**, 45°)**	**(3** m/s**, 30°)**	**(5** m/s**, 15°)**	**(5** m/s**, 45°)**
NONE	1.366E-26**	1.190E-89**	6.842E-12**	0.00763**	0.455
LIM	2.723E-05**	9.289E-26**	2.471E-35**	1.550E-84**	4.788E-98**
CRS	1.040E-23**	1.341E-96**	3.566E-11**	0.00611**	0.17
GS	2.236E-161**	5.085E-185**	6.275E-94**	5.396E-40**	8.507E-16**
ALL	1.815E-60**	9.553E-99**	1.690E-48**	2.146E-36**	1.355E-10**

$^*p \leq 0.05$, $^{**}p \leq 0.01$

Table C.11: Medians of all data samples for the (absolute) average deviation from ground speed limits per geovector breach (DEV_{GS})

Median	**(1** m/s**, 15°)**	**(1** m/s**, 45°)**	**(3** m/s**, 30°)**	**(5** m/s**, 15°)**	**(5** m/s**, 45°)**
MVP	0.25762	0.38556	0.31747	0.24222	0.31131
NONE	0.28968	0.50216	0.35233	0.24784	0.30907
LIM	0.25703	0.3473	0.39067	0.3725	0.4525
CRS	0.28623	0.50512	0.35109	0.24796	0.31539
GS	0.36645	0.55876	0.45166	0.33297	0.36198
ALL	0.39539	0.57546	0.46423	0.35677	0.36227

Table C.12: P-values of the Mann-Whitney U tests performed on samples for the (absolute) average deviation from course limits per geovector breach (DEV_{χ})

P-value	**(1** m/s**, 15°)**	**(1** m/s**, 45°)**	**(3** m/s**, 30°)**	**(5** m/s**, 15°)**	**(5** m/s**, 45°)**
NONE	7.950E-90**	1.193E-61**	2.836E-74**	3.335E-169**	5.249E-79**
LIM	1.477E-82**	3.390E-107**	9.177E-14**	1.806E-08**	2.217E-45**
CRS	3.409E-149**	8.997E-102**	9.133E-105**	9.494E-183**	7.731E-91**
GS	9.408E-92**	1.617E-97**	3.013E-78**	2.542E-165**	4.691E-85**
ALL	0.0**	0.0**	0.0**	0.0**	1.414E-287**

$^*p \leq 0.05$, $^{**}p \leq 0.01$

Table C.13: Medians of all data samples for the (absolute) average deviation from course limits per geovector breach (DEV_{χ})

Median	**(1** m/s**, 15°)**	**(1** m/s**, 45°)**	**(3** m/s**, 30°)**	**(5** m/s**, 15°)**	**(5** m/s**, 45°)**
MVP	1.7861	2.6058	3.2164	3.9306	5.0827
NONE	2.8374	3.9936	4.6221	5.2582	6.5613
LIM	2.7962	4.5576	3.8308	4.1691	6.1583
CRS	3.1821	4.5496	4.9215	5.3006	6.6656
GS	2.8248	4.4601	4.6579	5.2372	6.6458
ALL	4.1559	6.5396	6.5755	5.819	8.0475

Table C.14: P-values of the Wilcoxon signed rank-tests performed on samples for the number of conflicts (n_{conf})

P-value	**(1** m/s**, 15°)**	**(1** m/s**, 45°)**	**(3** m/s**, 30°)**	**(5** m/s**, 15°)**	**(5** m/s**, 45°)**
NONE	0.121	0.0489*	0.204	0.128	0.127
LIM	0.91	0.427	0.605	0.0017**	4.823E-05**
CRS	0.0379*	0.06	0.137	0.109	0.0445*
GS	0.389	0.015*	0.236	0.351	0.325
ALL	0.00638**	7.109E-05**	6.828E-06**	6.751E-09**	2.289E-09**

$*p \leq 0.05$, $**p \leq 0.01$

Table C.15: Medians of all data samples for the number of conflicts (n_{conf})

Median	**(1** m/s**, 15°)**	**(1** m/s**, 45°)**	**(3** m/s**, 30°)**	**(5** m/s**, 15°)**	**(5** m/s**, 45°)**
MVP	545.5	645.5	738.0	816.0	934.5
NONE	543.5	647.0	727.5	812.5	935.0
LIM	552.5	644.5	731.0	820.5	954.0
CRS	548.5	644.0	724.5	815.0	939.0
GS	546.5	645.0	726.5	813.5	938.5
ALL	565.5	675.5	755.5	853.5	980.5

Table C.16: P-values of the Wilcoxon signed rank-tests performed on samples for the number of intrusions (n_{intru})

P-value	**(1** m/s**, 15°)**	**(1** m/s**, 45°)**	**(3** m/s**, 30°)**	**(5** m/s**, 15°)**	**(5** m/s**, 45°)**
NONE	0.385	0.0826	0.0109*	0.745	0.716
LIM	0.0129*	5.653E-06**	0.00225**	0.453	0.465
CRS	0.478	0.0517	0.0146*	0.751	0.657
GS	0.367	0.0133*	0.0153*	0.812	0.708
ALL	9.692E-04**	6.846E-07**	3.015E-04**	0.605	0.11

$*p \leq 0.05$, $**p \leq 0.01$

Table C.17: Medians of all data samples for the number of intrusions (n_{intru})

Median	**(1** m/s**, 15°)**	**(1** m/s**, 45°)**	**(3** m/s**, 30°)**	**(5** m/s**, 15°)**	**(5** m/s**, 45°)**
MVP	4.0	5.0	4.5	3.0	4.0
NONE	4.0	5.0	3.0	3.5	4.0
LIM	3.0	3.0	3.0	4.0	4.0
CRS	4.0	5.0	3.0	4.0	4.0
GS	4.0	4.0	3.0	4.0	4.0
ALL	3.0	3.0	3.0	4.0	4.0

Table C.18: P-values of the Mann-Whitney U tests performed on samples for the intrusion severity (LOS_{sev})

P-value	**(1** m/s**, 15°)**	**(1** m/s**, 45°)**	**(3** m/s**, 30°)**	**(5** m/s**, 15°)**	**(5** m/s**, 45°)**
NONE	0.124	0.44	0.156	0.0429*	0.222
LIM	0.0882	0.00484**	0.00274**	0.107	0.0524
CRS	0.0339*	0.304	0.189	0.0865	0.347
GS	0.159	0.39	0.0899	0.0736	0.25
ALL	5.580E-04**	0.00125**	4.321E-06**	0.0169*	9.380E-04**

$^{*}p \leq 0.05$, $^{**}p \leq 0.01$

Table C.19: Medians of all data samples for the intrusion severity (LOS_{sev})

Median	**(1** m/s**, 15°)**	**(1** m/s**, 45°)**	**(3** m/s**, 30°)**	**(5** m/s**, 15°)**	**(5** m/s**, 45°)**
MVP	0.42102	0.29483	0.482	0.69389	0.55319
NONE	0.58189	0.29701	0.49144	0.83043	0.64479
LIM	0.64042	0.42102	0.61897	0.74375	0.72992
CRS	0.66297	0.27961	0.48781	0.76851	0.59825
GS	0.57317	0.28179	0.51613	0.76523	0.62297
ALL	0.76268	0.4624	0.79837	0.82496	0.77725

Table C.20: P-values of the Wilcoxon signed rank-tests performed on samples for the percentage of resolution maneuvers involving multiple intruders simultaneously ($\%MACC$)

P-value	**(1** m/s**, 15°)**	**(1** m/s**, 45°)**	**(3** m/s**, 30°)**	**(5** m/s**, 15°)**	**(5** m/s**, 45°)**
NONE	0.178	0.0921	0.958	0.0297*	0.836
LIM	0.0831	0.00783**	0.449	0.851	0.229
CRS	0.094	0.0412*	0.295	0.0429*	0.761
GS	0.534	0.0375*	0.896	0.0578	0.866
ALL	0.191	0.0884	9.138E-08**	6.214E-04**	3.785E-09**

$^{*}p \leq 0.05$, $^{**}p \leq 0.01$

Table C.21: Medians of all data samples for the percentage of resolution maneuvers involving multiple intruders simultaneously ($\%MACC$)

Median	**(1** m/s**, 15°)**	**(1** m/s**, 45°)**	**(3** m/s**, 30°)**	**(5** m/s**, 15°)**	**(5** m/s**, 45°)**
MVP	2.0913	2.9611	2.4011	2.1424	3.3313
NONE	1.8981	2.7951	2.2611	1.9616	3.2486
LIM	1.734	2.5388	2.5507	2.1212	3.3547
CRS	1.8745	2.5906	2.2726	1.8095	3.325
GS	1.8501	2.6694	2.2444	2.0079	3.2273
ALL	2.3784	3.3679	3.4213	2.8155	4.9095

Table C.22: P-values of the Mann-Whitney U tests performed on samples for the change in magnitude of relative velocity per conflict resolution maneuver (f_{Vrel})

P-value	**(1** m/s**, 15°)**	**(1** m/s**, 45°)**	**(3** m/s**, 30°)**	**(5** m/s**, 15°)**	**(5** m/s**, 45°)**
NONE	6.345E-06**	8.654E-37**	2.016E-04**	3.147E-92**	7.079E-07**
LIM	7.039E-08**	1.570E-78**	0.332	0.0**	0.399
CRS	1.606E-05**	6.408E-44**	2.924E-04**	1.678E-91**	1.048E-07**
GS	2.836E-05**	2.319E-40**	0.0724	3.020E-93**	0.0202*
ALL	0.323	5.079E-14**	3.460E-138**	0.0**	1.157E-189**

$*p \leq 0.05$, $**p \leq 0.01$

Table C.23: Medians of all data samples for the change in magnitude of relative velocity per conflict resolution maneuver (f_{Vrel})

Median	**(1** m/s**, 15°)**	**(1** m/s**, 45°)**	**(3** m/s**, 30°)**	**(5** m/s**, 15°)**	**(5** m/s**, 45°)**
MVP	1.0275	1.036	1.0084	1.0005	1.0036
NONE	1.0285	1.0298	1.0067	1.0074	1.0017
LIM	1.0276	1.0211	1.0105	1.026	1.0036
CRS	1.0283	1.0285	1.0068	1.0073	1.0015
GS	1.0295	1.0289	1.0091	1.008	1.0024
ALL	1.031	1.03	1.0295	1.0372	1.0171

Table C.24: P-values of the Mann-Whitney U tests performed on samples for the absolute course change per resolution maneuver performed by each individual UAV ($||\Delta\chi_{CR}||$)

P-value	**(1** m/s**, 15°)**	**(1** m/s**, 45°)**	**(3** m/s**, 30°)**	**(5** m/s**, 15°)**	**(5** m/s**, 45°)**
NONE	4.156E-23**	5.440E-140**	2.766E-12**	1.917E-25**	3.009E-12**
LIM	0.0**	0.0**	2.396E-146**	3.616E-51**	2.025E-50**
CRS	6.319E-09**	3.013E-111**	7.176E-09**	2.803E-26**	5.554E-14**
GS	8.759E-28**	2.593E-193**	7.226E-14**	1.658E-27**	1.929E-18**
ALL	0.0**	0.0**	9.569E-130**	3.785E-250**	7.989E-52**

$*p \leq 0.05$, $**p \leq 0.01$

Table C.25: Medians of all data samples for the absolute course change per resolution maneuver performed by each individual UAV ($||\Delta\chi_{CR}||$)

Median	**(1** m/s**, 15°)**	**(1** m/s**, 45°)**	**(3** m/s**, 30°)**	**(5** m/s**, 15°)**	**(5** m/s**, 45°)**
MVP	1.102	1.3376	2.0763	2.9061	2.9372
NONE	1.2428	1.6335	2.2286	2.8342	3.0867
LIM	1.767	2.7244	2.5042	2.7296	3.1953
CRS	1.2045	1.6027	2.2136	2.8323	3.1022
GS	1.2502	1.6873	2.2309	2.8278	3.1168
ALL	1.8007	3.1461	2.5723	2.5125	3.2163

Table C.26: P-values of the Wilcoxon signed rank-tests performed on samples for the Domino Effect Parameter (DEP)

P-value	**(1** m/s**, 15°)**	**(1** m/s**, 45°)**	**(3** m/s**, 30°)**	**(5** m/s**, 15°)**	**(5** m/s**, 45°)**
NONE	0.128	0.0513	0.201	0.151	0.137
LIM	0.902	0.395	0.615	0.00157**	3.737E-05**
CRS	0.0441*	0.053	0.146	0.114	0.0478*
GS	0.418	0.0136*	0.231	0.347	0.368
ALL	0.00603**	6.300E-05**	5.837E-06**	6.759E-09**	2.365E-09**

$^*p \leq 0.05$, $^{**}p \leq 0.01$

Table C.27: Medians of all data samples for the Domino Effect Parameter (DEP)

Median	**(1** m/s**, 15°)**	**(1** m/s**, 45°)**	**(3** m/s**, 30°)**	**(5** m/s**, 15°)**	**(5** m/s**, 45°)**
MVP	0.17404	0.22222	0.20656	0.22346	0.26687
NONE	0.17055	0.20604	0.19932	0.21915	0.27509
LIM	0.17584	0.21465	0.21869	0.23928	0.28589
CRS	0.16775	0.20499	0.20067	0.21995	0.27314
GS	0.17034	0.2042	0.20145	0.21669	0.27472
ALL	0.20683	0.25569	0.25545	0.27791	0.32103

Table C.28: P-values of the Mann-Whitney U tests performed on samples for the instantaneous airspace density (ρ_{inst})

P-value	**(1** m/s**, 15°)**	**(1** m/s**, 45°)**	**(3** m/s**, 30°)**	**(5** m/s**, 15°)**	**(5** m/s**, 45°)**
NONE	0.411	0.411	0.471	0.406	0.479
LIM	0.339	0.362	0.326	0.191	0.365
CRS	0.416	0.413	0.462	0.406	0.475
GS	0.417	0.42	0.481	0.409	0.479
ALL	0.306	0.233	0.266	0.0524	0.296

$^*p \leq 0.05$, $^{**}p \leq 0.01$

Table C.29: Medians of all data samples for the instantaneous airspace density (ρ_{inst})

Median	**(1** m/s**, 15°)**	**(1** m/s**, 45°)**	**(3** m/s**, 30°)**	**(5** m/s**, 15°)**	**(5** m/s**, 45°)**
MVP	49.0	48.0	49.0	50.0	49.0
NONE	49.0	48.0	49.0	50.0	49.0
LIM	49.0	48.0	49.0	50.0	49.0
CRS	49.0	48.0	49.0	50.0	49.0
GS	49.0	48.0	49.0	50.0	49.0
ALL	49.0	48.0	49.0	50.0	49.0

Appendix D

BlueSky Unit Tests

Unit tests have been performed in BlueSky in order to verify the computation of resolution maneuvers along the leg of the VO. A conflict was created using the following commands:

```
00:00:00.00>ZONER 0.0134989201
00:00:00.00>DTLOOK 10.0
00:00:00.00>BOX SECTOR,52.4554,2.213505,51.588555,3.878969
00:00:00.00>GEOVECTOR SECTOR,9,12,345,15,,,
00:00:00.00>CRE UAV1,M600,51.871288,3.387089,345.0,100.0,10.0
00:00:00.00>CRECONFS UAV2,M600,UAV1,30.0,0.005,9.0,0.0,9.0,10.5
```

Figure D.1 shows the input distance, bearing, time to CPA, and distance at CPA for the conflict resolution module. Output of the MVP resolution module is shown in Figure D.2. The expected output for the ALL, GS, CRS, LIM, and NONE strategies was computed by hand and shown in Table D.1 and Table D.2, for UAV1 and UAV2 respectively. Comparing the expected output to the actual output of the resolution module shows the maneuvers are computed correctly.

Table D.1: Expected output of resolution module for UAV1, where the maneuver satisfying all limits does not exceed the threshold. All strategies are therefore expected to use the same maneuver, satisfying all limits.

Resolution strategy	Expected GS	Expected course	Correct?
ALL	12.0	348.16	Yes
GS	12.0	348.16	Yes
CRS	12.0	348.16	Yes
LIM	12.0	348.16	Yes
NONE	12.0	348.16	Yes

Table D.2: Expected output of resolution module for UAV2, where the maneuver satisfying all limits exceeds the threshold.

Resolution strategy	Expected GS	Expected course	Correct?
ALL	9.0	357.66	Yes
GS	9.0	36.39	Yes
CRS	8.496	15.0	Yes
LIM	8.831	1.06	Yes
NONE	8.503	20.08	Yes

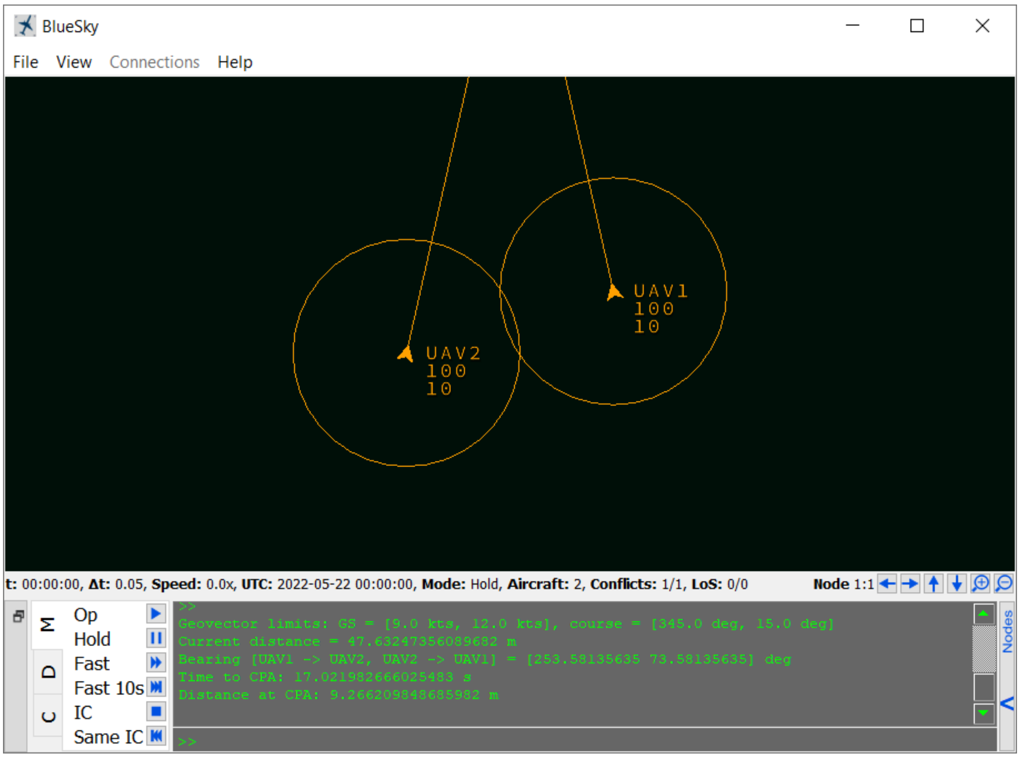

Figure D.1: Distance, bearing, time to CPA, and distance at CPA the start of the conflict

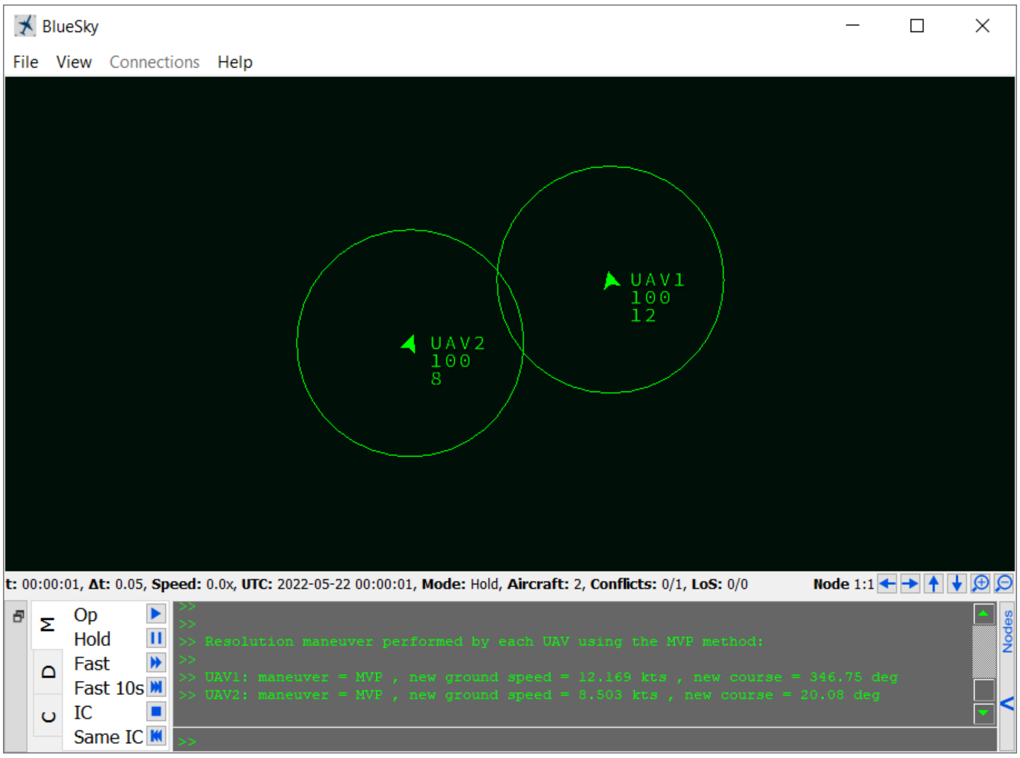

Figure D.2: Output of resolution module using the MVP method

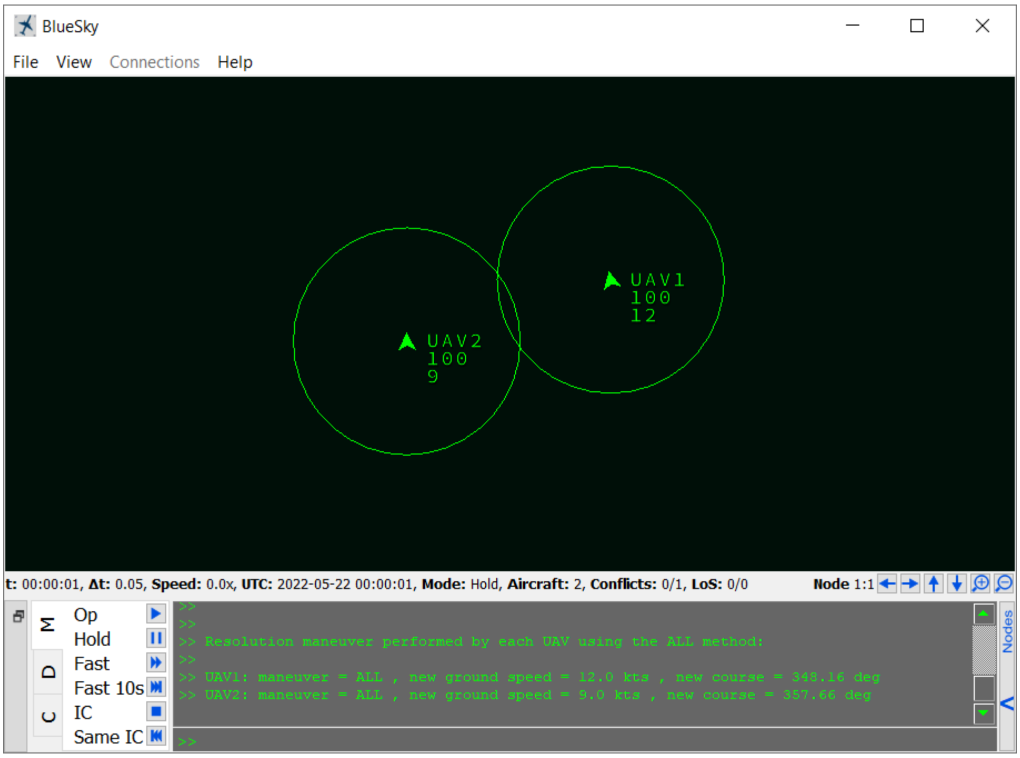

Figure D.3: Output of resolution module using the ALL method

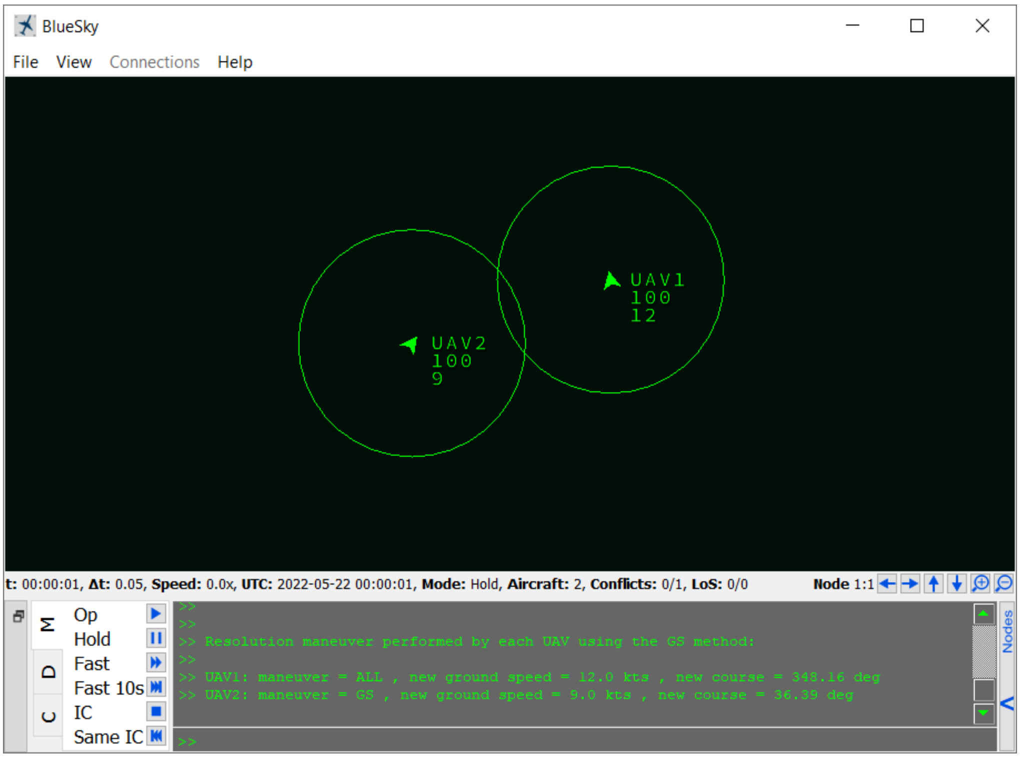

Figure D.4: Output of resolution module using the GS method

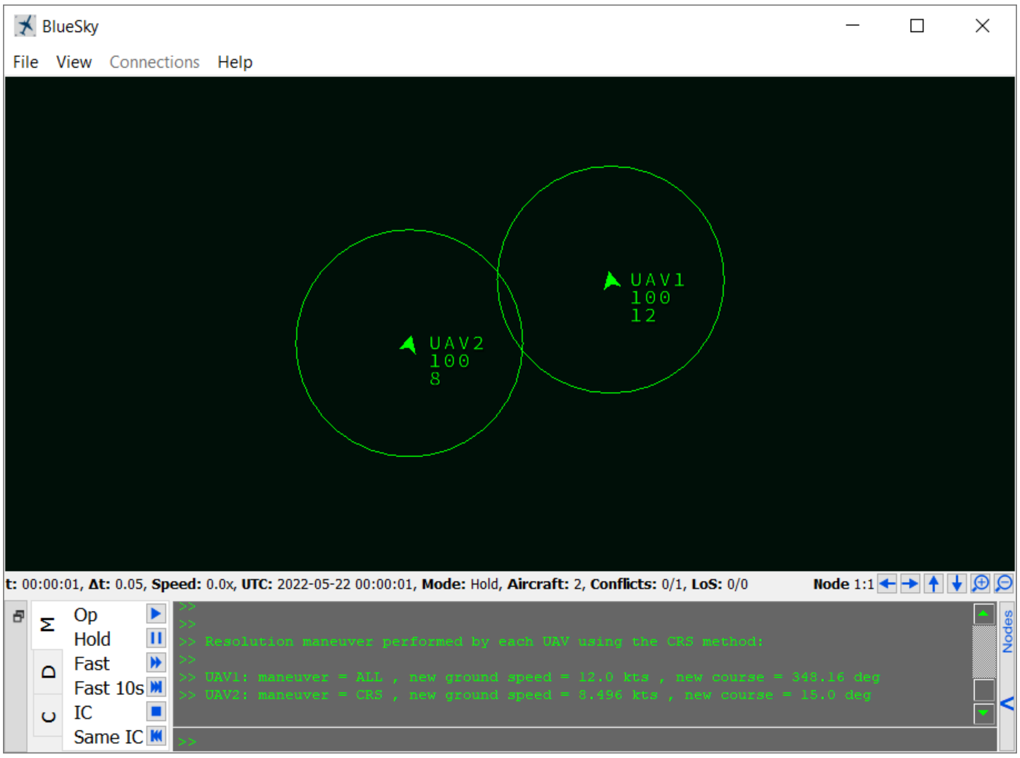

Figure D.5: Output of resolution module using the CRS method

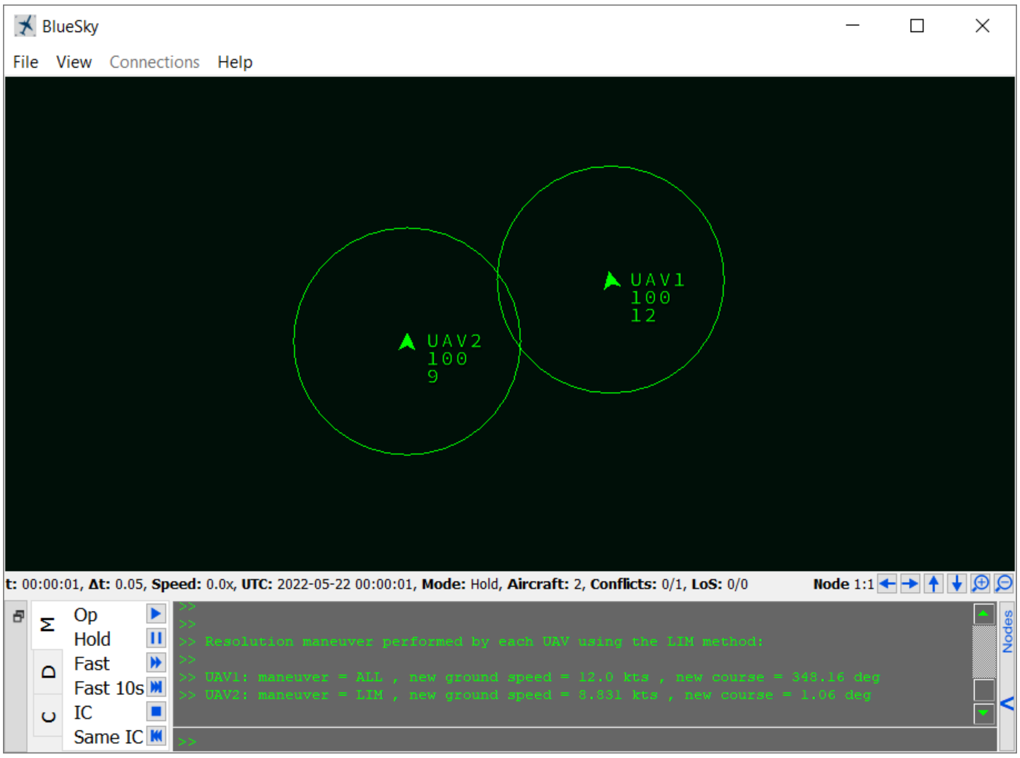

Figure D.6: Output of resolution module using the LIM method

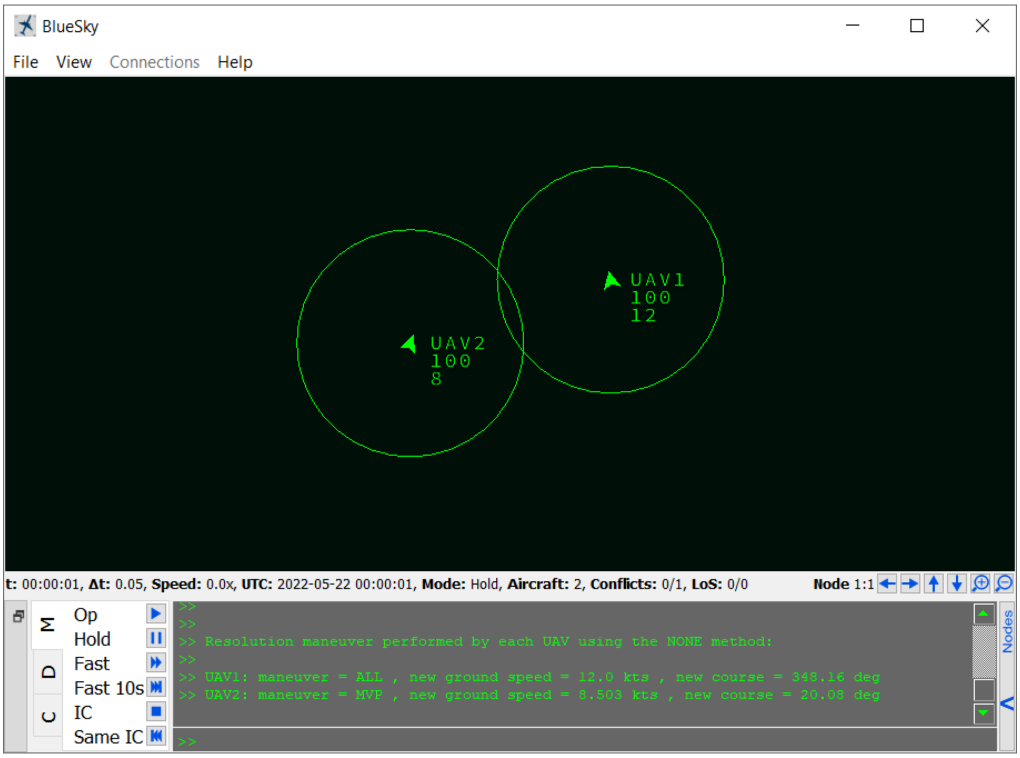

Figure D.7: Output of resolution module using the NONE method

Part III

Preliminary Report (already graded)

Chapter 1

Introduction

In a drone outlook study performed by the SESAR Joint Undertaking (2016) [39], it is mentioned that the use of drones in civil airspaces will significantly grow over the coming decades. It is expected that by 2050, around 7 million leisure drones and 400,000 commercial drones or drones used by governments will be present across Europe. Furthermore, it is mentioned that these drones will mostly operate at altitudes below 150 metres. In order to accommodate for this growth of traffic, new procedures and technologies need to be developed in terms of airspace management.

Sunil et al. (2015) [49] have investigated the relationship between airspace structure and capacity. Four airspace concepts were compared on capacity, safety, and efficiency through simulations, varying from completely unstructured to completely structured. It was found that a layered airspace concept is optimal in terms of these metrics. This concept uses so called segmentation and relative speed reduction to reduce the amount of conflicts encountered by an aircraft. The former reduces the combinations of aircraft that can encounter each other in a conflict, while the latter reduces the rate at which aircraft encounter each other. Hoekstra et al. (2018) [21] generalized these definitions for Unmanned Aerial Vehicle (UAV) control methods. Two methods to control airspace density are often considered in studies for the improvement of airspace capacity: geofencing and geocaging. The former implies defining no-go areas for vehicles, while the latter is focused on defining areas in which vehicles are confined to move. It was concluded that both geofencing and geocaging incorporate the segmentation effect, found in the study from Sunil et al. (2015). In order to also exploit the effect of relative speed reduction, a new tool was proposed: geovectoring. This concept implies setting limits on the allowed 3-D speed vector of a vehicle existing within a specified 3-D area, which result in the approximate alignment of the speed vectors of vehicles in the same area. Hoekstra et al. (2018) propose to add geovectoring as a 3rd concept for the implementation of UAV airspace, on top of the already planned concepts of geofencing and geocaging. In order to practically implement this concept in future UAV airspace, it is mentioned that it is necessary to investigate how the concept of geovectoring can be used to control the capacity of UAV airspace [21].

According to the U-space Blueprint by the SESAR Joint Undertaking (2017) [40] and the UTM Concept of Operations by NextGen (2020) [14], services deployed for UAV airspace should enable high-density operations of automated drones. This will require some form of Conflict Detection and Resolution (CD&R), which will mostly rely on sensor data and algorithms instead of a human controller. A problem arising when implementing geovectors in dense UAV airspace is that UAVs cannot always satisfy the geovector rules in the conflict resolution maneuvers dictated by the Conflict Resolution algorithm. It could occur that all possible maneuvers to solve a conflict exist outside the geovector limits. This research aims to investigate how geovectors can be considered in the conflict detection and resolution process. A method will be proposed and experimentally verified in a series of simulations using the open source ATC simulator BlueSky [20]. Recommendations will be given for the combination of geovectors and CD&R in UAV airspace.

1.1 Research Objective, Framework, and Questions

The objective of this research is *to contribute to a conflict resolution algorithm for UAVs in future UAV airspace subject to geovector constraints by defining a set of maneuvering rules based on literature and testing this ruleset in a series of simulations.* Following from this objective, the main research question is formulated as follows.

> What recommendations can be made for the combination of CD&R methods and geovector rules in UAV airspace?

The research question is split into multiple levels of sub-questions:

1. What is the expected layout of future UAV airspace?
   (a) Which types of air traffic services are envisioned for UAV airspace?
   (b) What are typical airspace parameters relevant for the current study?
2. What CD&R methods are feasible for future UAV airspace?
   (a) How can existing CD&R methods be categorized?
   (b) Which existing CD&R method is most suitable as baseline method in this study?
3. How can geovector rules be incorporated in the CD&R process?
4. What metrics are relevant for the performance evaluation of the combined CD&R-geovector method?
5. How does the combined CD&R-geovector method perform in an experimental simulation based on the relevant metrics?
   (a) To what extent is the method effective in satisfying geovector rules?

(b) How does the proposed method perform on CD&R, compared to the baseline method?

6. What is the influence of the assumptions on the validity of the experiment results?

A research framework (Figure 1.1) was created in order to visualize the steps that need to be taken in this research. The diagram shows where each sub-question (1-6) is answered in the research process.

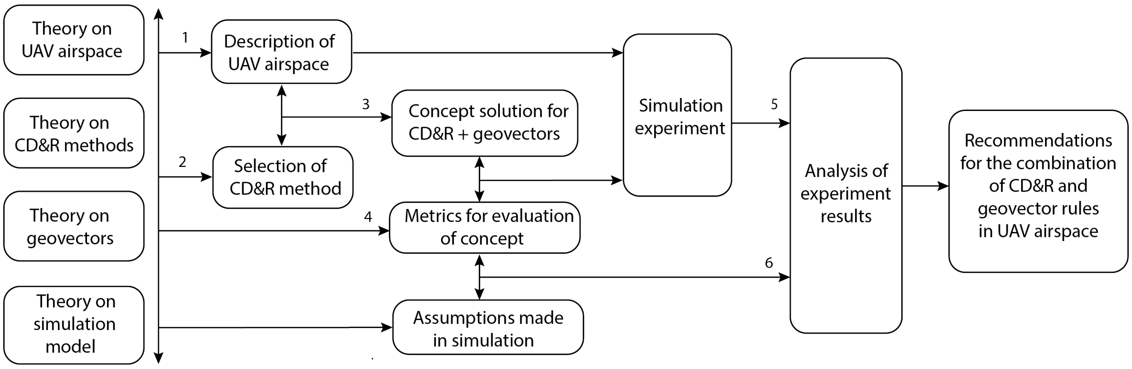

Figure 1.1: Research Framework

1.2 Report Outline

This report is structured as follows. Chapter 2 includes a literature review on the expected of future UAV airspace. Existing CD&R methods are described in Chapter 3. This is followed by a description of the concept of geovectoring in Chapter 4. In Chapter 5, a method is proposed to combine CD&R with geovectoring rules. Finally, Chapter 6 proposes an experiment design to verify the proposed method in a series of simulations.

Chapter 2

UAV Airspace

Unmanned Aerial Vehicles (UAVs) are a relatively novel concept in the field of aviation. Nevertheless, rapid technological advancements have boosted the potential of unmanned flight. Several aviation authorities have set up projects for the development of procedures and services for UAVs, in order to enable them to integrate into the already existing airspace. In Section 2.1, a brief overview of the European U-Space program is provided, followed by its American counterpart UTM. Afterwards, Section 2.2 presents typical parameters like expected airspace density and structure. Finally, Section 2.3 briefly presents the main conclusions of this chapter.

Different terminology is used to refer to UAV airspace or UAVs in particular. The following are used throughout this report:

Definition 1. **Unmanned Aerial Vehicle (UAV):** Airborne vehicle which is either remotely piloted or performing completely autonomous flight [18].

Definition 2. **Drone:** Pilotless aircraft [18], in this report used as synonym for UAV.

Definition 3. **Personal Air Vehicle (PAV):** Airborne vehicle for personal use, alternative for cars.

2.1 Enabling Unmanned Flight

The potential of drones and therefore the need to enable UAV flight is acknowledged across the globe. Next to the economical benefits of commercial drone usage, UAVs can also be employed to increase public safety, provide medical services, preserve national parks and wildlife, and reduce greenhouse gas emissions. This section highlights two important research projects from Europe and the USA to realize UAV airspace, in Subsection 2.1.1 and Subsection 2.1.2 respectively.

2.1.1 Europe's U-Space Project

The U-Space project is established by the SESAR Joint Undertaking (SESAR JU). Specifically, "U-space is a set of new services and specific procedures designed to support safe, efficient and secure access to airspace for large numbers of drones" [40, p.2]. A planning has been made for the incremental development and deployment of these services, as is shown in Figure 2.1. As can be derived from the figure, four major packages have been identified in the roll-out process of the U-Space services: U1, U2, U3, and U4. From left to right, each builds upon an increased level of knowledge and technical developments, while incorporating updated versions of already existing services in previous packages [41]. Initially planned dates for the deployment of each set of services are indicated in Table 2.1.

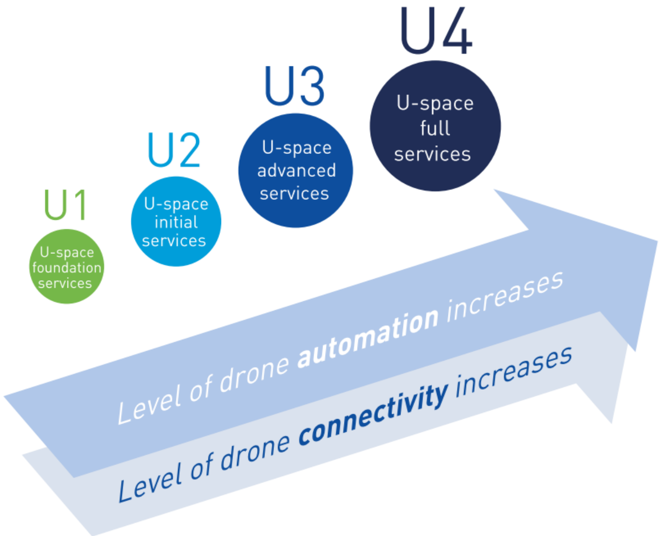

Figure 2.1: U-Space Deployment of Services [40]

Table 2.1: Initially Planned Deployment Dates of U-Space Services [41]

U-Space Package	Initially Planned Deployment Date
U1: Foundation Services	2019+
U2: Initial Services	2022+
U3: Advanced Services	2027+
U4: Full Services	2035+

The Foundation Services (U1) form the fundamental requirements for the integration of drones into European airspace, enabling flights on a basic level. The main objectives are the facilitation of registration and identification of UAVs, as well as the provision of restricted airspace data to drone operators (geo-awareness). Two approaches are envisioned to realize the latter: geofencing and geocaging. The former implies defining restricted areas for vehicles, while the latter relies on defining areas which vehicles are not allowed to leave [34]. As indicated in Table 2.1, the SESAR Joint Undertaking has planned that U1 services were ready to be deployed from 2019 onwards. In a preliminary summary of

U-Space research and innovations from 2017 to 2019 [42], SESAR JU mentions that U1 services are assumed to be ready for deployment. Several projects were set up to test this assumption. Although it was found that most services are already available, more work is required for successful implementation.

The goal of the Initial U-Space services (U2) is to enable the basic management of drone operations. This entails that drone flights can occur on a more routine basis. Beyond Visual Line Of Sight (BVLOS) flights will become more and more feasible, enabling more complex UAV missions. Some overlap with manned aviation will be envisioned by providing a basic interface with current ATM systems. Other important services envisioned to be released in U2 are strategic conflict resolution (de-conflicting flight plans, see Section 3.1), flight planning and approval, tracking, and airspace/traffic information. [41]

The Advanced U-Space services (U3) will build on the knowledge and experience gained in the process of developing U2 services. While these Initial Services aim to enable the safe management of drone operations, U3 services will incorporate more advanced methods of drone management. These will allow for UAV operations in dense and complex airspace. An important service planned in U3 is tactical conflict resolution ('detect and avoid', refer to Section 3.1). Another U3 service of interest is dynamic capacity management, which will be used to prevent the airspace from reaching its maximum capacity limit by managing access to dense parts [41]. Sunil et al. (2015) [49] have indicated that it is necessary to manage the traffic complexity, since UAV airspace is expected to be extremely dense with a high variety of applications. Therefore, Hoekstra et al. (2018) [21] propose to add geovectoring as component to the Dynamic Capacity Management service.

U4 is the ultimate goal in the deployment of the U-Space services. It entails full operation of the set of services, enabling full integration of manned and unmanned aviation. Currently, no services are planned for U4, but it is expected that these will follow from the roll-out of U3. [41]

2.1.2 United States' UTM Project

The Unmanned aerial system Traffic Management (UTM) project is the American counterpart of U-Space, led by the FAA's NextGen program. NASA first published a document describing the concept in 2013. As cited from a conceptual framework published by NASA (2014), "the goal of UTM is to enable safe and efficient low-altitude airspace operations" [29]. In 2015, the FAA highlighted its responsibility for managing low-altitude operations. Following this, the FAA and NASA joined forces to perform research on and eventually implement UTM in the USA. In 2017, the UTM Pilot Program (UPP) was set up in order to realize initial UTM services by developing prototypes. The FAA (2020) [15] has already demonstrated three UTM capabilities in phase one of the UPP: sharing of flight intent; sending notifications to drone operators about air and ground activities; and sharing information about these activities with other stakeholders.

The FAA (2020) [14] mentions that research is currently focused on enabling drone flight below 400 ft above ground level (AGL), in both controlled (classes B-E) and uncontrolled (class G) airspace. BVLOS flights are envisioned as well. As is the case for manned aviation, ATC will not provide services below 400 ft AGL. Drone operators need to adhere to the regulations installed by the FAA. They will be, for example, responsible for maintaining a safe separation distance. UTM services will be provided to support operators in this process, as is the case with U-Space. Examples of planned services are strategic de-conflictation assistance, contingency management in dangerous situations, and airspace capacity optimization. A Flight Information Management System will be installed to realize data exchange between the FAA and UTM users.

2.2 Urban Airspace

The drone outlook study performed by SESAR JU (2016) [39] maps the expected growth of UAV use in Europe for the coming decades, until the year 2050. Several categories applications of UAVs are identified, which are expected to foster this growth. These are presented Subsection 2.2.1. Furthermore, Subsection 2.2.2 presents literature on the most optimal structure for urban airspace.

2.2.1 Airspace Use

In Figure 2.3, SESAR JU (2016) presents the most prominent sectors in which the use of UAVs will grow significantly. These are military, government and commercial, and leisure applications. Furthermore, SESAR JU (2016) estimated the amount of hours and kilometers that will be anually flown by UAVs around the year 2050. These are presented in Figure 2.2.

As can be deducted from Figure 2.3, the number of leisure drones is expected to grow rapidly over the coming years. Nevertheless Figure 2.2 indicates that these will only make up a small portion of actual use of very low level (VLL) airspace, since most will only be used a few hours per year. On the contrary, UAV flight in densely populated areas is expected to be the most significant. Operations in this airspace are mainly performed by the government and commercial sector. Examples of these include police and firefighter surveillance, emergency medical drones, and delivery of packages and food [39]. Given the figures indicated in Figure 2.2, VLL airspace in densely populated areas can be expected to become relatively crowded.

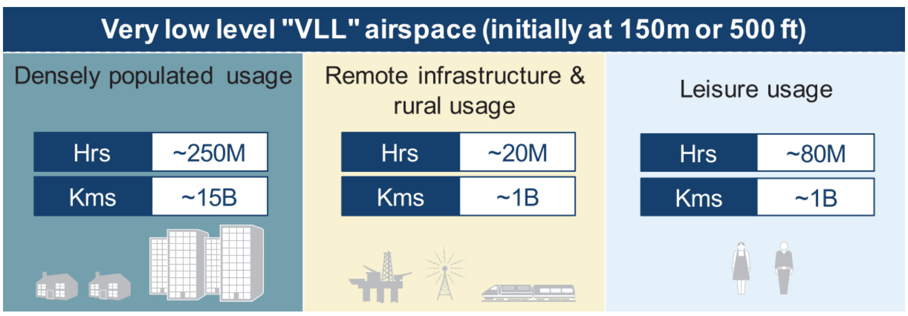

Figure 2.2: Expected Use of Airspace by UAVs in 2050, copied from SESAR JU (2016) [39, p.38]

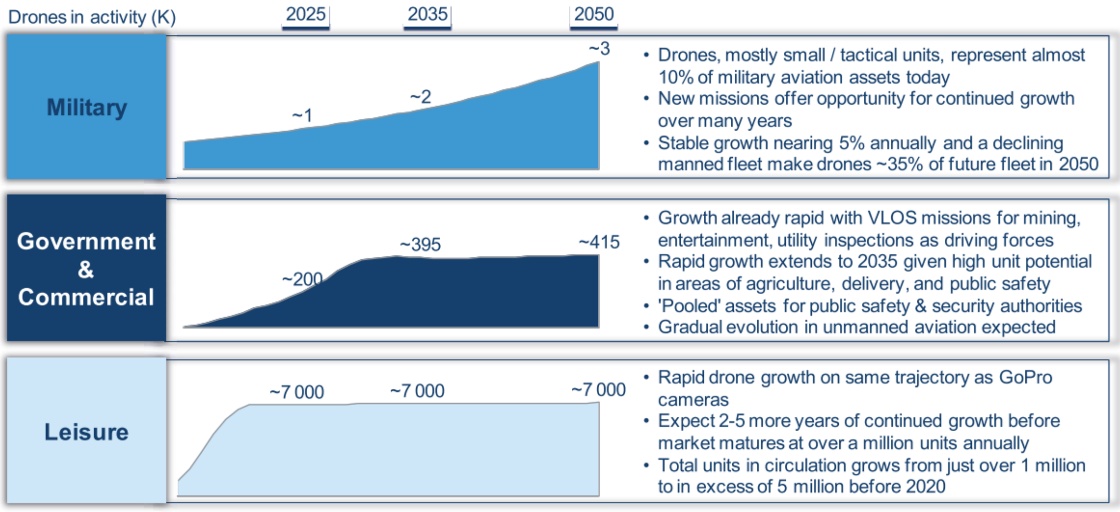

Figure 2.3: Total European Drone Fleet Size Expected over the Coming Decades, copied from SESAR JU (2016) [39, p.17]

Doole et al. (2018) [6] estimated traffic density in future European cities based on package delivery drone demand. Later, Doole et al. (2020) [7] extended their study and updated the statistics used in the previous research. The amount of parcels delivered annually in five countries was converted to the expected urban drone traffic density in the years 2035-2050. Use was made of the annual growth rate of parcel delivery, as well as factors to estimate the percentage of these parcels that will actually be delivered using drones in a city. Three estimations for the annual parcel delivery growth were used, based on the expected economic growth: one based on the average annual economic growth of 1.8% in 2019; one twice this value; and one conservative (half this value). Instantaneous parcel delivery traffic density was estimated for the metropolitan area of Paris (Île-de-France region), which covers an area of 12.012 km^2 or 3502.1 NM^2. The figures estimated by Doole et al. (2018) for the years 2035 and 2050 are presented in Table 2.2.

Furthermore, Doole et al. (2020) investigated the economical viability of food delivery drones for the metropolitan area of Paris. It was found that delivery UAVs can significantly reduce delivery costs compared to e-bike delivery, mainly due to the fact that e-bikes are harder to automate. Delivery drone traffic densities were estimated for the Île-de-France region, like was done for package delivery. Three scenarios were considered: low, medium, and high. In these scenarios, public acceptability of UAV food delivery and technological advancements increase from low to high. The higher, the lower the operational costs. Estimated figures are presented in Table 2.3.

Personal Air Vehicles (PAVs) encompass another type of airspace use. Considered an alternative for cars, PAVs enable a reduction of traffic on the streets and are a possible solution to the increasing amount of traffic congestion in urban regions. In the Metropolis project, Sunil et al. (2015) [49] assumed that approximately 4% of the population of Paris will be using PAVs by 2050. These vehicles will most likely be larger than the delivery UAVs described before and rely on a fixed-wing design where maintaining a relatively high airspeed is required to stay airborne. For this reason, Sunil et al. (2015) decided to separate the door-to-door delivery drones from PAVs in their research by assigning

Table 2.2: Instantaneous Package Delivery Drone Airspace Density Estimation (UAVs/NM^2) in Paris by [7]

Scenario	2035	2050
Low	9.6809	11.148
Medium	11.148	14.668
High	14.815	25.229

Table 2.3: Instantaneous Food Delivery Drone Airspace Density Estimation (UAVs/NM^2) in Paris by [7]

Scenario	2035	2050
Low	6.0829	6.9577
Medium	7.0114	9.1627
High	9.2812	15.776

different cruising altitudes. Interference only occurred during take-off and landing of PAVs.

For simplicity, the current study is limited to unmanned aerial vehicles only. Therefore, PAVs will not be used in the simulation experiments proposed in Chapter 6. Use will be made of only 1 type of quadcopter UAV capable of hover, which represents the parcel delivery drones and food delivery drones for which the airspace density estimation was performed in [7].

2.2.2 Airspace Structure

In the Metropolis project performed by Sunil et al. (2015) [49], four concepts for urban airspace structure were proposed and compared in a simulation using airspace capacity, safety, and route efficiency metrics. The concepts varied in level of structure in an increasing order: unstructured, layers, zones, and tubes. The layered airspace concept, previously investigated in several studies [36, 25, 33], was found to be optimal in terms of maintaining a balance between safety and route efficiency. It makes use of the so called 'segmentation' effect, which is further described in Section 4.1.

The layered airspace concept consists of vertically stacked altitude bands (layers) with fixed height. Allowed headings are confined to a specified interval in each layer, where the allowed heading range is constant. By separating traffic this way, the overall conflict rate can be reduced [23]. The amount of layers necessary to cover the entire compass range of 0° to 360° depends on the heading range. Furthermore, in order to safely separate aircraft in adjacent layers, the height of each layer should at least equal the vertical separation minimum for aircraft. An example is provided in Figure 2.4, illustrating the vertically stacked layers with a height of 300 ft and allowed heading range of 45°. In this case, 8 layers are necessary to allow flight in each direction.

Depending on the bearing between the origin and destination of aircraft, a different layer has to be used. Since each layer corresponds to a certain altitude, it was decided that aircraft cruising in a specific layer should maintain safe separation by only performing maneuvers horizontally.

2.2.3 Automatic Dependent Surveillance-Broadcast

Current-day tracking of aircraft is performed using radar technology. With advancements in technology, new methods are envisioned in order to improve this process. An example

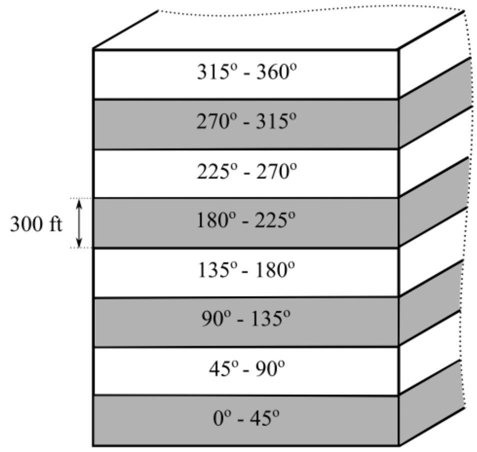

Figure 2.4: Layers structure as defined for the Metropolis Project [45]

of such a system is Automatic Dependent Surveillance-Broadcast (ADS-B). Specifically, ADS-B stands for:

- Automatic: without intervention of an operator, automatic process
- Dependent: retrieval of state information depends on other systems
- Surveillance: the information is used for the function of airspace surveillance
- Broadcast: data is transmitted to any ADS-B receiver in range

ADS-B is currently being enrolled to replace the Secondary Surveillance Radar (SSR) for manned aviation. Using navigation systems such as Global Navigation Satellite Systems (GNSS) or the Flight Management System (FMS), aircraft determine their own state information and share this using the 1090 MHz extended squitter link (ADS-B Out) [13]. This enables the use of more precise and more frequently updated surveillance information. Furthermore, aircraft with ADS-B receivers can get information of other aircraft in the area, as well as flight information service notifications (ADS-B In). Other messages transmitted using ADS-B technology include the aircraft identification number, operational status, but also flight information service messages from ground stations [43, 13].

Direct reception of state information from aircraft in the neighborhood allows for decentralized traffic management, where each aircraft separately performs the task of airspace surveillance. Although data can be transmitted at high rates, ADS-B has some limitations which could potentially impose constraints on the use of this technology in very dense UAV airspace. Langejan et al. (2016) [31] investigated the effects of system and situation related limitations, like measurement accuracy and signal interference, on the performance of airborne conflict detection and resolution systems used for decentralized traffic management in manned aviation. No direct implications were found for the feasibility of self-separation, but interference effects become significant with increasing airspace density. Furthermore, the study mentions a GPS accuracy of $\leq 7.8m$ on a 95% confidence interval. Using a minimum required horizontal separation of 50 m (based on a previous study [27]), this deviation can reach up to 15% of the required separation. For manned aviation, which typically has to stay 5 NM apart, this percentage would only be 0.08%.

Although the use of ADS-B in UAV airspace should be more carefully examined, this is considered out of scope for this research. Therefore, this study assumes ADS-B will be fully available for self-separation of UAVs, enabling all necessary data to be transmitted instantly to any receiver in the airspace.

2.3 Conclusions

The following conclusions can be drawn from the literature review on UAV airspace:

- Several research projects exist to enable future UAV airspace. Examples are the U-Space project in Europe and UTM in the United States.
- The concept of geovectoring is proposed to be added as a component of the Dynamic Capacity Management service in U3.
- Research has been performed on expected use of future UAV airspace, as well as expected airspace density figures. UAVs will be utilized for military, government and commercial, and leisure applications.
- Density of parcel delivery drones for the Île-de-France region range from 9.7 UAVs/NM^2 to 14.8 UAVs/NM^2 by 2035. For 2050, these numbers increase to 11.1 UAVs/NM^2 to 25.2 UAV/NM^2.
- The expected airspace density of food delivery drones in the Île-de-France region ranges from 6.1 UAVs/NM^2 to 9.3 UAVs/NM^2 in 2035. In 2050, the expectations increase to 7.0 UAVs/NM^2 to 15.8 UAVs/NM^2.
- Next to the previously mentioned UAVs, 4% of the population of the Île-de-France region is expected to make use of PAVs by the year 2050. Since these manned aircraft will be larger and rely on a fixed-wing structure (with higher airspeeds than quadcopters), it is expected they will make use of a different flying altitude. This type of aircraft is not included in the current study for simplicity, only one type of quadcopter UAV will be involved in the simulation experiments proposed in Chapter 6.
- In previous research, it was found that a layered airspace concept is optimal for urban airspace in terms of airspace capacity, safety, and route efficiency metrics. In this concept, the airspace is divided into vertically stacked layers of a fixed height, each allowing aircraft to fly in a different heading range. This concept will be considered in the current study.
- ADS-B allows aircraft to directly receive surveillance data from aircraft in the neighborhood. This allows for decentralized traffic management. Although some limitations can occur with state measurement accuracy and signal interference at high airspace density, the current study assumes aircraft can instantly receive all necessary surveillance data noise-free from all aircraft in the airspace.

Chapter 3

Conflict Detection & Resolution

Since UAVs are unmanned and are expected to operate in very crowded airspace, it is expected that they will be equipped with automatic Conflict Detection and Resolution (CD&R) systems. Over the past decades, research has been performed into several CD&R methods for use in both manned and unmanned aviation. The chapter starts by introducing the concept of CD&R methods, as well as existing taxonomy to categorize them Section 3.1. Afterwards, the most commonly used CD&R methods for UAVs are considered. Velocity obstacle based methods are described in Section 3.2. A method for non-moving (static) obstacle avoidance is presented in Section 3.3. Section 3.4 describes a voltage potential based method. Finally, conclusions are given in Section 3.5.

3.1 CD&R taxonomy

In order to understand the fundamental principle behind CD&R methods, its definition should be clarified. To start, CD&R comprises two processes, namely *conflict detection* and *conflict resolution*. Both are aimed at handling conflicts between vehicles. The definition of a conflict, together with other relevant definitions, are given below.

Definition 4. **Protected Zone (PZ):** A virtual 3-dimensional area around a vehicle, which should not be entered by other vehicles, in order to maintain a safe separation distance [11]. Dimensions of the area can differ per vehicle and phase of flight. For aircraft, the PZ usually looks like a 3-dimensional disc with radius equal to the minimum required horizontal separation S_h and height equal to twice the minimum required vertical separation S_v. An illustration of the PZ is given in Figure 3.1 and Figure 3.2.

Definition 5. **Closest Point of Approach (CPA):** A point on the trajectory of a vehicle which corresponds to its location when it is closest to another vehicle passing by.

Definition 6. **Loss of Separation (LoS):** A situation in which two or more vehicles pass each other through their PZ, meaning the CPA lies within the PZ of the vehicles [31].

Definition 7. **Lookahead time:** The time between a conflict warning is issued and first instant at which LoS will occur [32].

Definition 8. **Conflict:** A predicted future LoS, which will occur within a specified lookahead time [38].

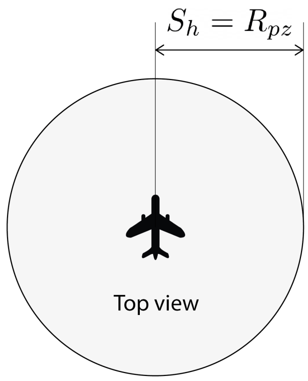

Figure 3.1: Top view of the Protected Zone, indicating the minimum horizontal separation S_h. A commonly used term for horizontal separation is the protected zone radius, R_{pz}.

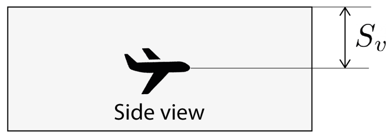

Figure 3.2: 3-D side view of the Protected Zone, indicating the minimum vertical separation S_v.

With regard to the description of a conflict given above, the two processes covered by a CD&R method can be explained as given hereafter. In these descriptions, the term *ownship* refers to the vehicle executing the CD&R process and the term *intruder* relates to another vehicle which is in conflict with the ownship.

- **Conflict Detection (CD)**: The process of determining whether the ownship is in conflict with one or more intruders.
- **Conflict Resolution (CR)**: The process of determining and executing a maneuver or set of maneuvers which are aimed at resolving the conflict or set of conflicts.

Over the past decades, a large amount of research has been published about possible implementations of CD&R methods in current day and future airspace. Nevertheless, these publications vary widely in terms of the approach that should be taken. In order to compare these methods, several review articles have been created, including frameworks to categorize them. Two decades ago, Kuchar et al. (2000) [30] did this for research on CD&R methods for manned flight. More recently, Jenie et al. (2017) [28] have created a framework for CD&R specifically tailored towards UAVs. This framework is based on the multi-layered CD&R architecture for manned flight, in which several layers of safety are defined based on the time to collision [5]. Furthermore, Ribeiro et al. (2020) [37] reviewed a large number of CD&R methods and created an elaborate framework that can be used to categorize CD&R methods for both manned and unmanned aviation.

In the framework from Ribeiro et al. (2020), classification of methods is performed using 10 categories in total, 3 of which are used for the conflict detection process and 7 for the conflict resolution process. The framework is presented in Table 3.1. The table indicates how the Modified Voltage Potential (MVP) CR method can be categorized, which is introduced later in the chapter.

Table 3.1: CD&R Method Taxonomy for both Manned and Unmanned Aviation [37]

Surveillance**	***Trajectory Propagation*****	***Predictability Assumption*****	**Control**	**Method Categories**
Centralized Dependent Distributed Dependent Independent	State-Based Intent-Based	Nominal Probabilistic Worst-Case	Centralized Distributed*	Exact Heuristic Prescribed Reactive* Explicitly Negotiated

Multi-Actor Conflict Resolution	**Avoidance Planning**	**Avoidance Maneuver**	**Obstacle Types**	**Optimization**
Sequential Concurrent Pairwise Sequential Pairwise Summed* Joint Solution	Strategic Tactical* Escape	Heading* Speed* Vertical* Flight Plan	Static Dynamic* All	Flight Path* Flight Time Energy Consumption

*Taxonomy conform with the MVP method
***Conflict detection category*

The **surveillance** category for conflict detection indicates the way surveillance data is gathered, necessary to gain awareness of surrounding traffic and objects. Three options are identified. With Centralized Dependent Surveillance, data is gathered by a central system on the ground. Distributed Dependent Surveillance relies on aircraft directly sharing data between each other, such as with the ADS-B system. If Independent Surveillance is implemented, no communication is performed and each aircraft gathers its own data using on-board equipment.

Trajectory propagation concerns the way of estimating future positions of aircraft, used to check if two or more aircraft are in conflict. Trajectory propagation can be State-Based or Intent-Based. The former relies on linear extrapolation of the current state of a vehicle (position and velocity vector), while the latter assumes a vehicle will follow its intended trajectory which is not necessarily a straight line.

The **predictability assumption** category classifies methods based on the level of uncertainty that is considered in the conflict detection process. If no uncertainty is incorporated at all, a method is classified as Nominal. In increasing order, the Probabilistic and Worse-Case Predictability Assumption do take into account uncertainty in the trajectory propagation of a vehicle. This results in the conflict detection system considering more possible trajectories.

The first category for conflict resolution, **control**, comprises how decisions are made in the conflict resolution process. In Centralized Control, a central unit such as an ATC center is responsible for making decisions on separation management and communicating them to the appropriate aircraft. The central unit tries to find a global optimum for the conflict resolution process. On the contrary, in Distributed Control this task is distributed to the individual aircraft without involvement of a centralized system.

Method categories indicates to a further extent how the conflict resolution process is performed. Five categories are identified: Exact, Heuristic, Prescribed, Reactive, and Explicitly Negotiated. The first two correspond with a Centralized Control strategy, the latter three with Distributed Control. The algorithm used to find a global optimum in Centralized Control can be Exact, hence searching until it finds the best solution. For a Heuristic algorithm, it also satisfies to return a sub-optimal solution, which is not the most optimal but can save time on the computation process. A Prescribed method relies on implicit coordination, through a set of previously determined rules. Similarly, a Reactive method uses implicit coordination, but in this case the resolution strategy depends on the geometry of the conflict. Finally, Explicitly Negotiated methods rely on communication between the vehicles in conflict. They negotiate until a solution is found that satisfies all.

The **multi-actor conflict resolution** category indicates how conflicts are handled if more than two vehicles are involved. Sequential and Concurrent handling of conflicts can be used in a Centralized Control strategy. The former sequentially solves conflict pairs (between two vehicles), the latter solves all conflicts at once. For a Distributed Control strategy, three options exist. Pairwise Sequential Conflict Resolution is similar to the Sequential method mentioned before. In a Pairwise Summed method, one single resolution maneuver is found by summing the separate resolution vectors of each conflict pair. Finally, a Joint Solution can be found by similarly considering all intruders and finding a single maneuver that solves all conflicts at once.

Avoidance planning relates to the timescale in which action is undertaken to solve a conflict. Firstly, Strategic Avoidance Planning relies on acting tens of minutes or even hours before LoS, resulting in a significant change of the trajectory of a vehicle. Secondly, Tactical Planning (also called 'detect and avoid') typically occurs several minutes before LoS. Deviation of the trajectory is smaller, but the required maneuver (e.g. heading change) is larger. Finally, an Escape maneuver is executed seconds before collision.

The **avoidance maneuver** can be obtained by varying one or more states of the vehicle. Combinations can be made of a Heading change, Speed change, and Vertical (altitude) change. Furthermore, the Flight Plan of a vehicle can be adapted to change its future trajectory.

CD&R methods can be designed for different **obstacle types**. These can be Static, which are stationary objects such as buildings, or Dynamic, e.g. other vehicles in the airspace. Some methods can also be used for both types simultaneously, these are classified as being able to handle All obstacles.

Finally, several types of **optimization** exist which aim to increase the efficiency of a method. CD&R methods can be designed such that they minimize Flight Path, Flight Time, or Fuel/Energy Consumption of a vehicle.

3.2 Velocity Obstacle Based Methods

Fiorini et al. (1998) [17] designed a method to visualize conflicting velocities using the so called Velocity Obstacle (VO). A VO represents a set of velocities which would result in a future LoS with another aircraft [16], given a certain lookahead time for conflict detection. The construction of a velocity obstacle is visualized in Figure 3.3.

Let the ownship be at position denoted with vector $\mathbf{x}_{own}$ and intruder at position $\mathbf{x}_{int}$. The velocity of the ownship relative to the intruder, denoted by $\mathbf{V}_{rel}$ can be computed using Equation 3.1. A collision cone (CC) can be constructed which contains all relative velocities that would result in a predicted LoS within the lookahead time t_{LA}. This cone originates at the ownship and is defined by the area between the two lines that are tangent to the protected zone of the intruder. The latter is represented by a circle around the intruder position with radius R_{pz}.

$$\mathbf{V}_{rel} = \mathbf{V}_{own} - \mathbf{V}_{int} \tag{3.1}$$

All relative velocities that point trough the intruder protected zone yield LoS in the future, but the time to LoS depends on its magnitude. As the relative velocity approaches the tip of the CC, the time to LoS increases to infinity. Since a finite lookahead time is used for conflict detection, denoted by t_{LA}, a certain region at the tip of the CC describes relative velocities with time to LoS larger than the lookahead time. These velocities are, by definition, conflict free at the moment of constructing the CC and can therefore be excluded as explained hereafter.

Let the vector $\mathbf{d}$ with magnitude d denote the distance from the ownship to the intruder (as indicated in Equation 3.2). By dividing the distance over the specified conflict detection lookahead time (which yields a velocity) and scaling the protected zone of the intruder by the same amount (also resulting in a set of velocities), the boundary of all velocity vectors leading to LoS within this timeframe can be determined [50]. These are illustrated in grey in figure Figure 3.3.

In order to obtain the VO, which indicates all absolute conflict free ownship velocity vectors, the CC is translated by the intruder velocity (which follows logically from Equation 3.1). As is illustrated in the figure, the current ownship velocity would result in LoS within the lookahead time t_{LA}, since it coincides with the VO.

Ellerbroek (2013) [10] describes a velocity obstacle using three unit vectors. Let $\mathbf{n}_d$ be the first unit vector which points from the ownship position towards the intruder position (Equation 3.2). The second and third unit vector, describing the tangent lines of the collision cone, can subsequently be computed as provided in Equation 3.3 using the rotational matrix R given in Equation 3.4 [10]. Finally, adding the intruder velocity vector to the collision cone tangent unit vectors yields a description of the velocity obstacle for absolute velocities.

$$\mathbf{n}_d = \frac{\mathbf{d}}{d} = \frac{\mathbf{x}_{int} - \mathbf{x}_{own}}{||\mathbf{x}_{int} - \mathbf{x}_{own}||} \tag{3.2}$$

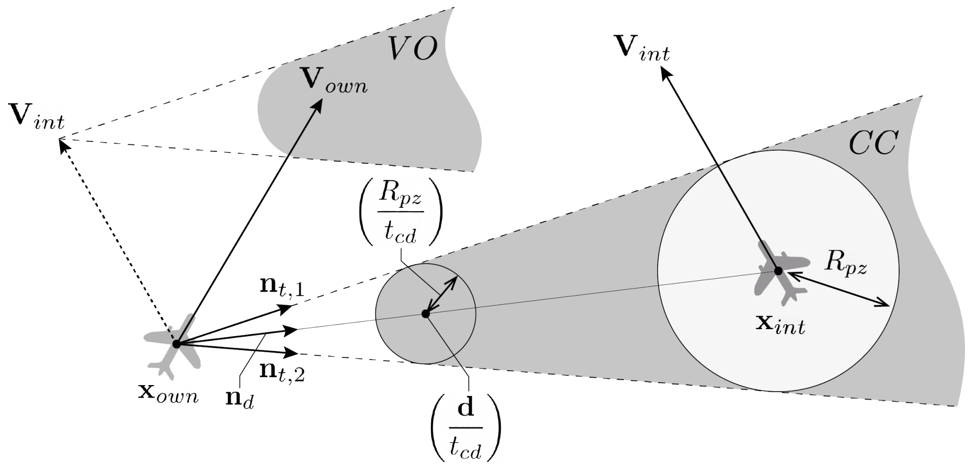

Figure 3.3: Illustration of the Collision Cone (CC) and the Velocity Obstacle (VO) [50] [10]

$$\begin{aligned} \mathbf{n}_{t1} &= R\mathbf{n}_d \\ \mathbf{n}_{t2} &= R^T\mathbf{n}_d \end{aligned} \tag{3.3}$$

$$R = \begin{bmatrix} \sqrt{1-\left(\frac{R_{pz}}{d}\right)^2} & \frac{R_{pz}}{d} \\ -\frac{R_{pz}}{d} & \sqrt{1-\left(\frac{R_{pz}}{d}\right)^2} \end{bmatrix} \tag{3.4}$$

Due to the rotational symmetry of the problem, the VO as seen from the intruder perspective (not illustrated in the figure) is actually rotationally symmetric to the VO from the ownship perspective (illustrated in Figure 3.3). Obviously, this VO originates at the tip of the ownship velocity vector drawn from the intruder position.

Since conflict detection and resolution relies on the manipulation of velocity vectors, a commonly used method is to visualize all velocities which would yield a conflict free solution. This method was first explored by Hermes et al. [19] in order to estimate the workload for air traffic controllers (ATCOs) in situations where horizontal traffic flows have to be merged. It relies on construction of the so called Solution Space Diagram (SSD). More research has been performed into possible use of the SSD as a workload *estimation* tool. Furthermore, Mercado Velasco et al. (2010) [35] investigated the possibilities of using the SSD as a workload *alleviating* tool for ATCOs, in order to aid them in the decision making process. This use of the SSD was further explored by Balasooriyan (2017) [2], who concretized and tested the SSD as a CD&R method for horizontal traffic scenarios.

The layout of the SSD is shown in Figure 3.4. Let the set of Reachable Velocities (RV) be defined by the area between the circles denoting the minimum and maximum velocity of a vehicle, V_{min} and V_{max} respectively. It can be mathematically represented by Equation 3.5 [2], using x and y as coordinates to denote velocity in the easterly and northerly direction.

A separate velocity obstacle (VO) is constructed for each intruder with protected zone (PZ), as described in Section 3.2. Note that the tips of the VOs indicated in Figure 3.4 are not cut off for simplicity. Since the i-th velocity obstacle represents all forbidden velocities for the i-th conflict, the set of all Forbidden Velocities (FV) for N conflicts is composed of the union of all Velocity Obstacles (Equation 3.6 [2]).

The set of Forbidden Reachable Velocities (FRV) and Allowed Reachable Velocities (ARV) can be subsequently determined from the definitions given above. They are represented by Equation 3.7 and Equation 3.8, respectively [2]. The former is illustrated by the union of grey areas (velocity obstacles) in Figure 3.4, the latter by the white area encircled by the circles denoting the minimum and maximum ownship velocity. Using the SSD, it is possible to simultaneously find a joint solution for all conflicts encountered by the ownship. In fact, any velocity chosen in the set of ARV can be considered a solution.

$$RV = \{(x,y) \in \mathbb{R}^2 | \mathrm{x}^2 + \mathrm{y}^2 \geq \mathrm{V}_{\mathrm{min}}^2, \mathrm{x}^2 + \mathrm{y}^2 \leq \mathrm{V}_{\mathrm{max}}^2\} \tag{3.5}$$

$$FV = \bigcup_{i=1}^{N} VO_i \tag{3.6}$$

$$FRV = FV \cap RV \tag{3.7}$$

$$ARV = FV^C \cap RV \tag{3.8}$$

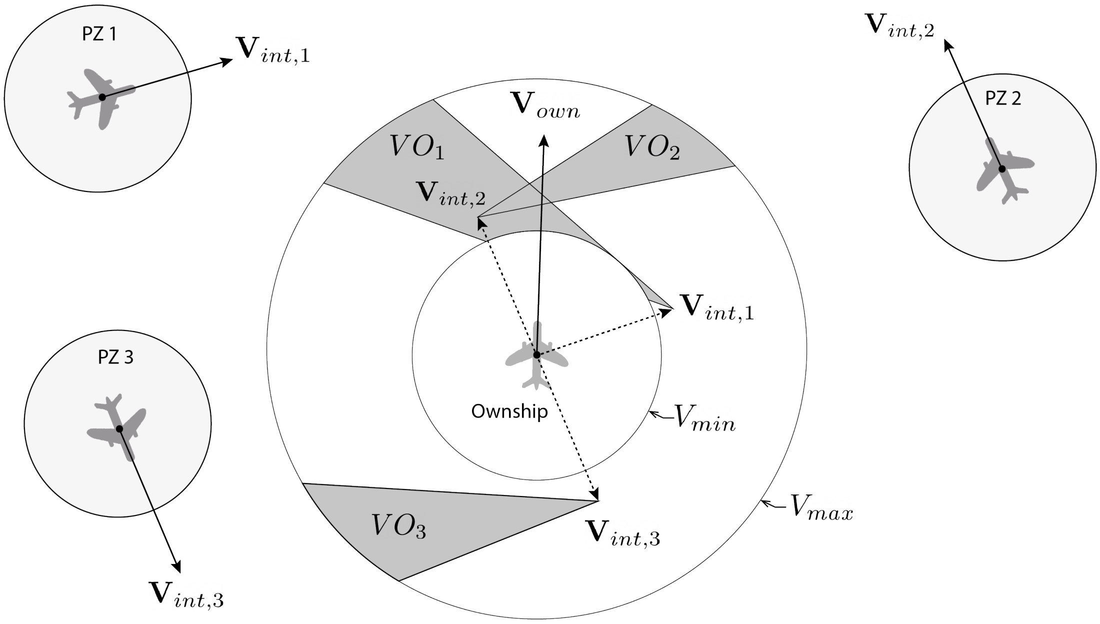

Figure 3.4: Layout of the Solution Space Diagram (SSD)

Although the method of finding a joint solution for all conflicts appears very efficient, it can occur that the union of velocity obstacles covers the entire set of reachable velocities.

In this case, no conflict resolution maneuver can be determined at all using the SSD. Other methods, like the Modified Voltage Potential, avoid this problem by relying on pairwise summed multi-actor conflict resolution. Nevertheless, the SSD can be considered a powerful tool for visualization of the maneuvering possibilities of aircraft.

3.3 Static Obstacle Avoidance Using Collision Cones

Next to dynamic obstacles, like other aircraft, conflicts can occur with static obstacles as well. These can include avoiding buildings, terrain, or prohibited airspace. In order to derive forbidden velocities which would result in a collision, a collision cone (CC, previously explained in Section 3.2) can be constructed for the static obstacle. Any ownship velocity outside the CC can be chosen to resolve the conflict and avoid collision. An example of such a CC for a static obstacle is given in Figure 3.5. The unit vectors $\mathbf{n}_{t,1}$ and $\mathbf{n}_{t,2}$ describe the legs of the CC.

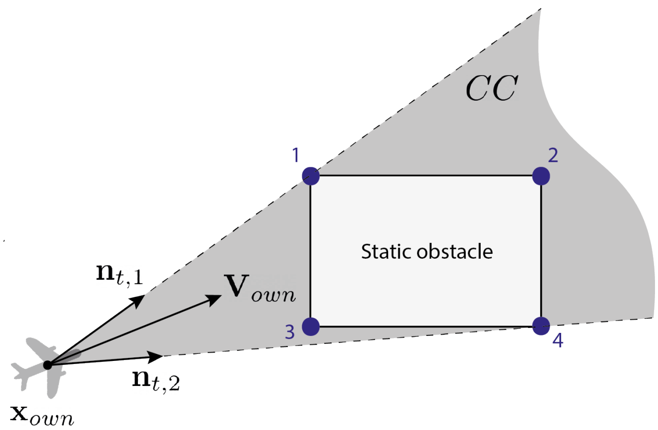

Figure 3.5: Collision Cone for a static obstacle

The CC for a rectangular obstacle, such as the one given in the figure, is relatively straightforward to derive. Chakravarthy et al. (1998) [4] describe a method for the derivation of a CC for irregularly shaped objects. However, if it is assumed that all static obstacles encountered will be in the form of a polygon, the derivation process can be simplified. A polygon has a clearly defined set of vertices. The legs of the CC will coincide with the two outermost vertices as seen from the perspective of the ownship (1 and 4 in the example figure). Checking all vertices allows for the derivation of the CC legs. Subsequently, the aircraft's heading can be altered in order to reach the nearest leg. This method was employed by Jacobse (2020) [26] in his master's thesis and can be used in the current study as well.

3.4 Modified Voltage Potential

The Modified Voltage Potential (MVP) is a tactical conflict resolution (CR) method which allows for decentralized traffic management. The method, descibed by Hoekstra et al. (2001) [22], is based on the comparison of aircraft with charged particles that repel each other away from their CPA [9]. By computing the amount of intrusion at CPA and dividing this *distance* by the *time* left until the CPA is reached, a resolution *velocity* can be determined in both the horizontal and vertical dimension. Aircraft involved in a conflict separately compute a resolution maneuver, which follows implicitly from the conflict geometry. Each conflict encountered by the ownship is treated separately, yielding a single resolution maneuver for that specific conflict. Resolution vectors are summed in case of multi-aircraft conflicts, according to the pairwise summed method presented in Section 3.1.

Ribeiro et al. (2020) [37] showed that the MVP algorithm scores best on the efficiency and safety metrics. Another study by Balasooriyan et al. (2017) [2] directly compared the MVP method to the SSD method for manned aviation. Balasooriyan showed that the MVP method scores better on safety, efficiency, and airspace stability metrics. The MVP method, feasible for autonomous CR for UAVs, is therefore chosen as nominal conflict resolution method in the current study.

The MVP method allows for the separate calculation of resolution maneuvers in the horizontal and vertical plane. These are presented in Subsection 3.4.1 and Subsection 3.4.2, respectively. Both maneuvers can be combined into a 3D resolution vector, where the indices $(1, 2, 3)$ represent the portions of the resolution vector along the three axes in the Cartesian coordinate system presented in Section A.1 (Part III, Appendix A). Adding this resolution vector to the ownship velocity vector allows for conflict resolution. A choice can be made to either solve the conflict in the horizontal or the vertical plane, or to use the combination of both stored in the resolution vector.

In case of n simultaneous conflicts, n resolution vectors can be determined for each conflict. Afterwards, all conflict resolution vectors are summed with the initial ownship velocity to determine a new ownship velocity for conflict resolution ($\mathbf{V}_{own,mvp}$, Equation 3.9), according to the pairwise summed method described in Section 3.1. Doing this ensures that complex conflict situations can be solved through the interaction of the resolution behaviour of each separate aircraft. For more information, the reader can refer to the "super conflict" and "wall" scenarios presented in [24].

$$\mathbf{V}_{own,mvp} = \mathbf{V}_{own} + \sum_{i=1}^{n} \mathbf{V}_{r,mvp_i} \tag{3.9}$$

3.4.1 Horizontal Resolution Maneuvers

Figure 3.6 shows an arbitrary conflict in the horizontal plane and illustrates the vectors necessary for the computation of the horizontal MVP resolution vector. The velocity of the ownship *relative* to the intruder ($\mathbf{V}_{rel}$) can be determined using Equation 3.1. The flight path of the ownship relative to the intruder is the extension of the relative velocity

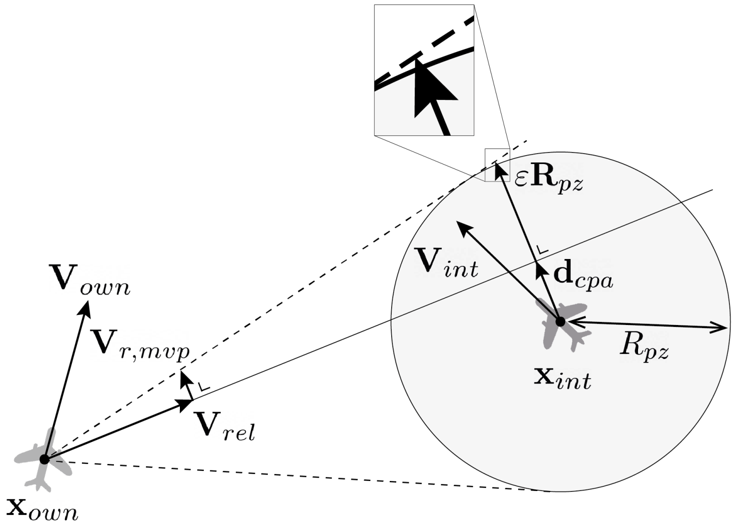

Figure 3.6: Illustration of MVP resolution maneuver mapped onto the horizontal plane

vector. Since the ownship will pass through the PZ of the intruder in the future, LoS will occur. The horizontal closest point of approach (CPA) on this relative flight path is located at $(\mathbf{x}_{int} + \mathbf{d}_{cpa})$. The latter vector in this sum indicates the distance at CPA.

The horizontal portion of the resolution vector, $\mathbf{V}_{r,mvp}(1,2)$, represents the required state change to solve the conflict, hence "push" the horizontal CPA to the edge of the PZ. This vector is computed using Equation 3.10 [22]. In this equation, t_{cpa} represents the time until the CPA is reached. The vector $\varepsilon\mathbf{R}_{pz}$ points in the same direction as $\mathbf{d}_{cpa}$, which is perpendicular to the relative velocity $\mathbf{V}_{rel}$. In order to solve the conflict it should touch the tangent of the collision cone (refer to Figure 3.3). As is illustrated in the magnified portion of Figure 3.6, its magnitude will be slightly larger than the radius of the protected zone R_{pz}. This is indicated by the factor ε, which is computed using Equation 3.11 [22]. In this equation, d_{cur} represents the current distance between the ownship and the intruder and d_{cpa} represents the magnitude of the distance vector at horizontal CPA.

$$\mathbf{V}_{r,mvp}(1,2) = \frac{\varepsilon\mathbf{R}_{pz} - \mathbf{d}_{cpa}}{t_{cpa}} \tag{3.10}$$

$$\varepsilon = \frac{1}{\left|\cos\left(\arcsin\left(\frac{R_{pz}}{d_{cur}}\right) - \arcsin\left(\frac{d_{cpa}}{d_{cur}}\right)\right)\right|} \tag{3.11}$$

The maneuver computed using Equation 3.10 assumes that the intruder does not perform any heading or speed change. Nevertheless, it can be expected that the intruder will perform a conflict resolution maneuver as well. As is the case for velocity obstacles, the resolution maneuver computed by the intruder is equal but opposite to the maneuver computer by the ownship. This is due to the rotational symmetry of the conflict geometry. Therefore, it actually suffices if both actors only execute half of the maneuver they computed. This allows for a cooperative resolution strategy without excessive maneuvering.

3.4.2 Vertical Resolution Maneuvers

A resolution maneuver based on a change in vertical speed can be computed as well, as is explained by Hoekstra (2001) [22]. A distinction can be made between two cases: the relative vertical speed between the two actors in the conflict can either be zero or nonzero.

In the former case, the amount of intrusion in the vertical plane is constant over time. Similar to the horizontal case, the vertical resolution speed ($\mathbf{V}_{r,mvp}(3)$) is found by dividing the amount of vertical intrusion by the time left until the first moment of LoS (denoted by t_{los}). The amount of vertical intrusion equals the required vertical separation S_v minus the difference between ownship altitude (alt_{own}) and intruder altitude (alt_{int}):

$$\mathbf{V}_{r,mvp}(3) = \frac{S_v - (alt_{own} - alt_{int})}{t_{los}} \tag{3.12}$$

In case of a nonzero vertical speed component of the relative velocity, the intervals for horizontal and vertical LoS do not coincide entirely (except if the relative vertical speed is very small). In this case, the time to CPA (t_{cpa}) is determined by considering the mid-point of the combined vertical and horizontal LoS interval. At this point, the altitudes of the ownship and intruder will be equal. Since the vertical intrusion equals S_v, the vertical resolution speed can be computed as follows:

$$\mathbf{V}_{r,mvp}(3) = \frac{S_v}{t_{cpa}} \tag{3.13}$$

3.5 Conclusions

The main conclusions drawn from the literature study performed on CD&R methods are:

- Extensive frameworks exist for the categorization of CD&R methods, which could be useful in the analysis of this current study. Many CD&R methods have already been investigated.
- Static obstacles can be avoided using a heading maneuver to the nearest leg of the collision cone (CC) corresponding to the obstacle.
- Two commonly investigated resolution methods for UAVs, Velocity Obstacle (VO) based methods and the Modified Voltage Potential (MVP), have been compared in previous research. The MVP method scored better on safety, efficiency, and stability metrics than the SSD. Furthermore, MVP is more effective in solving complex multi-aircraft conflicts. It will therefore be used as nominal CR method in the current study.

Chapter 4

Geovectors

It is important to investigate how future UAV airspace can enable the expected airspace densities, mentioned in Chapter 2. Challenges arise as these figures are not comparable to current-day situations in manned aviation. Novel mechanisms have to be invented to allow for this new type of airspace. Numerous research projects are already focused on tackling this matter. This chapter highlights a portion of this research that led to the development of the concept of geovectoring, a tool which can enable an increase UAV airspace capacity. Firstly, Section 4.1 explains the theory behind the concept. Secondly, Section 4.2 describes the concept of geovectors in further detail. Finally, Section 4.3 provides main conclusions of this chapter.

4.1 Airspace Capacity

A logic approach to facilitate the high number of drone operations is to aim at maximization of UAV airspace capacity. Hoekstra et al. (2018) [21] mention that this can be achieved by maximizing the safety and efficiency of an airspace. Furthermore, they explain that the conflict rate is a good metric for both these properties, which therefore is a good indicator for the capacity of an airspace.

If decreasing the conflict rate is proportional to increasing airspace capacity, how is a reduction in conflict rate achieved? According to Hoekstra et al. (2000) [24], the global conflict rate in the entire airspace can be calculated as follows:

$$CR_{global} = \frac{1}{2}N(N-1)p_2 \tag{4.1}$$

In this equation, CR_{global} represents the global conflict rate, N refers to the number of aircraft in the airspace, and p_2 is the average probability that two arbitrary aircraft in the airspace get in conflict. Furthermore, Hoekstra et al. (2016) [23] explain that the global conflict rate depends on the relative velocity of vehicles through the following relationship, where $\bar{V}_{rel}$ is the average relative velocity of all aircraft pairs and *const* is a constant:

$$p_2 = const \cdot \bar{V}_{rel} \tag{4.2}$$

Equation 4.1 and Equation 4.2 show that the global conflict rate depends on the amount of aircraft in the airspace, but also the relative velocity of these aircraft. This effect was noted by Sunil et al. (2015) [49] in the Metropolis project mentioned in Subsection 2.2.2. Assuming a layered airspace structure, use is made of the two effects that reduce the global conflict rate [21, 23]:

- **Segmentation**: separating aircraft in layers means they can not encounter a conflict with each other. Dividing the airspace into multiple zones converts Equation 4.1 to the following, where CR_{layer} is the average conflict rate per layer and L represents the number of layers [23]:

$$CR_{global,L} = L * CR_{layer}$$

$$CR_{layer} = \frac{1}{2}\frac{N}{L}\left(\frac{N}{L} - 1\right)p_2$$

  Combining the two equations above results in the global conflict rate for a layered airspace:

$$CR_{global,L} = \frac{1}{2}N\left(\frac{N}{L} - 1\right)p_2 \tag{4.3}$$

  Comparing Equation 4.1 with Equation 4.3 shows that segmentation (in this case by layers) can decrease the global conflict rate.

- **Relative speed reduction**: only allowing aircraft to fly in a certain direction lowers the average relative velocity of the vehicles. As explained by Hoekstra et al. (2016), the relative speed of two aircraft is proportional to their heading difference as follows [23]:

$$V_{rel} = 2V \sin\left(\frac{|\Delta hdg|}{2}\right) \tag{4.4}$$

  In this equation, V represents the average ground speed and $|\Delta hdg|$ the heading difference of two vehicles. Although this equation assumes that all aircraft fly at the same ground speed and will arrive at the same point at the same time, it illustrates how a decrease in heading difference can decrease the relative speed.

Hoekstra et al. identified that the segmentation effect is used by the concepts of geofencing and geocaging (explained in Chapter 2). In order to also benefit from the effect of relative speed reduction, a 3$^{\text{rd}}$ concept was created: geovectoring. It relies on partially aligning the velocity vectors of aircraft in the same segment of the airspace. The alignment is obtained by setting minimum and maximum limits on the allowed ground speed, course, and vertical speed. A practical explanation of this concept is provided in the next section.

In order to make optimal use of a the effect of relative speed reduction, Hoekstra et al. propose that use can be made of both *static* and *dynamic* geovectors. The former relies on pre-defined rules in a pre-defined area that are not subject to change. These can, for example, be implemented in an offline navigation system. The latter involves rules that can be adapted at any point in time by broadcasting them live to the relevant aircraft in a certain area of interest. The benefit is that use can be made of certain indicators, such as the instantaneous air traffic density, to only apply geovectors when and where necessary. Of course, this requires the use a broadcasting system, which is not required for static geovectors. Although dynamic geovectors are potentially useful in future airspace, the current study is limited to static geovectors for simplicity.

4.2 Concept of Geovectoring

As explained in the previous section, the concept of geovectoring can be used as a tool to reduce the relative velocity between aircraft in the same area. A geovector works by specifying allowed intervals on one or more of the three speed components of aircraft: ground speed, course angle, and vertical speed. The allowed intervals hold for all aircraft flying in the sector for which the geovector is specified. The sector can be represented by a series of (lat,lon) coordinates and altitudes (alt). The geovector can mathematically be represented by Equation 4.5, where the subscripts $_{min}$ and $_{max}$ represent the minimum and maximum limits of the allowed intervals, respectively:

$$\mathbf{V}_{geo} = \begin{Bmatrix} [GS_{min}, GS_{max}] \\ [\chi_{min}, \chi_{max}] \\ [VS_{min}, VS_{max}] \end{Bmatrix} = f(lat, lon, alt) \tag{4.5}$$

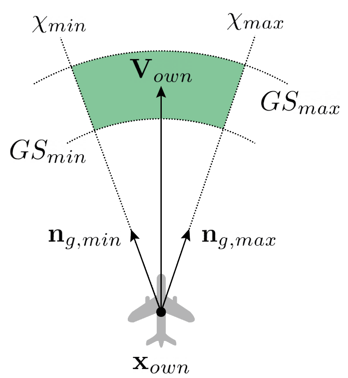

Figure 4.1: Top-view of geovector interval, in this case bound by the ground speed (GS) and course (χ) limits.

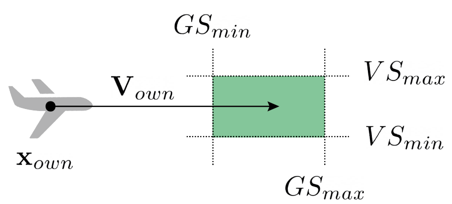

Figure 4.2: Cross-section of geovector interval, constrained by ground speed (GS) and vertical speed (VS) limits along the ownship velocity vector $\mathbf{V}_{own}$.

Figure 4.1 and Figure 4.2 present the visualization of the geovector limits in 2D velocity space from the horizontal and vertical (side-view) perspective. Ground speed limits are represented by the circles in Figure 4.1 centered at the ownship position $\mathbf{x}_{own}$ with radius equal to the magnitude of the limit. Next to ground speed, Figure 4.1 illustrates course limits as radials originating from the ownship position. Vertical speed limits are represented by the horizontal lines in Figure 4.2. In order to allow vector computations involving course limits, two unit vectors can be defined pointing in the direction of these radials: $\mathbf{n}_{g,min}$ and $\mathbf{n}_{g,max}$. Derivation of these vectors is provided in Appendix A (Part III) (Section A.2).

Finally, Figure 4.3 provides a categorization of all possible configuration types for geovectors in the horizontal plane, depending on whether a specific limit has been specified or not. These configurations are labeled 1-7 and can be used for the categorization of the experiment design in Chapter 6.

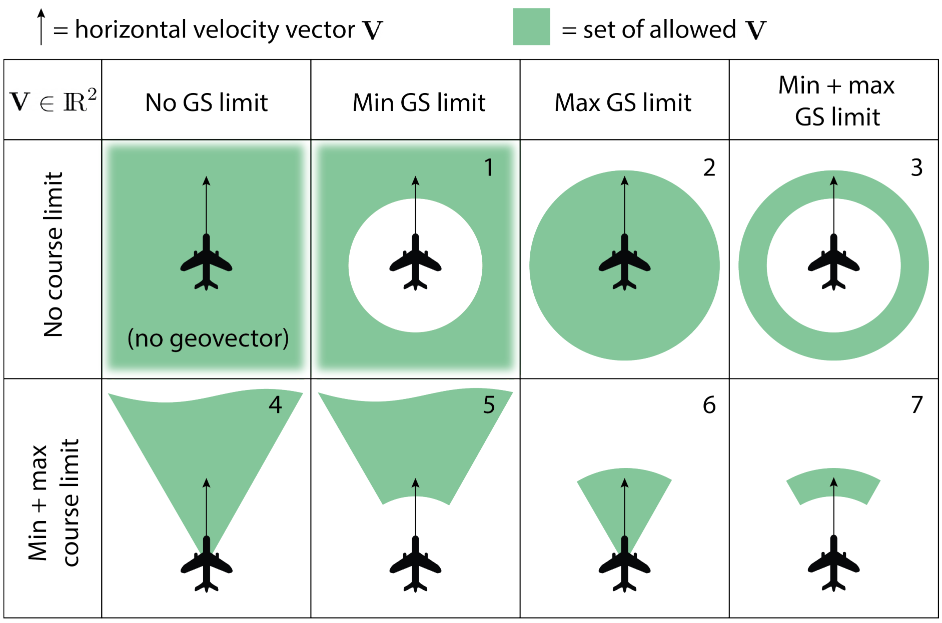

Figure 4.3: Categorization of all seven possible geovector configurations in the horizontal plane. Note that within each category, the shape of the geovector can differ, depending on the size of the intervals.

4.3 Conclusions

The main findings of this chapter are as follows:

- A decrease in conflict rate can lead to an increase in airspace capacity.
- While geofencing and geocaging can lower the conflict rate using the effect of segmentation, the concept of geovectoring aims to achieve this using relative speed reduction between aircraft.
- A geovector works by specifying minimum and maximum limits on the three components of a velocity vector: ground speed, course, and vertical speed. It is specified for a certain airspace section using (lat,lon) coordinates and altitude.
- Geovectors can be visualized in velocity space for analysis of the set of allowed velocity vectors.
- Static geovectors rely on pre-defined rules which are not subject to change. Dynamic geovectors can be adapted at any time to make optimal use of the concept. The latter would require a broadcast system to share the information with the aircraft in the sector. For simplicity, the current study is limited to the use of static geovectors.
- Many geovector configurations can be identified. A categorization was created for types of geovectors in the horizontal plane, depending on which limits are specified. This categorization can be used to differentiate between possible scenarios in the process of designing a simulation experiment.

Chapter 5

Combining Geovectors with CD&R

Both geovector rules and CD&R executing algorithms affect the velocity vectors of individual aircraft. Geovectors define a set of allowed velocity vectors, while CD&R algorithms compute necessary state changes to solve conflicts. Situations can arise in which the avoidance maneuver determined by the CD&R algorithm leads to a violation of one or more geovector limits. This chapter describes an alternative conflict resolution strategy, aimed towards preventing these situations.

The chapter is structured as follows. Firstly, Section 5.1 shortly describes the problem that occurs when combining conflict resolution maneuvers with geovectors. Secondly, Section 5.2 identifies the scope of this research and labels the proposed solution according to the CD&R taxonomy descibed by Ribeiro et al. (2020) [37]. Thirdly, the idea behind the proposed resolution method is presented in Section 5.3. This is followed by the description of how this resolution method can be incorporated into a decision scheme for uncooperative pairwise conflict maneuvers in Section 5.4. Afterwards, Section 5.5 indicates complications that arise when trying to adopt a cooperative resolution strategy, followed by a description of multi-actor conflicts in Section 5.6. Next, Section 3.3 describes how conflicts with static obstacles should be resolved. Finally, Section 5.8 concludes the chapter, combining all proposed resolution rules into an overall scheme.

5.1 Geovector Maneuvering Space

A problem occurs in the decision process when the computed resolution vector for an arbitrary conflict exceeds the available maneuvering space. In this context, let the available geovector maneuvering space for the ownship ($\mathbf{V}_{gms}$) be defined by Equation 5.1. Each interval represents the set of allowed changes in ground speed, course, and vertical speed within the geovector limits, given the current ownship velocity vector.

$$\mathbf{V}_{gms} = \mathbf{V}_{geo} - \mathbf{V}_{own} = \left\{ \begin{matrix} [GS_{min} - GS_{own}, GS_{max} - GS_{own}] \\ [\chi_{min} - \chi_{own}, \chi_{max} - \chi_{own}] \\ [VS_{min} - VS_{own}, VS_{max} - VS_{own}] \end{matrix} \right\} \tag{5.1}$$

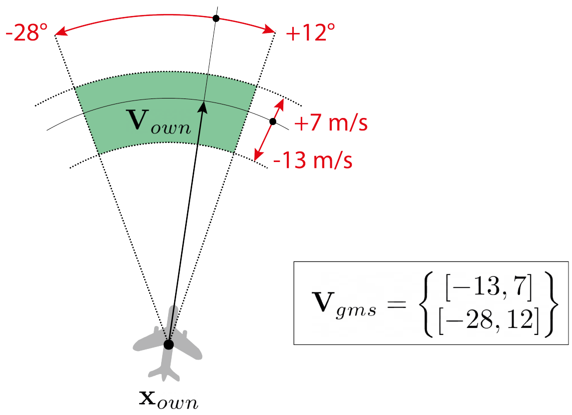

Figure 5.1: Illustration of an arbitrary set of geovector maneuvering space intervals in the horizontal plane

An example of the geovector maneuvering space in two dimensions is illustrated in Figure 5.1, indicating the lower and upper limits of the ground speed and course intervals in Equation 5.1. A similar image can be constructed for the vertical speed component (not shown).

5.2 Categorization of Solution

In previous research investigating the combined use of CD&R algorithms and geovectors in converging traffic flows [26], the CR maneuver was always given priority over the geovector rules in conflict situations. This ensured that conflicts could always be solved regardless of the limits imposed by the geovector. However, considering that geovectoring can be used as a tool to control traffic flows in UAV airspace, the assumption that the CD&R algorithm should always be able to violate the limits is not so straightforward. Frequent geovector violations lead to a reduction in the positive effects encountered from the relative speed reduction.

Solutions for the incorporation of geovector rules can be sought in both the conflict detection and conflict resolution process. Investigating the relationship between various conflict detection parameters and the rate at which geovector violations occur can provide insight into how the detection process can be adjusted in favor of the geovector. The scope of this research, however, is put on determining a different way to resolve the conflict in case nominal operation would in fact lead to a geovector violation.

According to the taxonomy proposed by Ribeiro et al. (2020) [37], CR methods can be classified into 5 categories. Assuming a distributed control strategy and implicit coordination, the "prescribed" and "reactive" methods remain as candidates for an alternative way of conflict resolution. The current study is limited to the investigation of a reactive method, relying on pairwise summed multi-actor conflict resolution. Conflict detection is performed using distributed dependent surveillance, relying on state-based trajectory propagation. This method is described in the remainder of this chapter.

5.3 The "GEO" Maneuver

Considering conflicts which only involve two actors at the same time, the process of determining an alternative horizontal resolution maneuver which satisfies the geovector constraints is relatively straightforward. Possible resolution maneuvers can be visualized in velocity space. An example conflict is illustrated in Figure 5.2. The ownship and intruder are represented by a dot on positions $\mathbf{x}_{own}$ and $\mathbf{x}_{int}$, respectively. They move with velocity $\mathbf{V}_{own}$ and $\mathbf{V}_{int}$. The velocity of the ownship relative to the intruder ($\mathbf{V}_{rel}$) can be computed by subtracting the intruder velocity vector from the ownship velocity vector (Equation 3.1). The vector denoting the distance at the horizontal closest point of approach is illustrated by $\mathbf{d}_{cpa}$. Since the magnitude of this vector is smaller than the radius of the protected zone, R_{pz}, a conflict exists.

Let the set of reachable velocities of the ownship (RV) be denoted by the area between the circles denoting the maximum (V_{max}) and minimum (V_{min}) ground speed (Equation 3.5). This set can further be subdivided into the sets of coordinated ("coord.") and uncoordinated ("uncoord.") velocities for this specific pair of aircraft. Uncoordinated resolution velocities would result in the ownship passing on the other side of the intruder, compared to if no maneuver was performed. In other words, any uncoordinated resolution vector would cross the dotted line denoting collision course with the intruder. This set ($U \in \mathbb{R}^2$) is illustrated in Figure 5.2.

Furthermore, the velocity obstacle ($VO \in \mathbb{R}^2$) represents the set of all possible ownship velocities which would result in future loss of separation. Its construction was explained in Section 3.2. The VO is represented by the grey area in the figure. On top of that, the illustration includes an arbitrary geovector, denoted by the green area in the figure ($G \in \mathbb{R}^2$). For the construction of geovectors, refer to Chapter 4.

Any ownship velocity vector which satisfies both the geovector rules and ensures coordinated conflict resolution is part of the set of geovector velocities, minus the union of the velocity obstacle and set of uncoordinated velocities. This subset of G is highlighted with a red border in the figure. Let any resolution vector (state-change), which results in the ownship velocity vector becoming part of this subset, be denoted by $\mathbf{V}_{r,geo}$. A mathematical expression is provided in Equation 5.2.

$$\mathbf{V}_{own} + \mathbf{V}_{r,geo} \in G \setminus (VO \cup U) \tag{5.2}$$

Sunil et al. (2017) [47] showed that the average conflict rate in an airspace increases with increasing average state-changes executed for conflict resolution. In order to minimize this effect, the resolution vector $\mathbf{V}_{r,geo}$ with the smallest possible magnitude should be chosen for resolution. Let this resolution be denoted by "GEO". Section A.3 (Part III, Appendix A) describes how this maneuver can be derived using the velocity obstacle.

Definition 9. **GEO maneuver:** Implicitly coordinated horizontal conflict resolution maneuver involving the smallest possible state change to simultaneously stay within the geovector limits and solve the conflict.

Including resolution maneuvers in the vertical plane makes the problem more complex. More extensive calculations are necessary to predict all suitable combinations of ground

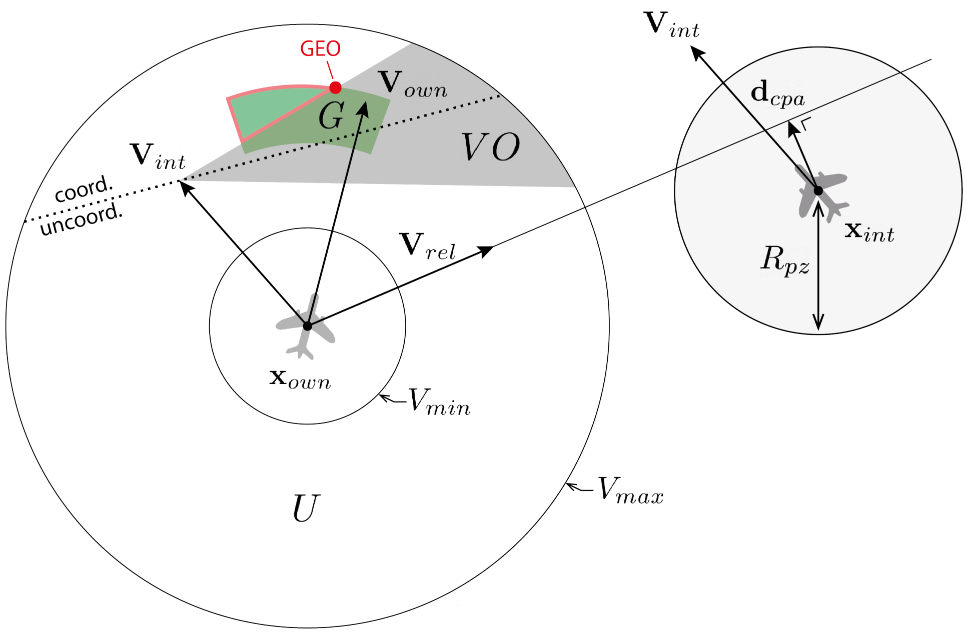

Figure 5.2: Illustration of the set of ownship velocities, in the horizontal plane, which both yield implicitly coordinated conflict resolution and satisfy the geovector constraints: $(G \setminus (VO \cup U))$. The corresponding "GEO" maneuver is indicated in red.

speed, course, and vertical speed for conflict resolution. This complexity follows to the disc-like shape of the PZ. Nevertheless, the assumption that vertical maneuvers will only involve a vertical speed change simplifies the problem. The required vertical conflict resolution speed can be computed as shown in Subsection 3.4.2. Two options exist: this speed either violates the vertical speed limit set by the geovector, or not. No alternative maneuver is considered for this dimension if vertical speed maneuvers are performed without considering a ground speed and/or heading change.

5.4 Uncooperative Pairwise Conflict Resolution

The GEO maneuver can be used as alternative for the horizontal MVP maneuver, in case the latter would cause a violation of one or more geovector limits. It can be incorporated into a decision scheme, which allows for the selection of the most optimal maneuver based on the geometry of the conflict. The scheme is shown in Figure 5.3. In the scheme, both horizontal and vertical maneuvers are considered. Using MVP as nominal CR method, both the horizontal and vertical MVP maneuver can be feasible (not leading to a geovector violation) or unfeasible (leading to a geovector violation). A distinction is made between three situations, depending on the feasibility of the MVP maneuver considering the geovector limits. The different maneuvers considered in each situation are shown on the right, where green means the geovector is not violated, while orange indicates a geovector violation. Ultimately, one of the maneuvers is chosen for the resolution of the pairwise conflict based on a set of decision criteria discussed hereafter.

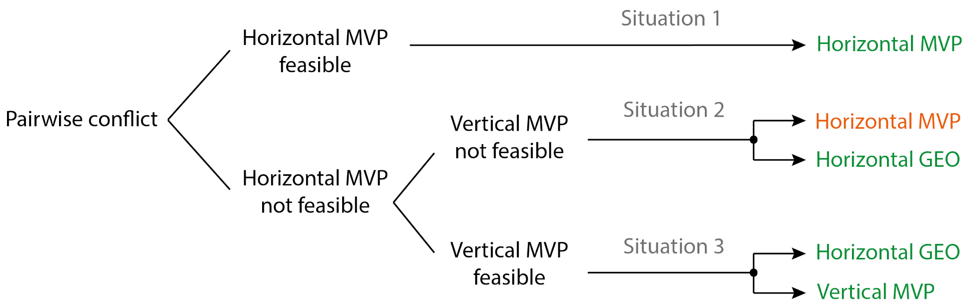

Figure 5.3: Decision scheme for horizontal and vertical resolution maneuvers in geovector airspace.

Situation 1

It is assumed that urban airspace will be layered, according to the findings of the Metropolis project [49]. Aircraft in cruising phase use a specific layer and ideally resolve conflicts horizontally within that layer. Therefore, whenever the horizontal MVP maneuver can be used without causing a geovector violation, this solution can be accepted.

Situation 2

In case both the horizontal and vertical MVP maneuver would result in a geovector violation, the GEO maneuver is considered. Depending on the maneuvering space within the geovector, this maneuver could be significantly larger in magnitude than the MVP maneuver. In order to prevent the geovector from significantly destabilizing the airspace, the GEO maneuver should only be selected if its magnitude does not exceed a certain threshold value. The reason for this consideration is the negative correlation between the average state change used for conflict resolution and the stability of the airspace [46]. The decision criterion can therefore be formulated as below, where f represents a scalar factor. If no GEO maneuver can be found, horizontal MVP will be used.

$$\texttt{CR strategy} = \begin{cases} \texttt{Horizontal GEO}, & \text{if } ||\mathbf{V}_{r,geo}|| \leq f \cdot ||\mathbf{V}_{r,mvp}(1,2)|| \\ \texttt{Horizontal MVP}, & \text{otherwise} \end{cases}$$

Situation 3

In case the vertical MVP maneuver is feasible within the geovector limits, it can be incorporated into the decision strategy. Nevertheless, assuming a layered airspace design, horizontal maneuvers are preferred over vertical ones in order to preserve airspace stability. The vertical MVP maneuver is therefore only used if the horizontal GEO maneuver would have a destabilizing effect as well. This is similar to situation 2, where the horizontal MVP maneuver is preferred if the GEO maneuver becomes too large. The only difference now is that instead of having to accept a horizontal solution which does not satisfy the geovector, the option exists to execute a vertical maneuver. The decision criterion is given below. If no GEO maneuver can be found for the conflict situation, vertical MVP will be used.

$$\texttt{CR strategy} = \begin{cases} \texttt{Horizontal GEO}, & \text{if } ||\mathbf{V}_{r,geo}|| \leq f \cdot ||\mathbf{V}_{r,mvp}(1,2)|| \\ \texttt{Vertical MVP}, & \text{otherwise} \end{cases}$$

Considering vertical maneuvers in a layered airspace would be performed into a resolution layer, an additional rule has to be added to perform the vertical maneuver. If both actors in a pairwise conflict were to simultaneously perform the vertical resolution maneuver into the same layer, the conflict would not be solved at all. In order to make sure the maneuver is only executed by one aircraft, a selection can be made based on the existing Standardised European Rules of the Air (SERA) [12, p.48]. These dictate which aircraft should perform an avoidance maneuver in case there is a risk of collision. Only allowing the aircraft which does not have right of way to perform the vertical maneuver results in the following logic:

- In case of *converging* trajectories, only the aircraft which has the intruder on its right is allowed to perform the vertical maneuver.
- In case of *overtaking* (same path), only the aircraft that is overtaking is allowed to perform the vertical maneuver.
- In case of *head-on* trajectories, no aircraft is allowed to perform the vertical maneuver. Although these situations are not expected to occur in geovector airspace, the logic can be implemented in the ruleset for consistency.

Differentiation between these types of trajectories is made based on the difference in heading between the two actors in the conflict. The same definition as used by Jenie et al. (2015) [27] is applied for the ruleset, shown in Figure 5.4.

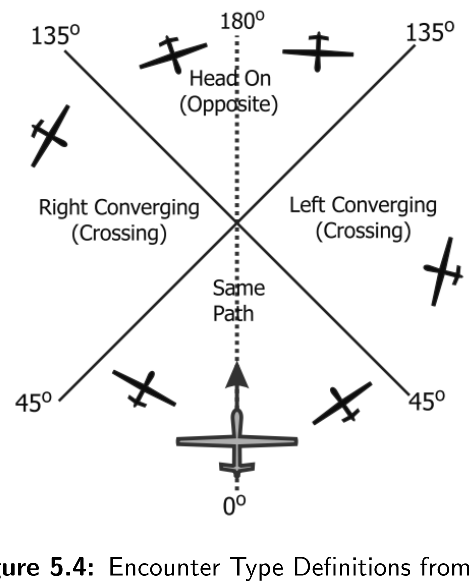

Figure 5.4: Encounter Type Definitions from [27]

5.5 Cooperative Pairwise Conflict Resolution

In case both aircraft simultaneously perform a resolution maneuver to solve a conflict, the resulting separation will be twice the required minimum. This can result in excessive maneuvering, which can have a negative effect on the airspace stability. Furthermore, if a smaller resolution maneuver is required per aircraft, the chances of violating a geovector limit are lowered. Therefore, it is interesting to analyze a possible resolution strategy for these kind of situations.

If it is safe to assume the intruder will also perform a maneuver, a cooperative resolution strategy can be applied. If both actors in the conflict perform 50% of their computed maneuver (or possibly a non-even distribution of weights), the conflict will still be solved. Although this strategy works well for MVP, some complications can arise when using the GEO maneuver.

Figure 5.5 sketches a situation in which performing 50% of the GEO maneuver, denoted by $\mathbf{V}_{r,geo}$ still leads to a geovector violation. The red arrow indicates where the ownship velocity vector would end up if only halve of the maneuver is performed. Although exaggerated for illustrative purposes, occurrence of these types of situations are theoretically possible when the GEO maneuver coincides with a minimum ground speed limit.

Furthermore, the resolution maneuver performed by the intruder will bring the leg of the VO closer to the ownship velocity vector. Therefore, the intersection with the geovector limit which corresponds to the GEO maneuver also shifts closer to $\mathbf{V}_{own}$, resulting in a smaller required resolution vector magnitude. Different calculations will have to be performed depending on whether the intruder is expected to perform maneuver or not.

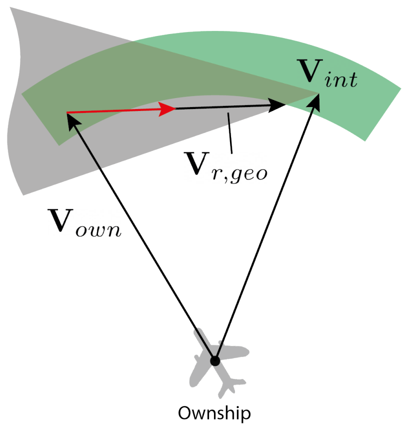

Figure 5.5: Theoretically possible situation in which performing 50% of the GEO maneuver denoted by $\mathbf{V}_{r,geo}$ still leads to a geovector violation, as opposed to performing the full maneuver.

Another possibility to prevent excessive maneuvering is the use of priority rules. In that case, only one aircraft will perform the entire maneuver. A simple implementation of such a strategy is to determine which aircraft has right of way according to the Standardised European Rules of the Air, which was presented in Section 5.4. Implementing this ruleset could be beneficial, as it is already widely known amongst aviators. Nevertheless, it does not take into account which vehicle has more maneuvering space to solve the conflict within the geovector limits. Priority rules could potentially be based on the geovector maneuvering space of the individual aircraft, which was presented in Section 5.1.

Although the question of cooperative resolution is interesting to consider, it is considered out of scope for the current study. Uncooperative conflict resolution could lead to more potential geovector violations, but this is actually beneficial when investigating the effectiveness of the GEO maneuver resolution strategy in these types of situations. Furthermore, the focus should be put on a more pressing topic, namely investigating how to deal with multi-aircraft conflicts. This is presented in the next section.

5.6 Multi-Actor Conflicts

Since the solution provided in Section 5.4 partially relies on performing alternative maneuvers, the behaviour of the system in case of multi-aircraft conflicts should be carefully examined. A multi-actor conflict occurs in case the ownship encounters conflicts with more than one intruder at once. Various methods to act in these situations have been previously investigated, as described in Section 3.1.

The benefits of the pairwise summed multi-actor CR method can be especially useful in future urban airspace, where large amount of aircraft are expected to simultaneously use the same section of airspace. This could potentially lead to multi-aircraft conflicts with many actors involved simultaneously. In order to be able to solve these conflicts, it is chosen to apply this method for the resolution strategy involving the GEO maneuver as well. Nevertheless, this could partially reduce the effectiveness of the resolution ruleset in obeying the geovector rules.

5.6.1 Pairwise Summed GEO

Although pairwise summing of resolution vectors works for the MVP maneuver, a problem arises when using this strategy for the GEO resolution method described in Section 5.4. Imagine the scenario depicted in Figure 5.6. The ownship encounters a conflict with intruder 1 and 2 simultaneously. Each conflict is evaluated separately, resulting in two resolution vectors for the GEO maneuver ($\mathbf{V}_{r,1}$ and $\mathbf{V}_{r,2}$). Both resolution vectors ensure the geovector is not violated when executed separately. Nevertheless, as shown on the right of the figure, summing them does in fact lead to a geovector violation.

Currently, no clear solution is found for this behaviour. Multi-aircraft conflict simulations of the proposed ruleset will be performed in order to investigate the frequency of geovector violations occurring due to pairwise summing. Recommendations can be made based on the observed behaviour in the simulations.

5.6.2 Pairwise Summed MVP

Opposed to the potential negative effects encountered when summing GEO resolution maneuvers, summing of multiple horizontal MVP resolution vectors can have a positive

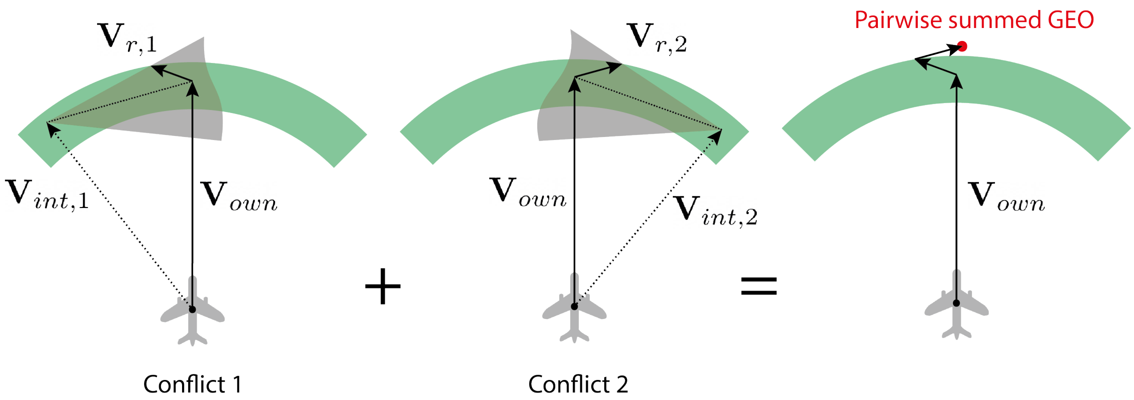

Figure 5.6: Example of a multi-aircraft conflict where pairwise summing of the individual GEO resolution vectors ($\mathbf{V}_{r,1} + \mathbf{V}_{r,2}$) still leads to a geovector violation.

effect. Imagine the ownship encounters two conflicts simultaneously, where both MVP resolution vectors would violate the geovector if they were executed individually. Now imagine both resolution vectors have approximately the same magnitude and act in opposite directions. The overall resolution maneuver found by summing these vectors will be relatively small, such that the geovector will not be violated after all. In this multi-aircraft conflict, it is not necessary to compute any GEO maneuver, saving on computation time and power.

In order to exploit this potential positive effect, the following logic should be added to the decision scheme given in Figure 5.3. Rather than first computing a resolution vector for each conflict based on the strategy provided in the scheme, a solution for each conflict should be computed using only horizontal MVP. Afterwards, it should be checked whether the pairwise summed solution violates the geovector. If this is not the case, the solution can be accepted before even considering an alternative maneuver for each separate conflict pair.

5.6.3 Vertical Maneuvers in Multi-Aircraft Conflicts

If the ownship is simultaneously overtaking two intruders, it could occur that the CR algorithm determines to resolve both pairwise conflicts using a vertical resolution maneuver. In this case, pairwise summation of the individual maneuvers leads to a vertical resolution speed which is larger than the required value. Although both vertical maneuvers separately satisfy the vertical speed limit of the geovector, this might not be the case after summation. In order to prevent the summation of vertical maneuvers, the following rule is added for the selection of the conflict resolution maneuver. Performing a second vertical resolution maneuver is not allowed when a first one is already active. This means that new conflicts detected while flying in the resolution layer can only be resolved horizontally. The aircraft is only allowed to revert back to the original layer after passing the CPA of the original conflict for which the vertical maneuver was performed.

5.7 Static Obstacle Avoidance and Decision Hierarchy

Airspace restrictions like geofences can limit the available space to solve a conflict. This can have a significant effect on the possibilities for solving conflicts within the geovector limits. This factor is especially interesting for this problem, as geovector rules are potentially useful for implementation in converging traffic flows like airspace corridor sections [26]. A method for static obstacle avoidance was previously presented in Section 3.3. A heading maneuver will be performed to reach the coordinated leg of the CC to prevent collision. After the maneuver is completed, the conflict can be regarded resolved.

In order to prevent geofence intrusions, this type of conflict will be given priority over conflicts with dynamic obstacles (i.e. other UAVs). This decision results in the decision hierarchy given in Figure 5.7, based on the method used by Jacobse (2020) [26]. The diagram states that if a conflict is detected with a static obstacle, the aircraft should solely focus on resolving this conflict first. Conflict resolution with other aircraft is only allowed after the heading maneuver is completed. Furthermore, following the nominal route by flying to the next waypoint is only allowed when a conflict-free situation arises.

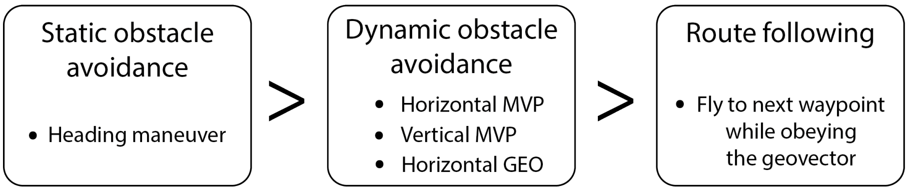

Figure 5.7: Decision hierarchy for the different types of maneuvers that can be performed, in order of importance, based on [26].

5.8 Conclusions

The individual rules necessary for a robust implicitly coordinated and uncooperative conflict resolution method in geovector airspace, presented throughout this chapter, can be combined into the following scheme. Upon detecting a conflict using state-based trajectory propagation, the following steps need to be executed:

1. If in conflict with a static obstacle, ignore all dynamic obstacles until the heading maneuver for the static obstacle is completed. If not, continue to step 2.

2. Check the pairwise summed solution for all conflicts if only horizontal MVP resolution vectors would be used. If this solution does not violate the geovector limits, it can executed to resolve the conflict. Otherwise, continue to step 3.

3. For each pairwise conflict:

   (a) Compute the horizontal GEO maneuver as explained in Appendix A (Part III). If the magnitude of the GEO maneuver is less or equal than f times the magnitude of the MVP maneuver ($||\mathbf{V}_{r,geo}|| \leq f \cdot ||\mathbf{V}_{r,mvp}(1,2)||$), where f represents a scalar value, the GEO resolution vector can be used for this conflict. , proceed to step 3b.

   (b) Check if the conflict situation allows the use of a vertical maneuver. This is the case if no other vertical maneuver is already executed and if the priority rules presented in Section 5.4 allow it. If not allowed, continue to step 3c. Otherwise, compute the vertical maneuver and check if it will lead to a violation the geovector limit. If this is not the case, the vertical MVP maneuver can be used. If not feasible, continue to step 3c
   (c) Select the horizontal MVP maneuver for resolution of this pairwise conflict.

4. Sum all solutions for the pairwise conflicts found in step 3 to find one overall resolution maneuver.

Chapter 6

Experimental Setup

In order to experimentally verify the effectiveness of the conflict resolution rules presented in Chapter 5, a series of simulations will be performed in the ATC simulator BlueSky. This chapter describes the experimental setup. Firstly, Section 6.1 describes the simulation environment. Secondly, Section 6.2 discusses the assumptions made in the simulation process. Afterwards, the general setup of the simulation scenarios, including the control variables, is discussed in Section 6.3. A list of metrics used to assess the performance of the proposed resolution ruleset is provided in Section 6.4. The proposed experiment consists of two parts, preliminary experiments presented in Section 6.5 and macro experiments given in Section 6.6. Hypotheses for both types of experiments are given in Section 6.7. Afterwards, Section 6.8 shortly discusses the relevance of the results. A research planning is given in Appendix B (Part III), including a Work Breakdown Structure and Gantt Chart to be able to keep track of the thesis progress. The Appendix includes a short description of all work packages which are identified.

6.1 BlueSky Simulator and OpenAP Performance Model

The simulation environment used for the experiments is the open source ATC simulator 'BlueSky', created in Python [20]. Its primary purpose is to allow ATM research to be more comparable, by providing a standard set of tools and data for research experiments. The simulator is open source and can be downloaded from GitHub [1].

BlueSky consists of several modules serving a different function. The two main functions are the simulation engine and the user interface. The user can give simulation commands in a format specially created for the BlueSky simulator ('TrafScript'). Scenarios can be created, allowing for the design of experiments. Data is vectorized in arrays, meaning that computations involving aircraft data can be performed for all aircraft at once. Data logs can be created, allowing the user to obtain .txt files with the desired data.

Navigation data, such as existing waypoints and airports, is included in BlueSky. Furthermore, the simulator is compatible with multiple aircraft performance data formats, BADA and OpenAP. This study uses the latter for the simulation. Short for open aircraft performance model, OpenAP is open source and consists of four main components: aircraft properties, kinematic performances, dynamic performances, and utilities [44]. The first includes aircraft configuration and engine data for simulation. The second involves aircraft performance parameters without considering forces acting on the aircraft, like take-off speed and cruise Mach number. The third provides a model for mass and forces including a drag and thrust, and fuel flow. Finally, utilities are additional data libraries, like a navigation database and a model for atmospheric conditions.

According to Sun et al. (2020) [44], the limitations of the OpenAP model are the following. Aircraft are assumed to be represented by a point with a certain mass, forces are assumed to act on its center of gravity. Furthermore, the model currently only works with turbofan engines. Although some UAV quadcopter models are included, they may not be accurately simulated. Finally, a Bayes estimator is used for the drag polar, which could result in uncertainties for drag force estimations.

6.2 List of Assumptions

The following assumptions are made the current study:

- The airspace will consist of two vertically adjacent layers with the same specified ground speed, course, and vertical speed intervals. The lower layer is used for normal cruise flight, the upper layer is a designated conflict resolution layer allowing resolution maneuvers in the vertical plane.
- Only level cruise flight is considered, with the exception of resolution maneuvers into an adjacent layer consisting of a predefined altitude change. Take-offs and landing are not accounted for.
- Only one type of UAV is used in all simulation experiments.
- The OpenAP model does not accurately represent UAV dynamics, but is assumed to be accurate enough to draw valid conclusions on the behaviour of the system of UAVs in the current experiments.
- The set of geovector velocities is a subset of the set of reachable velocities of the UAV model, hence all geovector limits can be exceeded by the UAVs.
- Per experiment scenario, all UAVs are subjected to the same geovector. Only one geovector is installed per scenario, hence it is not possible for a UAV to enter a new geovector area while performing a conflict resolution maneuver.
- Only static geovectors are considered, not dynamic geovectors.
- Required horizontal and vertical separation is constant for each UAV.
- All UAVs in the airspace use the same conflict detection and resolution strategy in one simulation scenario.

- The required state information for conflict detection of each UAV in the airspace is noise-free and instantly available to every other UAV in the airspace using ADS-B.
- Geofences in the airspace only exist in the form of a polygon.
- It is assumed no wind is present in the experiment.

6.3 Experiment Layout and Control Variables

A series of simulations will be performed in order to verify the effectiveness of the conflict resolution ruleset in geovector airspace (explained in Chapter 5). Two types of experiments will be conducted: *preliminary* and *macro* experiments. The former involves performing a series of 1-1 conflict simulations where two UAVs are spawned such that a conflict emerges in a geovector airspace without geofences. Geovector configurations are varied in order to verify the proposed resolution method and asses the effectiveness of the method with varying 3-D geovector intervals. The same set of simulations will also be performed using only the MVP method as a baseline scenario. The preliminary experiments are explained in Section 6.5. Afterwards, the geovector configurations which are found to involve a significant amount of GEO maneuvers will be used in a series of large-scale simulations (macro simulations). These involve simultaneous simulation of a large number of UAVs in an airspace corridor. The purpose of this type of experiment is to investigate system behaviour of a large number of UAVs all using the proposed resolution method, as well as determine relevant airspace metrics which allow for comparison of the resolution method with the baseline MVP method. The macro experiments are further explained in Section 6.6.

The drone model used in the simulation experiments is the *DJI Matrice 600.* This model is included in the BlueSky simulation environment. Relevant parameters of this rotorcraft UAV, found in the OpenAP database in BlueSky, are given in Table 6.1. Other control variables for the experiments are given in Table 6.2. A feasible value for the factor f of the resolution strategy needs to be determined from preliminary test runs in BlueSky.

Table 6.1: Parameters of the DJI Matrice 600

Parameter	Value
Reachable airspeeds	[-18, 18] m/s
Reachable vertical speeds	[-5, 5] m/s
Number of rotors	6
Maximum take-off weight	15.1 kg
Maximum altitude	2500 m

Table 6.2: Control Variables

Parameter	Value	Reference
Nominal flying altitude	500 ft (150 m)	[39, p. 38]
Required horizontal separation (S_h)	164 ft (50 m)	[27]
Required vertical separation (S_v)	25 ft (7.6 m)	[8]
Conflict detection lookahead time	30 s	[8]
UAV type	DJI Matrice 600	
Factor f for the resolution strategy	t.b.d.	

6.4 List of Metrics

A number of metrics can be used to assess the performance of the proposed resolution method in the experiments. Since the solution is tailored towards both satisfying the geovector rules and solving a conflict simultaneously, the metrics can be subdivided into three groups. First of all, Subsection 6.4.1 describes the metrics used to measure how effective the resolution strategy is in meeting the geovector rules. Afterwards, Subsection 6.4.2 focuses on the ability to resolve conflicts. Finally, Subsection 6.4.3 describes metrics used to identify how the proposed resolution ruleset behaves in conflict situations.

6.4.1 Geovector Metrics

The following metrics can be used to determine the effectiveness of the resolution strategy in preventing aircraft from violating one or more geovector limits.

Geovector Intrusion Rate

The factor of conflict resolution maneuvers which lead to a geovector violation can be determined using Equation 6.1. This factor will be denoted by *geovector intrusion rate* (GIR). Let the amount of conflict resolution maneuvers be denoted by n_{CR}. The amount of maneuvers which violate a geovector limit, being a subset of all CR maneuvers, is denoted by $n_{CR,violation}$. The higher this factor, the more maneuvers have led to a geovector violation, hence the worse the performance it indicates.

$$GIR = \frac{n_{CR,violation}}{n_{CR}} \tag{6.1}$$

The geovector intrusion rate as presented above does not differentiate between the different limits that are violated. Therefore, this factor can further be subdivided into violations of the ground speed (GS), course (χ), and vertical speed (VS) limits, where the amount of geovector violations is only measured for one specific limit. It should be noted that it is possible one maneuver exceeds multiple limits simultaneously. Therefore, summing the individual geovector intrusion rates of the separate limits can result in a higher value than computed using Equation 6.1.

Amount of Intrusion per Geovector Limit

It is possible the velocity vector resulting after performing a CR maneuver for a pairwise conflict exceeds one or multiple limits. When this occurs, the amount of excess state change of a CR maneuver outside the geovector maneuvering space ($\mathbf{V}_{gms}$, refer to Section 5.1) can be used to describe the severity of the geovector intrusion. Excess ground speed (ΔGS in m/s), course ($\Delta\chi$ in degrees), and vertical speed (ΔVS in m/s) can be separately computed.

Since the process of CD&R is iteratively performed each timestep t, the amount of geovector intrusion might not be constant over the entire duration the limit is violated. Therefore, the average value is used of the intrusion at each timestep t over the interval. Let the first time of exceeding a geovector limit be denoted by $t_{geo,out}$ and the last by $t_{geo,in}$. Using a timestep Δt, the amount of timesteps over this interval, $n_{\Delta t}$, can be denoted computed as:

$$n_{\Delta t} = \frac{t_{geo,out} - t_{geo,in}}{\Delta t} + 1 \tag{6.2}$$

The average value can be computed using Equation 6.3 - Equation 6.5. In these equations, the subscript $_{own}$ represents the value corresponding to the velocity vector of the ownship, while $_{lim}$ refers to the value corresponding to the limit that is being violated. Since both minimum and maximum limits can be violated, the absolute value is used. The computed values can subsequently be stored for visualization in separate boxplots. The plots give an indication of the distribution of the severity of geovector violations. The larger the amount of intrusion, the worse the resolution method performs on staying within the geovector rules.

$$\overline{\Delta GS} = \sum_{t=t_{geo,out}}^{t_{geo,in}} \frac{||GS_{own} - GS_{lim}||_t}{n_{\Delta t}} \tag{6.3}$$

$$\overline{\Delta \chi} = \sum_{t=t_{geo,out}}^{t_{geo,in}} \frac{||\chi_{own} - \chi_{lim}||_t}{n_{\Delta t}} \tag{6.4}$$

$$\overline{\Delta VS} = \sum_{t=t_{geo,out}}^{t_{geo,in}} \frac{||VS_{own} - VS_{lim}||_t}{n_{\Delta t}} \tag{6.5}$$

Geovector Intrusion Duration

For each geovector intrusion situation that occurs, it can be logged how long it takes before the situation resolves. This gives a measure of how long geovector violations last on average. Using the same definitions as above, the amount of time a geovector violation lasts, denoted by $t_{violation}$ can be computed using Equation 6.6. Values can be logged for each violation situation and combined into boxplots. The longer a violation, the worse the resolution method performs on satisfying the geovector rules.

$$t_{violation} = t_{geo,out} - t_{geo,in} \tag{6.6}$$

6.4.2 Conflict Resolution Metrics

Metrics used to measure the effectiveness of the resolution ruleset to resolve conflicts are given below.

Average Conflict Duration

A factor which is important is the average duration of a conflict. Since the GEO maneuver typically results in a relative speed reduction, conflicts may take a significant amount of time to be resolved. This can have negative effects on the efficiency of the resolution method. For each conflict, the time at the moment of conflict detection (t_{CD}) and at the moment of reaching CPA (t_{CPA}) will be logged. Afterwards, the conflict duration will be determined using the definition in Equation 6.7. The longer a conflict lasts, the worse the resolution method performs.

$$t_{conf} = t_{CPA} - t_{CD} \tag{6.7}$$

Intrusion Prevention Rate

If a loss of separation (LoS) occurs, the CD&R algorithm was unable to resolve a conflict in time. Logging the amount of LoS that occur during the experiment and comparing this value to the total amount of conflicts gives an indication of the effectiveness of the CR method for conflict resolution. Let the amount of LoS be denoted by n_{LoS} and the amount of conflicts by n_{conf}. The *intrusion prevention rate* (IPR) can be computed according to the method used by Sunil et al. (2017) [48]: The lower this value, the worse the resolution method performs.

$$IPR = \frac{n_{conf} - n_{LoS}}{n_{conf}} \tag{6.8}$$

LoS Severity

The severity of a conflict can be expressed as the amount of intrusion at CPA compared to the required minimum separation. Let the distance at CPA be denoted by d_{cpa}. The *LoS severity* can be computed using the definition specified by Ribeiro et al. (2020) [37] given in Equation 6.9. This metric can give an indication of the satefy of the airspace. The higher this value, the worse the performance of the resolution method.

$$LOS_{sev} = \frac{R_{pz} - d_{cpa}}{R_{pz}} \tag{6.9}$$

Domino Effect Parameter

Airspace stability can be measured using the *Domino Effect Parameter* (DEP). Defined by Bilimoria et al. (2000) [3]. This parameter expresses the degree to which new conflicts (secondary conflicts) are created by aircraft that are manoeuvring to resolve a conflict that has already occurred (primary conflict). Let the amount of conflicts in a scenario without conflict resolution be denoted by n_{conf}^{OFF}. Furthermore, denote the amount of conflicts that occur in a scenario with conflict resolution by n_{conf}^{ON}. Using these values, the DEP can be computed as follows:

$$DEP = \frac{n_{conf}^{ON}}{n_{conf}^{OFF}} - 1 \tag{6.10}$$

Positive values indicate a destabilizing effect of the resolution ruleset, as more conflicts occur due to the resolution maneuvers performed by the aircraft. Using the same reasoning, negative values would indicate a stabilizing effect.

Route Efficiency

The effect of the resolution ruleset on route efficiency can be expressed in terms of the extra path flown due to the resolution maneuvers performed. Denoting the route distance in the scenario without conflict resolution by d^{OFF} and with conflict resolution by d^{ON}, the *route efficiency* η_d can be expressed using Equation 6.11. The lower this value, the higher the impact of the conflict resolution strategy on the efficiency.

$$\eta_d = \frac{d^{OFF}}{d^{ON}} \tag{6.11}$$

Geofence Intrusions

Using the same definition as Jacobse (2020) [26], the amount of intrusions with restricted airspace or other static obstacles can give an indication of the effectiveness of the resolution ruleset to be used in the presence geofences. This factor is important, as urban airspace could be full of these types of restrictions. It can give an indication of the feasibility of the proposed method of static obstacle avoidance.

6.4.3 Resolution Strategy Metrics

It can be investigated how the proposed resolution strategy behaves in the simulation experiments. For each conflict, it can be logged whether the CR algorithm chooses to perform the horizontal MVP maneuver, vertical MVP maneuver, or horizontal GEO maneuver. Counting all situations and dividing them by the total amount of conflict resolution maneuvers gives the percentage of occurrence of each type of maneuver. These values indicate to what extent the simulation scenario was effective in triggering potential geovector violations. Furthermore, it can give insight into how the resolution ruleset behaves when geovector configurations are changed. Let the amount of horizontal MVP, vertical MVP, and horizontal GEO maneuvers be denoted by $n_{MVP,h}$, $n_{MVP,v}$, and n_{GEO}, respectively. Furthermore, let the total amount of conflict resolution maneuvers performed be denoted by n_{CR}. The percentages can be computed as follows:

$$
\begin{aligned}
\%\text{Horizontal MVP} &= \frac{n_{MVP,h}}{n_{CR}} \cdot 100\% \\
\%\text{Vertical MVP} &= \frac{n_{MVP,v}}{n_{CR}} \cdot 100\% \\
\%\text{Horizontal GEO} &= \frac{n_{GEO}}{n_{CR}} \cdot 100\%
\end{aligned}
\tag{6.12}
$$

6.5 Preliminary Experiments

In order to verify if the proposed pairwise resolution method is effective in solving conflicts within the geovector limits, a series of 1-1 conflict simulations will be conducted. Independent variables are provided in Subsection 6.5.1. Afterwards, Subsection 6.5.2 indicates the dependent measures used for the preliminary experiments. Hypotheses are provided in Section 6.7. The results of the preliminary study can be used as input for the macro experiments described in Section 6.6, narrowing down the range of independent variables to be used in the simulation. It also allows to verify if the implementation in BlueSky works correctly.

For each combination of geovector intervals indicated in Table 6.3, a series of i scenarios will be created involving randomly spawning two UAVs in conflict. Each scenario will be executed twice, once for the baseline MVP method and once for the proposed resolution method. Depending on the geovector that is present, the proposed resolution method will prescribe a different resolution maneuver.

As was assumed for the experiments, only two flight levels are allowed in the experiment: one nominal cruise layer and one resolution layer. Both UAVs will be spawned in the cruise layer but can use the resolution layer for conflict resolution. A sketch of this vertical layout is provided in Figure 6.2.

Furthermore, preliminary case studies involving multi-actor conflicts will give more insight into the feasibility of the proposed resolution method in these types of situations. How exactly these simulations will be performed still needs to be determined. If major problems arise during these experiments, the proposed resolution method will be updated accordingly. Snapshots will be created in order to report on the effectiveness of the proposed resolution method in multi-aircraft conflicts.

6.5.1 Indepdendent Variables for the Preliminary Experiments

The independent variables for the simulations are the specified minimum and maximum limits of the geovector, as well as the resolution method used by the UAVs in a specific simulation scenario. These are described hereafter.

The geovector ground speed intervals will be centered on halve of the maximum reachable ground speed (GS_{max}) of the type of UAV used in the simulation, in order to make sure the UAV can perform maneuvers exceeding the limits. According to Table 6.1, this equals 9 m/s for the DJI Matrice 600 UAV model. The intervals specified for the simulations are given in Table 6.3. Allowed ground speed intervals are varied between 3 and 9 m/s (up to halve the set of reachable set of forward velocities). Course intervals, centered around the north, are increased in three steps between 30 and 90°. Finally, the set of allowed vertical speeds was determined based on the vertical separation requirement given in Table 6.2. Given a conflict is detected 30 seconds prior to LoS, the required vertical resolution speed would equal $7.6/30 = 0.25 m/s$. Adding an extra 20% to account for delay, an allowed vertical speed of 0.3 m/s would allow conflicts detected at the specified lookahead time to be resolved vertically. Two more cases are added: one where no vertical speed is allowed at all; and one where vertical maneuvers are allowed in almost all (short-term) conflicts up to 3 seconds prior to LoS. All geovector parameters are combined, resulting in $3 \times 3 \times 3 = 27$ different configurations.

Note that ground speed and course intervals are not compressed to one allowed value, as this would imply using a different resolution strategy involving only speed or heading changes should be used for maneuvers (MVP is not feasible). These cases are less relevant for the resolution strategy proposed in this research.

Table 6.3: Variation of Geovector Intervals for the Pairwise Conflict Simulations

Ground speed interval
[7.5, 10.5] (3 m/s)
[6, 12] (6 m/s)
[4.5, 13.5] (9 m/s)

Course interval
[345, 15] (30 °)
[330, 30] (60 °)
[315, 45] (90 °)

Vertical speed interval
[0, 0] (0 m/s)
[-0.3, 0.3] (0.6 m/s)
[-3, 3] (6 m/s)

Another independent variable is the resolution method used by the UAVs. Two options exist:

1. The baseline MVP method, involving only horizontal MVP maneuvers
2. The proposed resolution rulset from Chapter 5

Combining the 2 resolution strategies with the 27 geovector configurations results in a total of 54 configurations for the preliminary simulation experiments.

6.5.2 Dependent Measures for the Preliminary Experiments

The following dependent measures from the list of metrics provided in Section 6.4 are used in the preliminary experiments. They give an indication of the effectiveness of the proposed resolution method in solving pairwise conflicts in the presence of a geovector, compared to the baseline MVP method.

- For each series of i simulations for one geovector configuration, one value can be computed for the Geovector Intrusion Rate *(geovector metric)*.

- For each simulation, the average amount of intrusion per geovector limit can be computed. For each series of i simulations per geovector configuration, a box plot can be created showing the distribution of average deviations per geovector violation *(geovector metric)*.
- For each simulation, the average duration of intrusion per geovector limit can be logged. Values can be visualized in a box plot for each series of i simulations *(geovector metric)*.
- For each simulation, the conflict duration can be logged. Each series of i simulations for one geovector configuration provides a box plot indicating the distribution of values *(CR metric)*.
- For each series of i simulations per geovector configuration, one value can be computed for the Intrusion Prevention Rate *(CR metric)*.
- For each simulation, one value can be determined for the LoS severity. These can be combined into box plots indicating the distribution per series of i simulations for one geovector configuration *(CR metric)*.
- Finally, for each series of i simulations, the percentage of horizontal MVP, vertical MVP, and horizontal GEO maneuvers will be logged and presented per geovector configuration. This gives insight into the distribution of choices made by the proposed method *(resolution strategy metric)*.

6.6 Macro Experiments

In order to test the large-scale effects of the proposed resolution method, a set of scenarios will be created involving simultaneous simulation of a large number of UAVs. The main purpose of this design is to trigger a significant amount of situations in which the MVP maneuver would lead to a geovector violation.

The independent variables used in the macro experiments are the same as for the preliminary experiments: geovector ground speed interval, course interval, vertical speed interval, and the proposed resolution method. However, the total of 54 combinations given in Subsection 6.5.1 would result in a very large number of data to be compared. This can impede the process of drawing useful conclusions from the experiments. Therefore, it is proposed to select only a number of geovector configurations for the macro experiments. This selection will be based on the findings of the preliminary experiments, which should give an indication of the range of geovector intervals which generally lead to a significant amount of geovector violations using the MVP method.

The entire list of metrics given in Section 6.4 is used as dependent measures for the macro experiments. Data will be logged for each combination of independent variables, such that a comparison can be made between the baseline MVP method and the proposed resolution method in varying geovector configurations.

The proposed scenario consists of an airspace corridor with the same two vertical layers as used in the preliminary experiments. A preliminary sketch of the corridor layout is

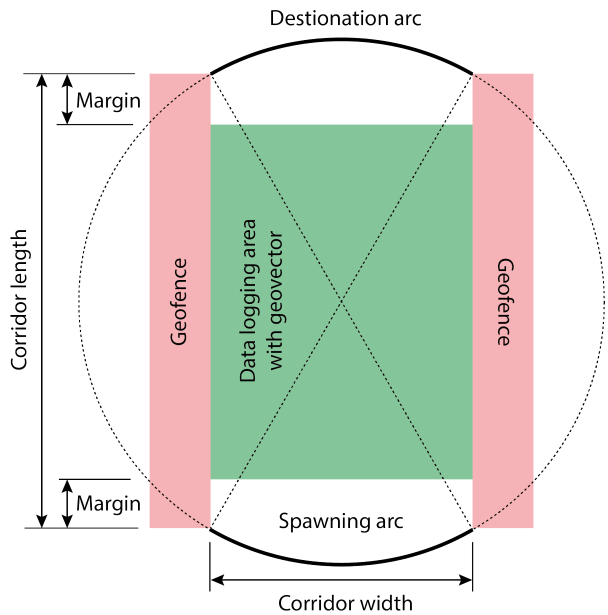

Figure 6.1: Sketched top-view of the proposed corridor experiment

provided in Figure 6.1 and Figure 6.2, where the former provides a top-view and the latter a cross-section in the vertical plane. A corridor was chosen in order to ensure that vehicles do not scatter over the experiment area, in which case the airspace density is not constant over the data logging period.

A large number of UAVs will be randomly spawned on the spawning arc and given a random destination waypoint on the destination arc. Conflicts emerging immediately after spawning can be resolved before the vehicles reach the data logging area, indicated by the margins. One geovector is specified in the logging area (indicated in green). The geovector intervals are independent variables, hence varied between different scenarios. The line segments connecting the outermost points on the spawning and destination arc indicate the maximum possible course a UAV can be assigned from origin to destination. These line segments should not exceed the maximum course constraints of the geovector, in order to allow each UAV to be able to reach its destination waypoint. Therefore, the ratio of the corridor length to width needs to be varied with varying geovector course constraints. Exact dimensions of the corridor still need to be determined, based on the final selection of independent variables. The hourly UAV throughput (t.b.d.) should be conform with the airspace density measures given in Table 2.2 and Table 2.3.

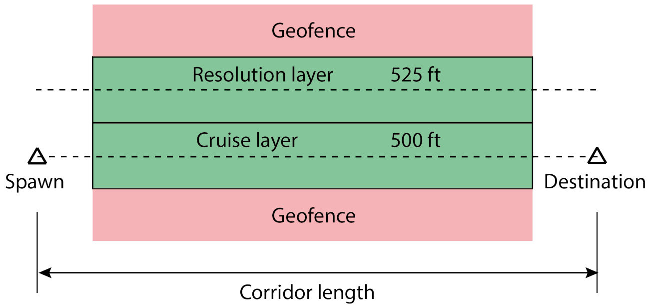

Figure 6.2: Sketched side-view of the proposed corridor experiment

6.7 Hypotheses

Varying the independent variables in both the preliminary and the macro experiments, the following hypotheses are made for the dependent measures:

1. Comparing the baseline MVP method to the proposed geovector resolution method ...
   (a) ... on the conflict resolution metrics, it is expected that all metrics show better performance for the baseline MVP method, since this method relies on more efficient resolution maneuvers.
   (b) ... on the geovector metrics, it is hypothesized that the proposed resolution strategy shows better performance on all metrics, since this method is tailored towards satisfying the geovector limits.
2. Analyzing only the baseline MVP method on ...
   (a) ... conflict resolution metrics, it is hypothesised that all metrics do not show a significant change in performance with decreasing ground speed, course, and vertical speed interval sizes of the geovector, as these limits do not influence the conflict resolution strategy of the MVP method.
   (b) ... the geovector metrics, it is hypothesised that all metrics indicate an increasingly worse performance with decreasing ground speed, course, and vertical speed interval sizes of the geovector, since the solution space for conflict resolution becomes more limited.
3. Analyzing only the proposed resolution method on ...
   (a) ... conflict resolution metrics, it is expected all metrics show worse performance with decreasing ground speed, course, and vertical speed interval sizes of the geovector, since less optimal solutions are chosen with a decrease in solution space for a conflict.
   (b) ... the geovector metrics, it is hypothesized all metrics do not show a significant change in performance with decreasing ground speed, course, and vertical speed interval sizes of the geovector, until a certain point is reached where the solution space is too small to consider alternative maneuvers within the geovector limits.

4. Analyzing the resolution strategy metrics for the proposed resolution method ...
   (a) ... it is expected the percentage of executed horizontal GEO maneuvers increases with decreasing ground speed and course interval size of the geovector, as the horizontal MVP maneuver would more often violate the geovector limits.
   (b) ... it is hypothesized the percentage of executed horizontal MVP maneuvers decreases with decreasing ground speed and course interval size of the geovector, as this maneuver more often violates the geovector limits.
   (c) ... it is expected the percentage of vertical MVP maneuvers used for resolution increases with decreasing ground speed and course interval size of the geovector. The magnitude of the horizontal GEO maneuver increases with decreasing solution space and the decision criterion to use it is more often violated.
   (d) ... it is expected the percentage of vertical MVP maneuvers used for resolution is zero when no vertical speed is allowed and increases with increasing vertical speed interval size of the geovector, since this option becomes available more often.

6.8 Results, Outcome, Relevance, and Planning

The hypotheses presented in Section 6.7 will be tested by logging relevant data in the proposed set of experiments and computing metrics for the dependent variables presented throughout this chapter. The metrics found for the baseline MVP method will be compared to those found for the proposed GEO resolution strategy. First of all, conclusions can be drawn about the effectiveness of the latter to prevent geovector violations for varying geovector configurations. Furthermore, comparison with the baseline method allows to draw conclusions about the effectiveness of the proposed method in solving conflicts. Recommendations can be given about the feasibility of the proposed method, its advantages, and its limitations.

Appendix A

Calculation of the GEO Maneuver

This appendix describes the method of determining the GEO maneuver for the ownship. Firstly, Section A.1 describes the reference frame used for the calculations. Afterwards, Section A.2 describes how to compute the unit vectors describing the course limits of the geovectors. These are necessary in the process of computing the GEO resolution vector, which is described in Section A.3.

A.1 Reference Frame

Velocity vectors of aircraft are expressed in terms of a cylindrical coordinate system using ground speed (GS), course (χ), and vertical speed (VS). However, vectorwise calculation of the GEO maneuver is more straightforward using a Cartesian coordinate system. The horizontal part of the velocity vector is therefore decomposed into a ground speed component in the easterly and northerly direction, denoted by $\mathbf{V}_E$ and $\mathbf{V}_N$ in Figure A.1. The transformation is performed using Equation A.1. All vectors calculations will be performed in the Cartesian reference frame, with the origin centered on the center of mass of the vehicle.

$$\mathbf{V}_{Cartesian} = \begin{pmatrix} GS \cdot \sin\chi \\ GS \cdot \cos\chi \\ VS \end{pmatrix} = \begin{pmatrix} \text{easterly ground speed} \\ \text{northerly ground speed} \\ \text{vertical speed} \end{pmatrix} \tag{A.1}$$

A.2 Geovector Unit Vectors

The unit vectors $\mathbf{n}_{g,min}$ and $\mathbf{n}_{g,max}$ describing the course limits of the geovector, as defined in Figure 4.1, can be found by rotating the unit vector pointing to the north ($\mathbf{n}_{north}$) with the corresponding course limits. Using the Cartesian coordinate frame aligned with the north, this unit vector is described by Equation A.2. The rotation matrices for this

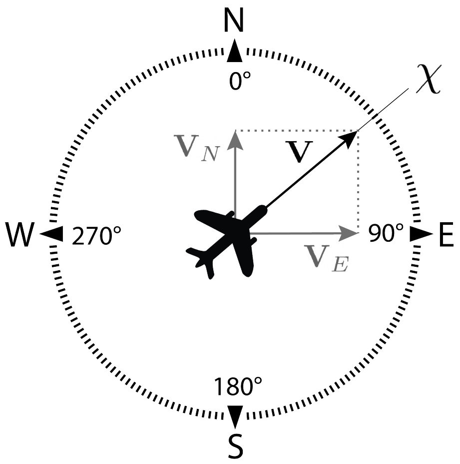

Figure A.1: Decomposition of vectors in northerly and easterly direction

operation, $R_{g,min}$ and $R_{g,max}$, are given in Equation A.3 and Equation A.4. The transpose of these matrices is used in order to account for the fact that compass bearings increase in the clockwise direction, as shown in Equation A.5 and Equation A.6.

$$\mathbf{n}_{north} = \begin{pmatrix} 0 & 1 \end{pmatrix}^T \tag{A.2}$$

$$R_{g,min} = \begin{bmatrix} -\sin(\chi_{min}) & -\cos(\chi_{min}) \\ \cos(\chi_{min}) & -\sin(\chi_{min}) \end{bmatrix} \tag{A.3}$$

$$R_{g,max} = \begin{bmatrix} -\sin(\chi_{max}) & -\cos(\chi_{max}) \\ \cos(\chi_{max}) & -\sin(\chi_{max}) \end{bmatrix} \tag{A.4}$$

$$\mathbf{n}_{g,min} = R^T_{g,min}\mathbf{n}_{north} \tag{A.5}$$

$$\mathbf{n}_{g,max} = R^T_{g,max}\mathbf{n}_{north} \tag{A.6}$$

A.3 GEO Maneuver

According to Definition 9, the GEO maneuver is chosen such that a minimum state change has to be applied for conflict resolution without violating the geovector rules. Computing this maneuver relies on two steps:

1. It is first checked whether the geometrically optimal solution lies on the allowed geovector intervals. This process is explained in Subsection A.3.1. If this solution is feasible, it can be accepted as the GEO maneuver.

2. If the geometrically optimal solution does not satisfy the geovector, the solution lies on the nearest intersection between the coordinated leg of the VO and the geovector limits. Subsection A.3.2 describes how this intersection is determined.

A.3.1 Geometrically Optimal Solution

The geometrically optimal solution corresponds to the smallest possible resolution vector magnitude and is denoted by "OPT". It is possible that this solution is actually feasible while MVP is not, as is shown in Figure A.2. The figure provides a zoomed section of a conflict situation, where the coorindated leg of the VO is described by the unit vector $\mathbf{n}_t$. As illustrated, the resolution vector corresponding to OPT is orthogonal to the leg of the VO, while the resolution vector for MVP is orthogonal to the relative velocity $\mathbf{V}_{rel}$.

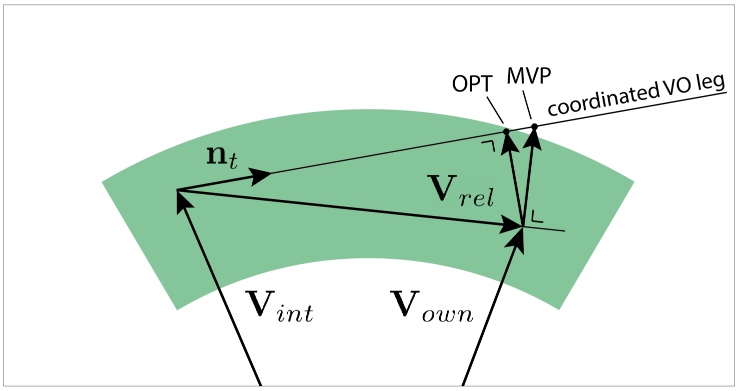

Figure A.2: Illustration of how the geometrically optimal maneuver (OPT) can satisfy the geovector limits, while the MVP maneuver does not.

Any velocity vector $\mathbf{V}_{sol}$ on the leg of the VO can be described by the vector given in Equation A.7, where c represents a non-negative scalar value.

$$\mathbf{V}_{sol} = \mathbf{V}_{int} + c \cdot \mathbf{n}_t \tag{A.7}$$

The value of c corresponding to the geometrically optimal solution can be computed using the fact that resolution vector is orthogonal to the leg of the VO [10]:

$$c = \mathbf{V}_{rel} \cdot \mathbf{n}_t \tag{A.8}$$

Subsequently, plugging the obtained value for c into Equation A.7, it can be checked whether the solution velocity $\mathbf{V}_{sol}$ violates the geovector limits.

A.3.2 Intersections with Geovector Limits

If the geometrically optimal solution is not feasible, the GEO maneuver lies on one of the intersections between the coordinated leg of the VO and the geovector limits. Figure A.3 provides an example of all intersections found for a geovector with ground speed and course limits (denoted by 1-6).

All intersections on the opposite side of where the unit vector $\mathbf{n}_t$ is pointing can be disregarded, since the leg of the VO actually does not exist on this side (1-4 in the example illustrated in Figure A.3). The same holds for the intersections that are not actually located on the intervals specified by the geovector (1, 2, 3, and 6 in the example). After subtracting all these infeasible points from the set of intersections, the following situations can occur:

1. It is possible no intersections remain if both aircraft already violate the geovector rules when the conflict is detected. In that case, the GEO maneuver is undefined.

2. One intersection remains, this solution corresponds to the GEO maneuver.

3. Two or more intersections remain. In this case, the intersection resulting in the smallest resolution vector magnitude (($||\mathbf{V}_{r,geo}||$)) corresponds to the GEO maneuver.

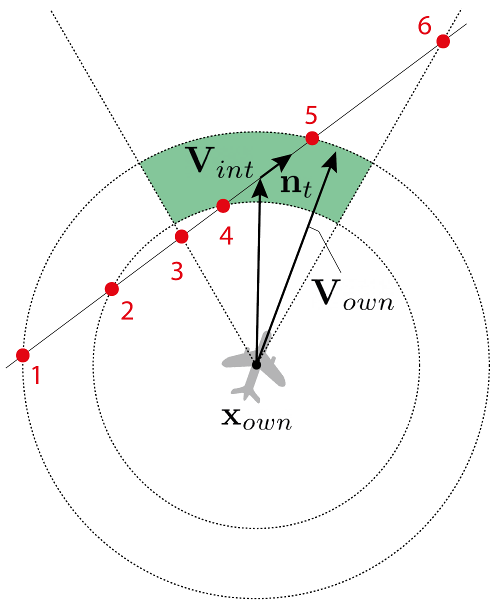

Figure A.3: Illustration of all points (1-6) found when computing the intersections between the horizontal geovector limits and the coordinated leg of the horizontal VO. The former are denoted by the dotted circles and radials originating at the ownship, enclosing the set of geovector velocities in green. The latter is visualized by the span of the unit vector $\mathbf{n}_t$.

Ground Speed Limits

Using Equation A.7, the value of c for which the leg of the VO crosses a ground speed limit can be computed by setting the magnitude of this vector equal to the value of the limit, represented by GS in Equation A.9.

$$||\mathbf{V}_{sol}||^2 = ||\mathbf{V}_{int} + c \cdot \mathbf{n}_t||^2 = GS^2 \tag{A.9}$$

Rearranging the terms results in the following second order polynomial which can be solved for c (note that the square of a unit vector equals 1):

$$c^2 + c\,(2 \cdot \mathbf{V}_{int} \cdot \mathbf{n}_t) + \left(\mathbf{V}_{int}^2 - GS^2\right) = 0$$

The discriminant Δ can be computed as given hereafter. If $\Delta < 0$, no real solutions can be found, meaning the GEO maneuver does not lie on this limit. If $\Delta = 0$, exactly one solution can be found for this limit. If $\Delta > 0$, two intersections are found.

$$\Delta = (2 \cdot \mathbf{V}_{int} \cdot \mathbf{n}_t)^2 - 4\left(\mathbf{V}_{int}^2 - GS^2\right)$$

Finally, the corresponding values of c for the intersection with the ground speed limit are computed using Equation A.10

$$c = \frac{-\,(2 \cdot \mathbf{V}_{int} \cdot \mathbf{n}_t) \pm \sqrt{\Delta}}{2} \tag{A.10}$$

Course Limits

The intersections found with a course limit will be either be one or infinitely many if the leg of the VO perfectly overlaps with the course limit radial. Computations rely on the fact that a cross product between two equal lines (resolution vector and course limit radial) is zero, as shown in Equation A.11. The resolution vector on the leg of the VO at the point of the intersection is described using Equation A.7. Let the course limit radial be described by the corresponding geovector unit vector $\mathbf{n}_g$.

$$\mathbf{V}_{sol} \times \mathbf{n}_g = (\mathbf{V}_{int} + c\mathbf{n}_t) \times \mathbf{n}_g = 0 \tag{A.11}$$

Rearranging the terms allows for the calculation of the value of c corresponding to the intersection:

$$c = \frac{-\mathbf{V}_{int} \times \mathbf{n}_g}{\mathbf{n}_t \times \mathbf{n}_g} \tag{A.12}$$

Appendix B

Experiment Planning

This appendix includes a Work Breakdown Structure (Figure B.1) and a Gantt Chart for the experiment phase, starting in week 26 (28-06-2021). The work packages defined in the Work Breakdown Structure are directly used as input for the Gantt Chart, including estimation of duration. Holidays are included in the planning. The estimated time of completion of the experimental phase lies at the end of week 48 (around 03-12-2021).

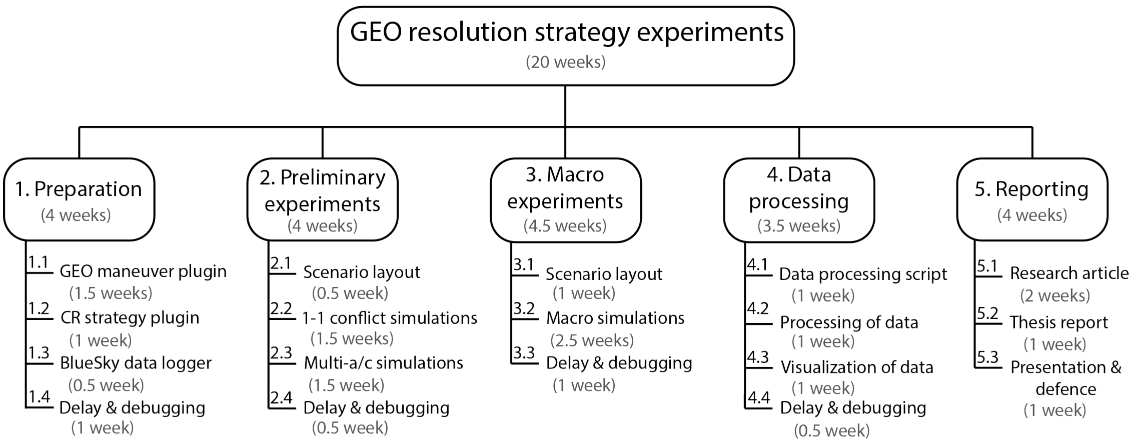

Figure B.1: Work Breakdown Structure for the experiment phase of the research

Five major work packages are recognized, dividing the experiment phase into approximately equal parts. Package 1 involves preparation of the experiment in the BlueSky simulator. A plugin will need to be created to implement computation of the GEO maneuer (Chapter A) and the overall resolution strategy (Section 5.8) such that it can be used by the simulated UAVs. Furthermore, additional data loggers will need to be realized in order to be able to obtain all necessary data for the metrics described in Section 6.4.

Packages 2 and 3 describe the preparation and execution of the various experiment proposed in Section 6.3. The preliminary experiments are used for verification and parameter tweaking of the proposed resolution method, while macro experiments refer to the simulations involving a large number of UAVs in the proposed corridor scenario.

Data processing is performed in package 4. A script will be created to convert the raw data .txt files from the BlueSky data logger to processed data .txt files. These files can further be used to efficiently create the required plots and other forms of data visualization required to test the hypotheses from Section 6.7. Finally, all results will be analyzed and included in a research article, which will be part of the overall thesis report. Package 5 also includes the preparation of the thesis presentation and defence.

Task	Duration	Start date	End date
1. Preparation	4 weeks	28-6-2021	23-7-2021
1.1 - GEO maneuver plugin	1.5 weeks	28-6-2021	6-7-2021
1.2 - CR strategy plugin	1 week	7-7-2021	13-7-2021
1.3 - BlueSky data logger	0.5 week	14-7-2021	16-7-2021
1.3 - Delay & debugging	1 week	19-7-2021	23-7-2021
2. Preliminary experiments	4 weeks	9-8-2021	3-9-2021
2.1 - Scenario layout	0.5 week	9-8-2021	11-8-2021
2.2 - 1-1 conflict simulations	1.5 weeks	16-8-2021	20-8-2021
2.3 - Multi-a/c simulations	1.5 weeks	30-8-2021	7-9-2021
2.4 - Delay & debugging	0.5 week	8-9-2021	10-9-2021
3. Macro experiments	4.5 weeks	13-9-2021	12-10-2021
3.1 - Scenario layout	1 week	13-9-2021	17-9-2021
3.2 - Macro simulations	2.5 weeks	20-9-2021	5-10-2021
3.3 - Delay & debugging	1 week	6-10-2021	12-10-2021
4. Data processing	3.5 weeks	13-10-2021	5-11-2021
4.1 - Data processing script	1 week	13-10-2021	19-10-2021
4.2 - Processing of data	1 week	20-10-2021	26-10-2021
4.3 - Visualization of data	1 week	27-10-2021	2-11-2021
4.4 - Delay & debugging	0.5 week	3-11-2021	5-11-2021
5. Reporting	4 weeks	8-11-2021	3-12-2021
5.1 - Research article	2 weeks	8-11-2021	19-11-2021
5.2 - Thesis report	1 week	22-11-2021	26-11-2021
5.3 - Presentation & defence	1 week	29-11-2021	3-12-2021

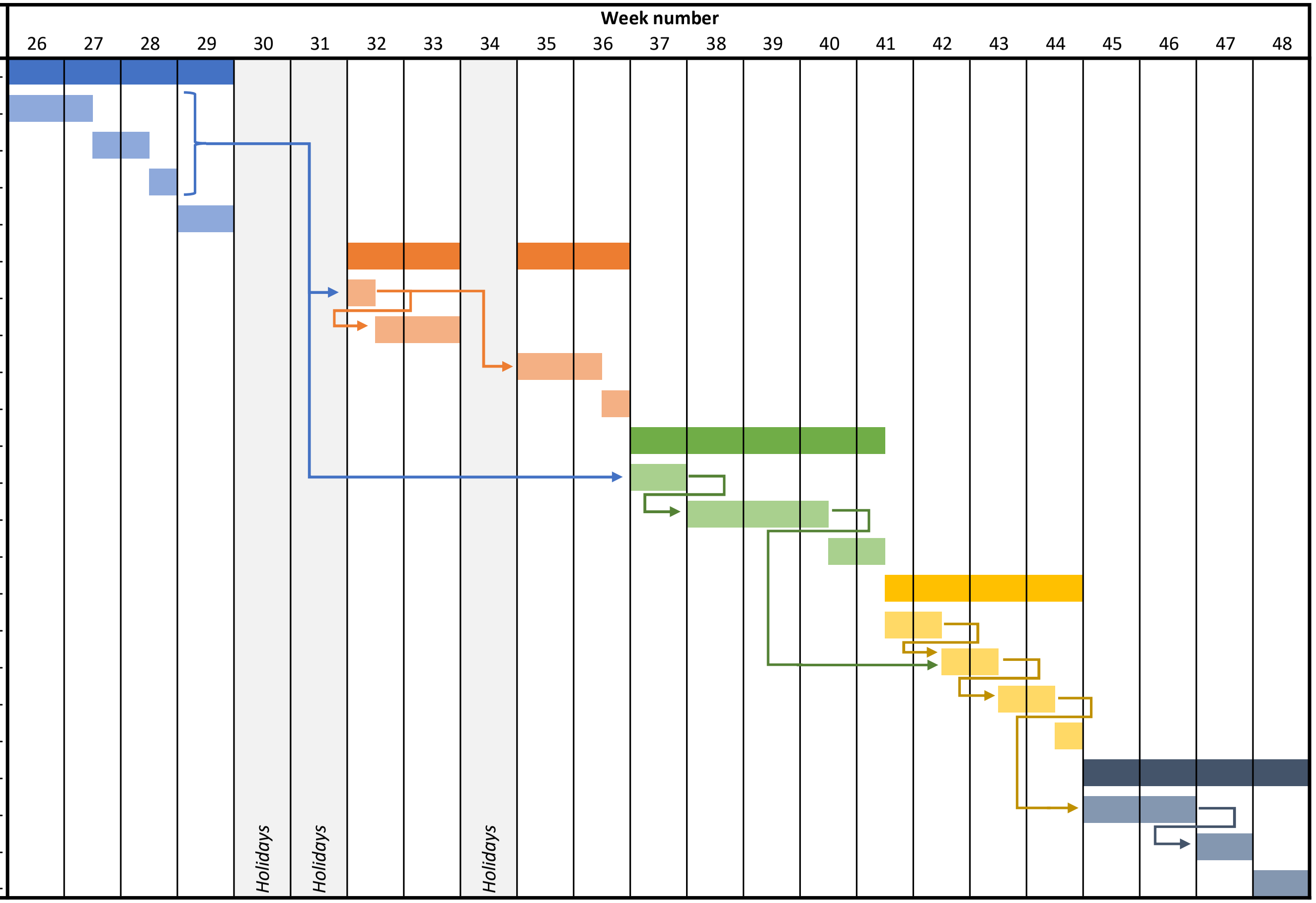

References

[1] TUDelft-CNS-ATM/bluesky: The open source air traffic simulator.

[2] S. Balasooriyan. *Multi-aircraft Conflict Resolution using Velocity Obstacles.* Master thesis, Delft University of Technology, 2017.

[3] K.D. Bilimoria, K.S. Sheth, H.Q. Lee, and S.R. Grabbe. Performance evaluation of airborne separation assurance for free flight. *18th Applied Aerodynamics Conference*, 2000.

[4] A. Chakravarthy and D. Ghose. Obstacle avoidance in a dynamic environment: A collision cone approach. *IEEE Transactions on Systems, Man, and Cybernetics Part A:Systems and Humans.*, 28(5):562–574, 1998.

[5] K. Dalamagkidis, K.P. Valavanis, and L.A. Piegl. *On Integrating Unmanned Aircraft Systems into the National Airspace System: Issues, Challenges, Operational Restrictions, Certification, and Recommendations.* Springer Science Business Media, 2 edition, 2011.

[6] M. Doole, J. Ellerbroek, and J.M. Hoekstra. Drone Delivery: Urban airspace traffic density estimation. *8th SESAR Innovation Days*, 2018.

[7] M. Doole, J. Ellerbroek, and J.M. Hoekstra. Estimation of traffic density from drone-based delivery in very low level urban airspace. *Journal of Air Transport Management*, 88, sep 2020.

[8] M. Doole, J. Ellerbroek, V.L. Knoop, and J.M. Hoekstra. Constrained urban airspace design for large-scale drone-based delivery traffic. *Aerospace*, 8(2):1–22, feb 2021.

[9] M.S. Eby. A Self-Organizational Approach for resolving Air Traffic Conflicts. *The Lincoln Laboratory Journal*, 7(2):239–253, 1994.

[10] J. Ellerbroek. *Airborne Conflict Resolution In Three Dimensions.* Doctoral thesis, Delft University of Technology, 2013.

[11] R.L. Ennis and Y.J. Zhao. A Formal Approach to the Analysis of Aircraft Protected Zone. *Air Traffic Control Quarterly*, 12(1):75–102, jan 2004.

[12] European Union Aviation Safety Agency (EASA). Easy Access Rules for Standardised European Rules of the Air (SERA), dec 2020.

[13] FAA. Equip ADS-B: Capabilities: Ins and Outs.

[14] FAA. Unmanned Aircraft System (UAS) Traffic Management (UTM): Concept of Operations v2.0, 2020.

[15] FAA. UTM Pilot Program (UPP), 2020.

[16] P. Fiorini and Z. Shiller. Motion planning in dynamic environments using the relative velocity paradigm. *Proceedings - IEEE International Conference on Robotics and Automation*, 1:560–566, 1993.

[17] P. Fiorini and Z. Shiller. Motion planning in dynamic environments using velocity obstacles. *International Journal of Robotics Research*, 17(7):760–772, 1998.

[18] S.I. Granshaw. RPV, UAV, UAS, RPAS ... or just drone? *The Photogrammetric Record*, 33(162):160–170, jun 2018.

[19] P. Hermes, M. Mulder, M.M. Van Paassen, J.H.L. Boering, and H. Huisman. Solution-Space-Based Analysis of the Difficulty of Aircraft Merging Tasks. *Journal of Aircraft*, 46(6):1995–2015, 2009.

[20] J. Hoekstra and J. Ellerbroek. BlueSky ATC Simulator Project: An Open Data and Open Source Approach. *7th International Conference on Research in Air Transportation: Philadelphia, USA*, 2016.

[21] J. Hoekstra, J. Ellerbroek, E. Sunil, and J. Maas. Geovectoring: Reducing Traffic Complexity to Increase the Capacity of UAV airspace. *2018 International Conference on Research in Air Transportation*, 2018.

[22] J.M. Hoekstra. *Designing for safety: The free flight air traffic management concept.* Doctoral thesis, Delft University of Technology, 2001.

[23] J.M. Hoekstra, J. Maas, M. Tra, and E. Sunil. How Do Layered Airspace Design Parameters Affect Airspace Capacity and Safety ? *7th International Conference on Research in Air Transportation: Philadelphia, USA*, 2016.

[24] J.M. Hoekstra, R.C.J. Ruigrok, and R.N.H.W. Van Gent. Free Flight in a Crowded Airspace? *Proceedings of the 3rd USA/Europe Air Traffic Management RD Seminar*, 2000.

[25] R. Irvine and H. Hering. Towards Systematic Air Traffic Management in a Regular Lattice. *7th AIAA Aviation Technology, Integration and Operations Conference (ATIO)*, 2007.

[26] R. Jacobse. *Extending the Modified Voltage Potential algorithm for use in converging traffic flows.* Master thesis, Delft University of Technology, 2020.

[27] Y.I. Jenie, E.J. Van Kampen, C.C. De Visser, J. Ellerbroek, and J.M. Hoekstra. Selective velocity obstacle method for deconflicting maneuvers applied to unmanned aerial vehicles. *Journal of Guidance, Control, and Dynamics*, 38(6):1140–1145, 2015.

[28] Y.I. Jenie, E.J. Van Kampen, J. Ellerbroek, and J.M. Hoekstra. Taxonomy of Conflict Detection and Resolution Approaches for Unmanned Aerial Vehicle in an Integrated Airspace. *IEEE Transactions on Intelligent Transportation Systems*, 18(3):558–567, mar 2017.

[29] P.H. Kopardekar. Unmanned Aerial System (UAS) Traffic Management (UTM): Enabling Low-Altitude Airspace and UAS Operations, 2014.

[30] J.K. Kuchar and L.C. Yang. A Review of Conflict Detection and Resolution Modeling Methods. *IEEE Transactions on Intelligent Transportation Systems*, 1(4):179–189, dec 2000.

[31] T. Langejan, E. Sunil, J. Ellerbroek, and J. Hoekstra. Effect of ADS-B Characteristics on Airborne Conflict Detection and Resolution. *6th SESAR Innovation Days (SID)*, 2016.

[32] K. Leiden and S. Green. Strategies for applying variable lookahead times to conflict detection and trial planning. *Collection of Technical Papers - 6th AIAA Aviation Technology, Integration, and Operations Conference*, 2:916–926, 2006.

[33] K. Leiden, S. Peters, and S. Quesada. Flight Level-based Dynamic Airspace Configuration. *9th AIAA Aviation Technology, Integration and Operations Conference (ATIO)*, 2009.

[34] G. Manfredi, E. Baskaya, J. Sharples, and Y. Jestin. Unmanned Aerial System Operations for Retail. *ICAS 2018: 14th International Conference on Autonomic and Autonomous Systems, IASFR: Intelligent Autonomous Systems for the Future of Retail*, 2018.

[35] G. A. Mercado Velasco, M. Mulder, and M. M. Van Paassen. Air traffic controller decision-making support using the Solution Space Diagram. *IFAC Proceedings Volumes (IFAC-PapersOnline)*, 11(PART 1):227–232, jan 2010.

[36] R.A. Paielli. A Linear Altitude Rule for Safer and More Efficient Enroute Air Traffic. *Air Traffic Control Quarterly*, 8(3):195–221, jul 2000.

[37] M. Ribeiro, J. Ellerbroek, and J. Hoekstra. Review of conflict resolution methods for manned and unmanned aviation. *MDPI Aerospace*, 7(6), jun 2020.

[38] A.J.G.T. Scholtes. *Structuring airspace into lateral zones for conflict prevention.* Master thesis, Delft University of Technology, 2018.

[39] SESAR JU. *European Drones Outlook Study.* November 2016.

[40] SESAR JU. *U-space Blueprint.* 2017.

[41] SESAR JU. European ATM Master Plan: Roadmap for the safe integration of drones into all classes of airspace, 2018.

[42] SESAR JU. Supporting Safe and Secure Drone Operations in Europe: A Preliminary Summary of SESAR U-Space Research and Innovation Results (2017-2019), 2020.

[43] SESAR JU. *EUROCONTROL Specification for Surveillance Data Exchange ASTERIX: Part 12 - Category 021 ADS-B Target Reports (SPEC-0149-12)*. 2.5 edition, 2021.

[44] J. Sun, J.M. Hoekstra, and J. Ellerbroek. OpenAP: An open-source aircraft performance model for air transportation studies and simulations. *Aerospace*, 7(8), aug 2020.

[45] E. Sunil. *Analyzing and Modeling Capacity for Decentralized Air Traffic Control.* Doctoral thesis, Delft University of Technology, 2019.

[46] E. Sunil, J. Ellerbroek, and J. Hoekstra. CAMDA: Capacity Assessment Method for Decentralized Air Traffic Control. *2018 International Conference on Research in Air Transportation*, 2018.

[47] E. Sunil, J. Ellerbroek, J. Hoekstra, and J. Maas. Modeling Airspace Stability and Capacity for Decentralized Separation. *12th Seminar Papers: 12th USA/Europe Air Traffic Management Research and Development Seminar*, page 12, 2017.

[48] E. Sunil, J. Ellerbroek, J. Hoekstra, A. Vidosavljevic, M. Arntzen, F. Bussink, and D. Nieuwenhuisen. Analysis of Airspace Structure and Capacity for Decentralized Separation Using Fast-Time Simulations. *Journal of Guidance, Control, and Dynamics*, 40(1):38–51, jan 2017.

[49] E. Sunil, J. Hoekstra, J. Ellerbroek, F. Bussink, D. Nieuwenhuisen, A. Vidosavljevic, and S. Kern. Metropolis: Relating airspace structure and capacity for extreme traffic densities. *Proceedings of the 11th USA/Europe Air Traffic Management Research and Development Seminar, ATM 2015*, 2015.

[50] J. Van Den Berg, S.J. Guy, M. Lin, D. Manocha, C. Pradalier, R. Siegwart, and G. Hirzinger. Reciprocal n-body Collision Avoidance. *Robotics Research: The 14th International Symposium ISRR, Springer Tracts in Advanced Robotics*, 70:3–19, 2011.